NASA CR-134390

JUNE 1974

LMSC-D401948

THE DEVELOPMENT OF A NON-CRYOGENIC NITROGEN/OXYGEN SUPPLY SYSTEM

(NASA-CR-134300) THE DEVELOPMENT OF A
NON-CRYOGENIC NITROGEN/OXYGEN SUPPLY
SYSTEM Final Report (Lockheed Missiles
and Space Co.) 131 p HC $9.75 CSCL 06K
G3/05
N74-31581
Unclas
47094

Prepared Under Contract NAS9-13051

by

Bioengineering Organization
LOCKHEED MISSILES & SPACE COMPANY, INC.
Sunnyvale, California

for

NATIONAL AERONAUTICS AND SPACE ADMINISTRATION
Johnson Spacecraft Center
Houston, Texas

JUNE 1974

LMSC/D401948

DEVELOPMENT OF A NON-CRYOGENIC NITROGEN/OXYGEN SUPPLY SYSTEM

FINAL REPORT

Prepared Under Contract NAS 9-13051

By

Bioengineering Organization

LOCKHEED MISSILES & SPACE COMPANY, INC.

B. M. Greenough

R. E. Mahan

February 1974

NATIONAL AERONAUTICS & SPACE ADMINISTRATION

Johnson Space Center

Houston, Texas

LIST OF CONTRIBUTORS

B. M. Greenough	Project Leader
E. J. Clisham	Power Controller Design
W. Connor	Pump/Bubble Separator Design
R. E. Mahan	Baseplate Design, System Test
R. B. Maine	Cell Design
P. A. Wagner	Reservoir Design

NASA TECHNICAL MONITOR

R. Martin

CREW SYSTEMS DIVISION

NASA, Johnson Space Center

TABLE OF CONTENTS

SUMMARY

A program was conducted to design, fabricate and test a prototype hydrazine/water electrolysis system module applicable to manned spacecraft requiring metabolic oxygen and both oxygen and nitrogen for cabin leakage makeup. This system because it allows nitrogen to be stored in the chemical form of hydrazine hydrate offers potential advantages of weight savings and less difficult resupply for long-term and intermediate duration missions compared to gaseous or cryogenic storage.

This phase of the program development of the hydrazine/water electrolysis technology primarily implemented the modular maintainable design concept derived in the previous work.

Individual components of the prototype assembly were fabricated and bench tested at the component level prior to full module assembly. The following are the key components which represent advances in technology in the system:

The baseplate contains internal manifold and routing passages for the electrolyte loop, interfaces with the liquid loop components, and serves as the structural support for the assembly.

A pump/bubble separator combines in one component, the function of electrolyte circulation and removal of entrained gas bubbles in the electrolyte loop.

An electrolyte reservoir pressure controller provides the the multiple functions of system operating pressure control, water and hydrazine feed control, and volume sensing for safety purposes.

The electrolysis cell design includes a new cell spacer design amenable to being produced by injection molding; and a new hydrophilic matrix configuration within the cell to improve its resistance to gas/liquid differential pressure fluctuations.

The power controller is capable of utilizing spacecraft solar cell power to provide selectable regulated current at an efficiency of 92 percent.

The above key components along with the necessary laboratory supporting equipment were assembled in a test setup and operated in modes which verified component designs and demonstrated the compatibility of the individual components as well as the feasibility of the modular system concept.

The sections that follow in this report describe the component fabrication and testing, the hydrazine sensor study, and the cell math model. Component and assembly detail drawings and process specifications are documented separately.

Section 1
INTRODUCTION

A nitrogen/oxygen cabin atmosphere will probably be utilized in all future manned space missions. The nitrogen serves not only as an inert diluent to reduce the fire hazard in the closed environment, but also, enhances the physiological habitability of the spacecraft cabin.

In a reclamation type life support system oxygen, that is consumed by the crew, can be recovered from metabolic wastes for recycle. Water electrolysis is an effective process that is being considered for use in this type of life support system.

However, because of cabin atmosphere leakage, there is also a need for storage of makeup oxygen and nitrogen. For relatively short missions sufficient makeup oxygen and nitrogen can be carried effectively using cryogenic or high pressure gaseous storage. For long duration missions, however, the weight penalty associated with these techniques becomes excessive. An electrolysis technique, in which hydrogen and oxygen are produced from water, and nitrogen is produced from hydrazine at the oxygen electrode, is a competitive method of leakage makeup. With this system, oxygen and nitrogen are stored chemically as water and hydrazine in low-pressure (and therefore low-weight) tankage. This system design has the capability, with the appropriate sensors, of providing automatic control of a cabin total pressure and oxygen partial pressure.

The initial feasibility study of the hydrazine/water electrolysis concept, the verification of the process with single cells and the derivation of a spacecraft atmosphere control model were accomplished under Control NAS 1-7706. (Ref. 1)

A one-man breadboard system was then assembled and checked out in combination with a cabin simulator under Contract 9-10405, Phase I. Operational data from this breadboard were used in the preliminary design of a full-scale 12-man spacecraft system. Testing of the breadboard system in Phase II of the Contract yielded an extensive data base for this technique, and supported the detailed design of the modular concept of a full-scale system.

The major objectives of the program described herein were to fabricate a unit of the modular system design, and to subject this module to design verification testing.

A study effort was conducted to determine the technology status of hydrazine vapor sensors, and to evaluate techniques that might be used to measure liquid hydrazine concentration. This consisted of a literature survey on the LMSC DIALOG computerized data retrieval system and contacts with the leading vendors of specialized analytical devices. The state-of-the-art in vapor detectors was found to be limited to colorimetric techniques and no suitable method for liquid concentration measurement was found.

A mathematical model of the hydrazine/water electrolysis cell was developed suitable for predicting heat and mass balances for a steady state condition. The model identifies the key variables and defines their interrelationship in the cell process. Both empirical and theoretical data are utilized. This cell math model represents the first step in the development of a model capable of predicting full scale system real duty cycle performance.

Section 2
TECHNICAL RESULTS AND DISCUSSION

This section describes the fabrication and testing of the individual components and the final prototype assembly. Laboratory test facilities and supporting equipment are also described. Supporting test logs and data are included in the Appendix.

2.1 SYSTEM DESCRIPTION

2.1.1 Design Concept

The design concept which is demonstrated under this contract was developed under Contract NAS 9-10405 (Ref. 2). In developing the design approach for the hydrazine water electrolysis system, the first consideration was an appropriate maintenance concept. Maintenance experience and a maintenance analysis revealed that it was desirable to minimize the handling of the electrolyte circuit parts, fittings and disconnects in zero gravity. The concept that evolved to meet these requirements consisted of providing individual, self-contained hydraulic assemblies with no electrolyte connections. In this concept these assemblies would be completely sealed with internal manifolding within each module for the electrolyte circuit. The modules would be mounted on rails to allow easy installation and removal from a cabinet as shown in Figure 1. The only disconnects would be provided in the rear of the module for connection to services and gas discharge ports and would incorporate check valves to prevent spillage when disconnected. Cooling would be provided by a conduction cold plate that the module interfaces with when it is installed in the cabinet. The cabinet would also contain individual replaceable electronic assemblies for each module and a central status panel for manual monitoring of selected data which also could be supplied to the on-board spacecraft computer system.

The following sections describe the implementation of this module concept.

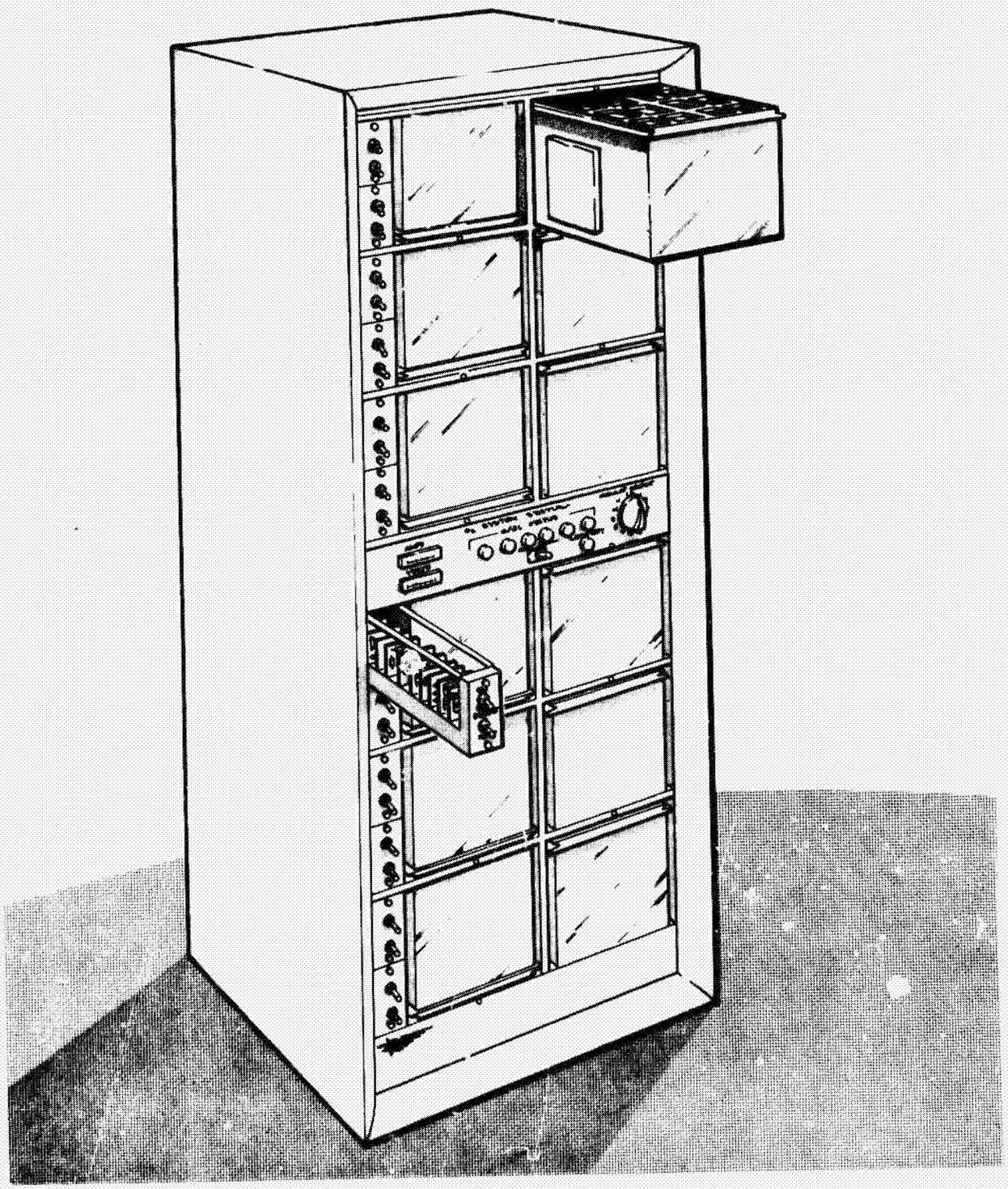

FIGURE 1 N_2/O_2 SUPPLY SYSTEM

2.1.2 Prototype Assembly

The prototype assembly contains all the mechanical features of the spacecraft module with the exception of the enclosure and mounting rails. A schematic of the unit is shown in Figure 2. The key components contained in the assembly are:

- A 22-cell electrolysis stack employing a new cell design.
- A zero-gravity design electrolyte reservoir incorporating water feed, volume control and pressure control.
- A zero-gravity design pump and bubble separator.
- A baseplate with integral manifolding for all system electrolyte passages and component connections.
- A contact heat exchanger for interfacing with a cabinet cold plate.

All of these individual components, their fabrication and performance in bench tests as well as their combined performance as a complete assembly in the laboratory test bed are described subsequently in this report.

One additional component, the power controller required to condition and control spacecraft power for the electrolysis cell stack, was also implemented and tested.

2.1.3 Laboratory Support Equipment

The laboratory test bed is shown in Figures 3 and 4. Mechanical support equipment includes a nitrogen cylinder for pressure reference and safety purge, water, a contact cold plate for cooling, and discharge connections for the generated gases and the separator gas vent. The hydrogen effluent and the separator gas vent are plumbed to an exhaust hood. The oxygen/nitrogen line vents to the room after passing through a PO_2 sensor chamber.

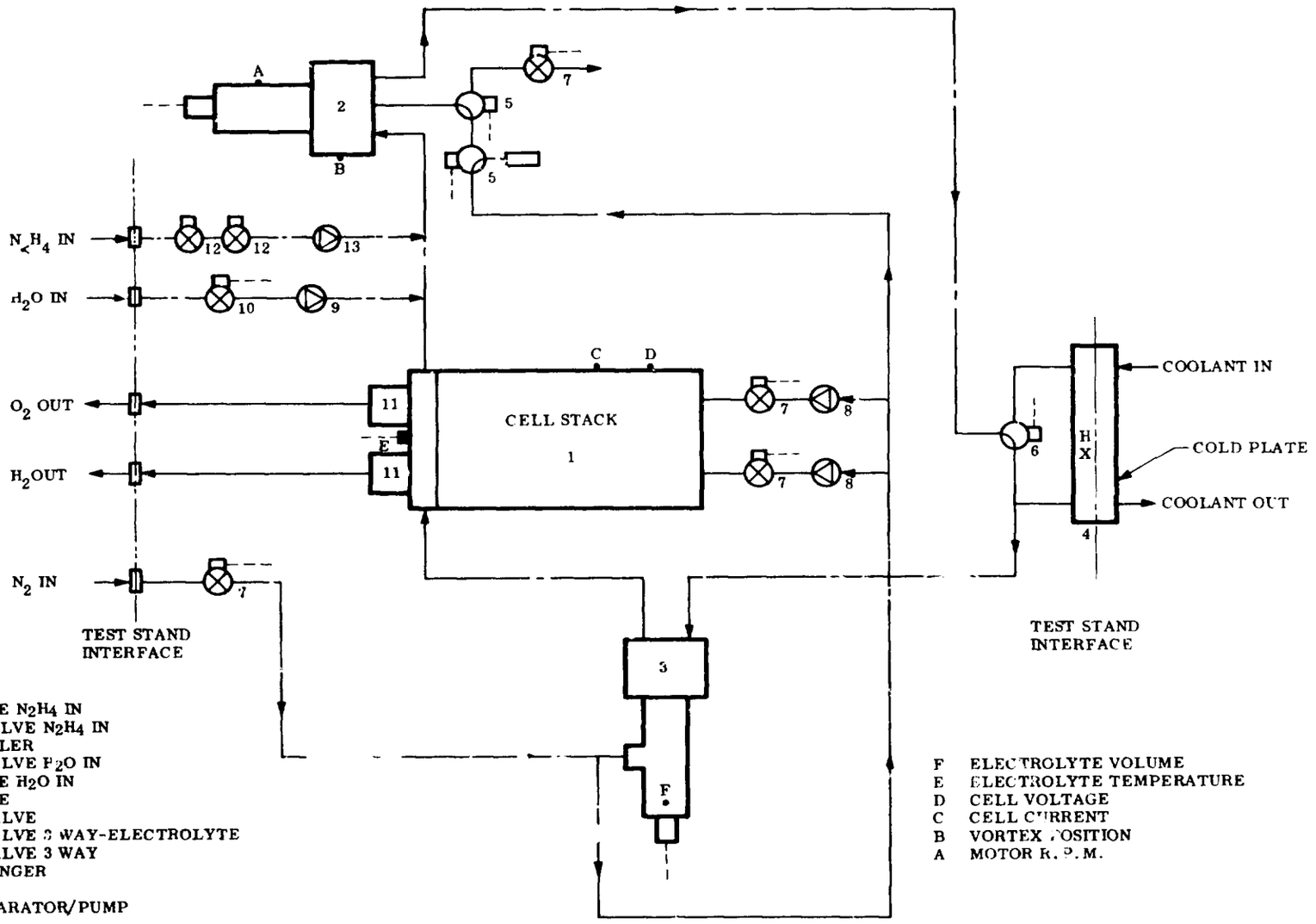

FIGURE 2 EARLY PROTOTYPE SCHEMATIC

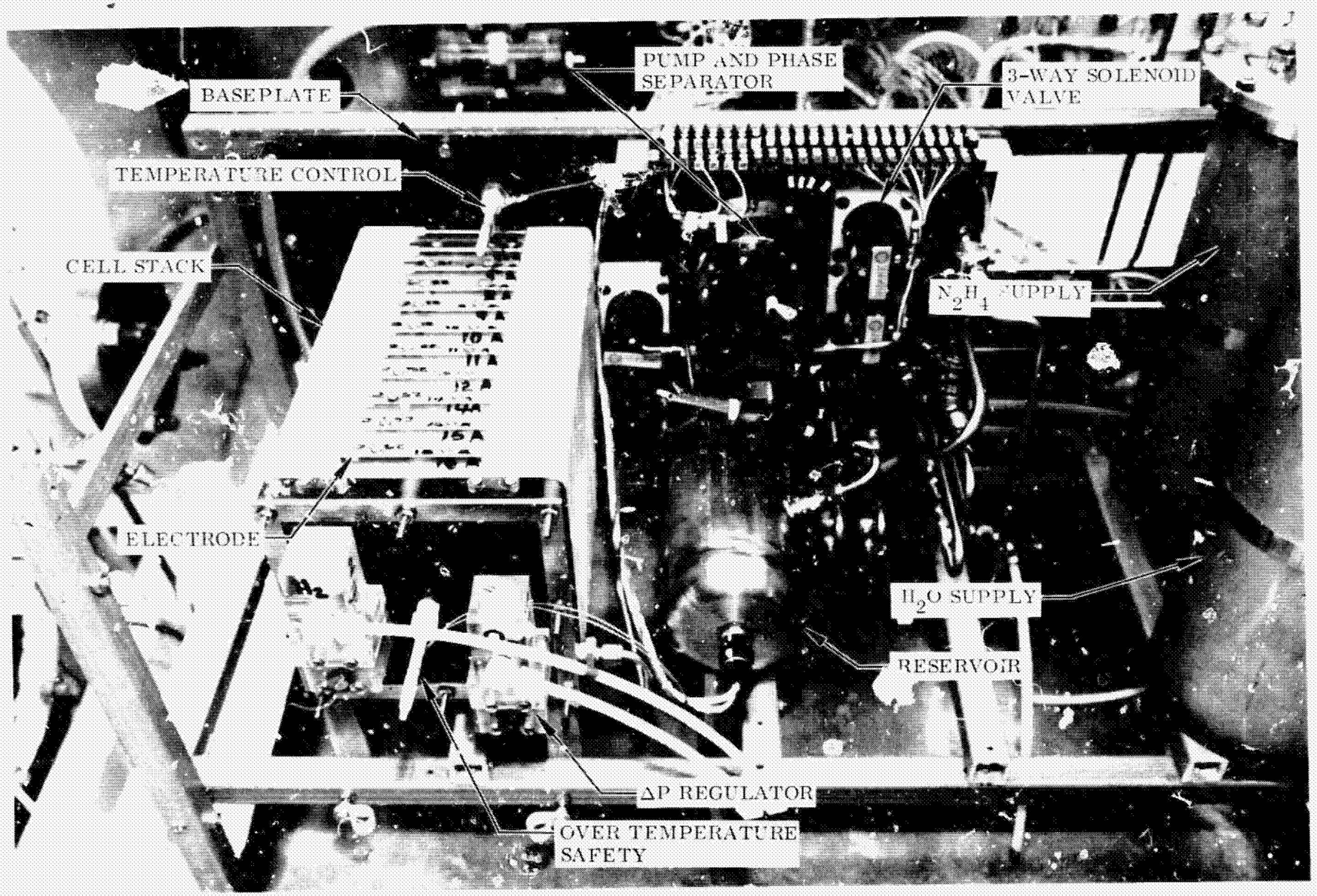

FIGURE 3 PROTOTYPE ASSEMBLY TEST SET UP FRONT VIEW

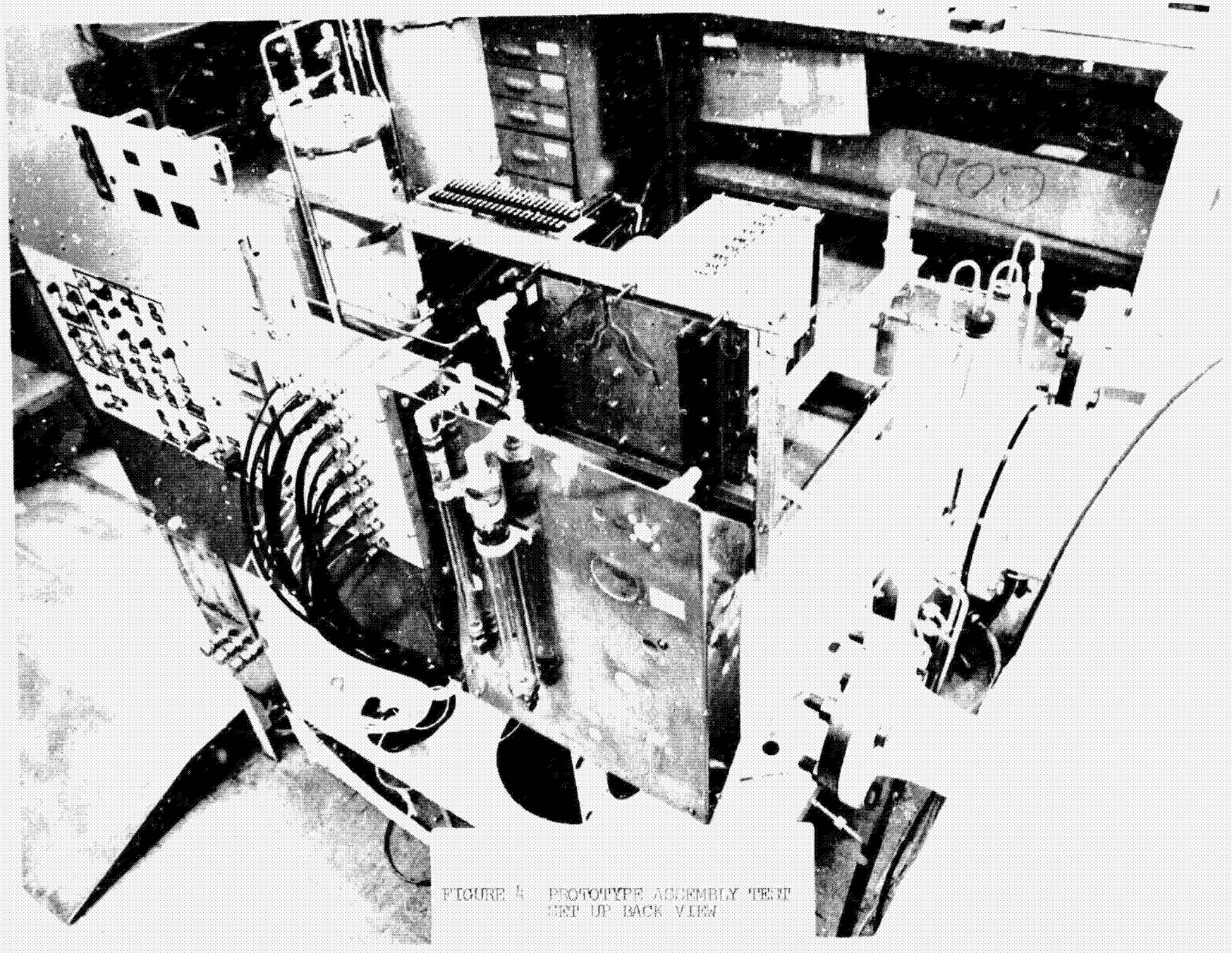

FIGURE 4 PROTOTYPE ASSEMBLY TEST SET UP BACK VIEW

2.1.4 Controls and Safety Circuits

Laboratory controls are used to operate the prototype assembly. A front view of the control panel is shown in Figure 3. The system requires manual startup, but normal operation is automatic with water feed, temperature control, and electrolysis current controlled internally. An electronic timer with adjustable duty cycles is used to simulate the cabin total pressure signal that determines whether the cell stack is to operate in high or low current. A manual switch is provided to simulate cabin oxygen partial pressure signals which determine the demand for hydrazine feed.

The safety sensors which are integral with the module components were integrated with the test bed safety shutdown circuits. In the event of a safety shutdown signal, all power to the components automatically is removed and the nitrogen purge of the cell stack comes on. The operational safety shutdown circuits include:

over temperature,
high or low electrolyte volume,
pump motor rpm (but not utilized for this program).

The additional safety circuits which automatically turn off the hydrazine feed, but do not shutdown the system are:

high electrolyte volume during hydrazine feed mode,
low PO_2: two levels depending on current mode.

Monitoring instrumentation includes an analog readout of cell stack current and anodic effluent PO_2 on strip chart recorders, and a multi-channel digital data logger with paper tape printout which reads and prints all individual cell voltages and total stack voltage once-an-hour on an around-the-clock basis.

2.2 COMPONENT FABRICATION AND TESTING

2.2.1 Pump/Bubble Separator (PBS)

Mechanical Design Requirements

The pump/bubble separator was designed and fabricated by Fluid Dynamics Corporation to LMSC specifications. The mechanical functions of the device are to circulate the electrolyte and to remove from the electrolyte loop gas bubbles which are introduced as dissolved gas in the feed water. The specifications called for all ports (both gas and liquid) to be located on the mounting surface with o-ring seals to interface with the baseplate manifolding ports. Materials of construction in contact with the electrolyte were limited to polysulfone and 316 stainless steel. Performance requirements were a minimum pressure with blocked flow of 41.4 kN/M^2 (6 psig) and a gas removal capability of at least 10 cc/min (0.61 in^3/MIN).

The unit as supplied by the vendor is shown in Figure 5. The clear plastic part at the opposite end from the motor is a test fixture to allow bench testing of the device independent of the baseplate.

Electronic Control Requirements

Two automatic control devices were required for the pump/bubble separator. First, a sensor of the gas vortex diameter was required to prevent discharge of liquid through the gas vent. Secondly, an rpm sensor was specified so that the total system would be capable of automatically responding to a failure of the pump/bubble separator motor. The controls delivered with the unit are shown in Figure 6.

Design Features

The as-built pump/bubble separator is a magnetically-coupled centrifugal pumping device with a single impeller which pumps the liquid and creates a sufficient force field to cause gas bubbles to collect in the center as a cylindrical core. A central non-rotating shaft contains a 10-mil I.D. teflon tube through which the gas is vented. The gas, as it is trapped in the unit grows in a cylindrical shape as shown in the sketch in Figure 7. As the

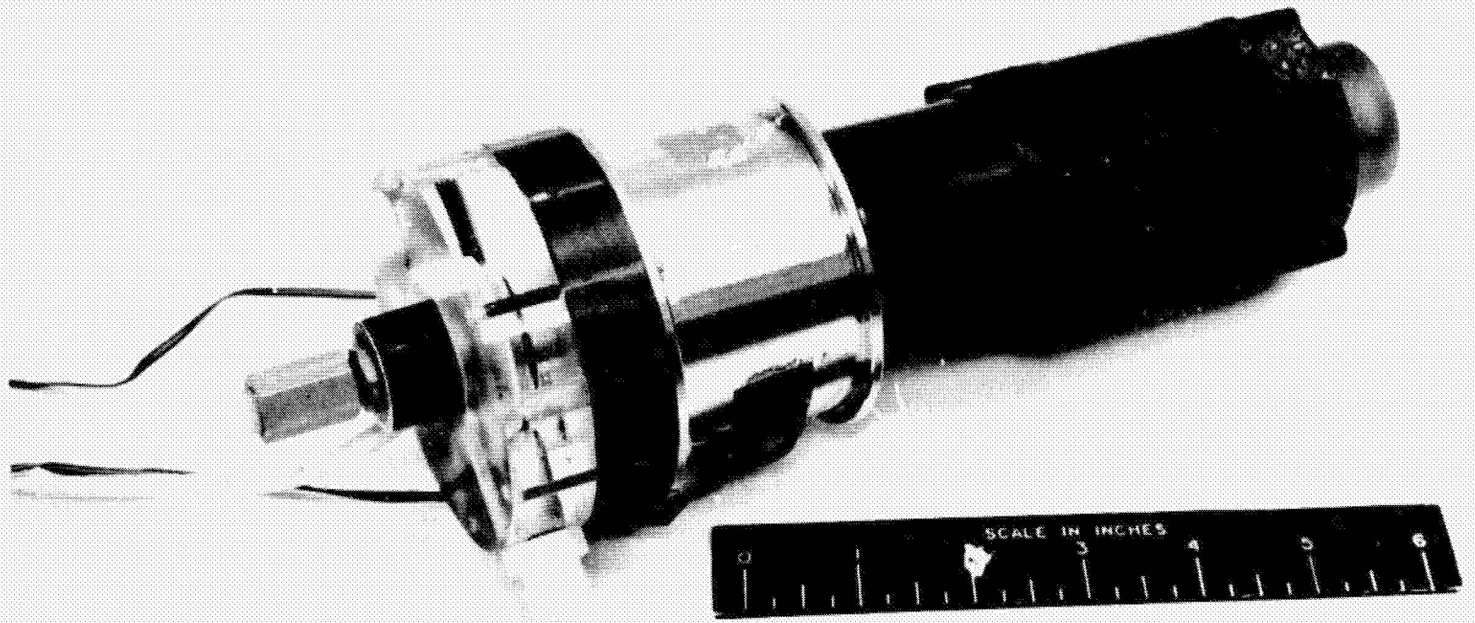

FIGURE 5 PUMP/BUBBLE SEPARATOR

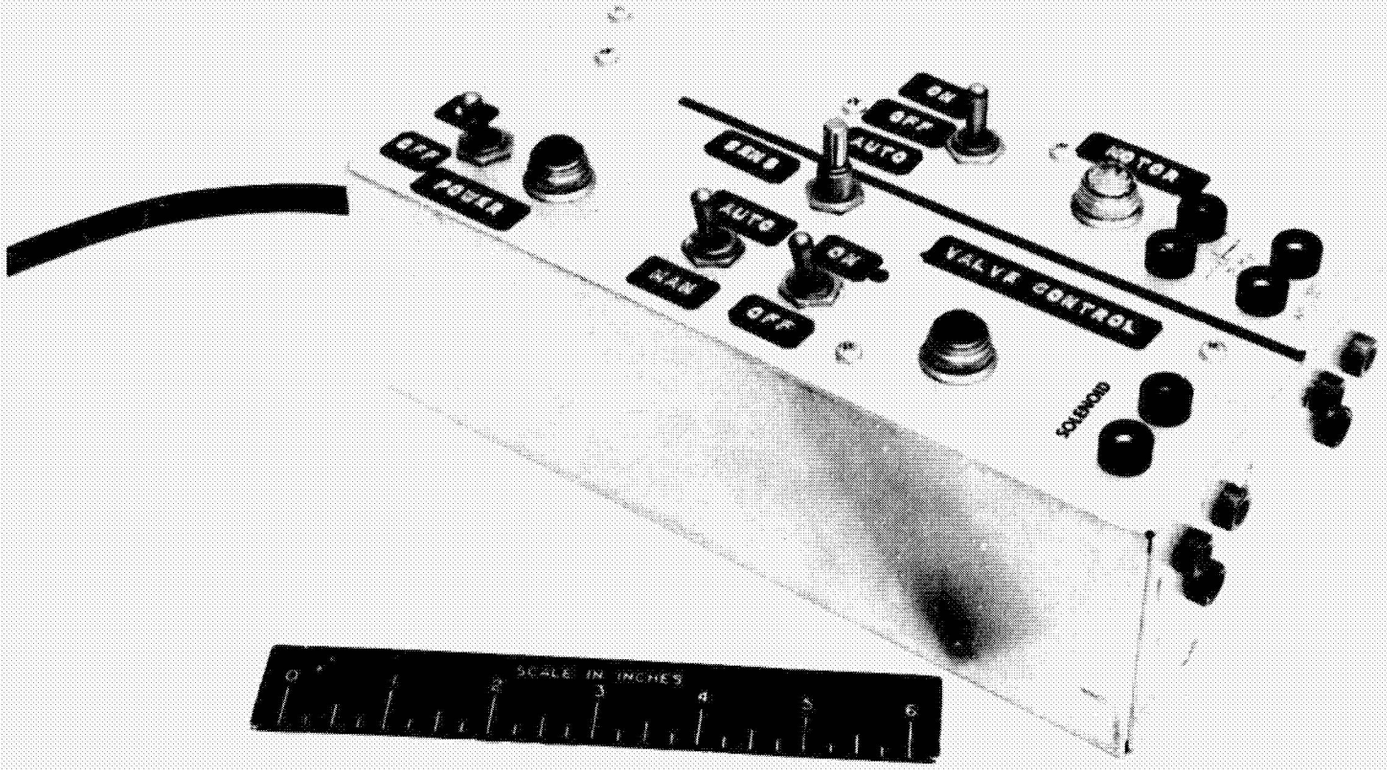

FIGURE 6 PUMP/BUBBLE SEPARATOR CONTROL

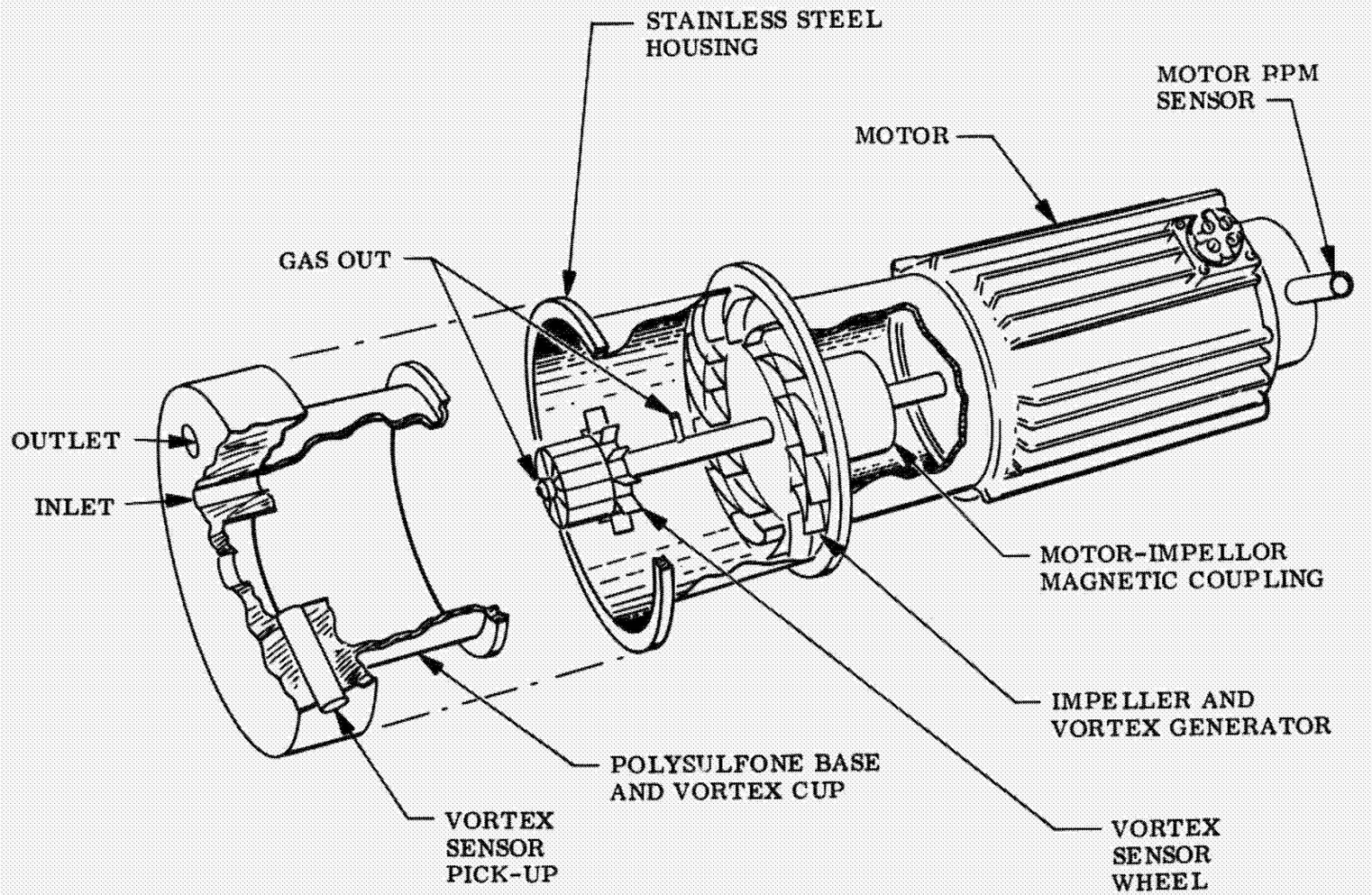

FIGURE 7 PUMP/BUBBLE SEPARATOR
FUNCTIONAL DIAGRAM

diameter of this gas core increases, a free-floating impeller slows its rotation, and an rpm sensor triggers a solenoid valve to discharge gas. As the gas core decreases in size and the inside diameter of the liquid annulus decreases the sensing impeller picks up speed and causes the rpm sensor to close the valve.

The motor rpm sensor receives its signal from a blade mounted on the shaft of the motor. When the motor stops turning the rpm sensor provides a signal which is used to actuate automatic shutdown of the entire system.

Performance Evaluation

The pump/bubble separator was bench tested in the laboratory configuration shown in Figure 8. Of interest in the bench tests were (1) maximum pressure developed by the pump under no-flow condition, (2) head-rise (ΔP) as a function of liquid flow rate, (3) the effect of gas introduction rate on performance, and (4) the effect of total system pressure. An additional requirement was to demonstrate insensitivity of the device to attitude orientation so as to prove as far as possible its zero-gravity capability.

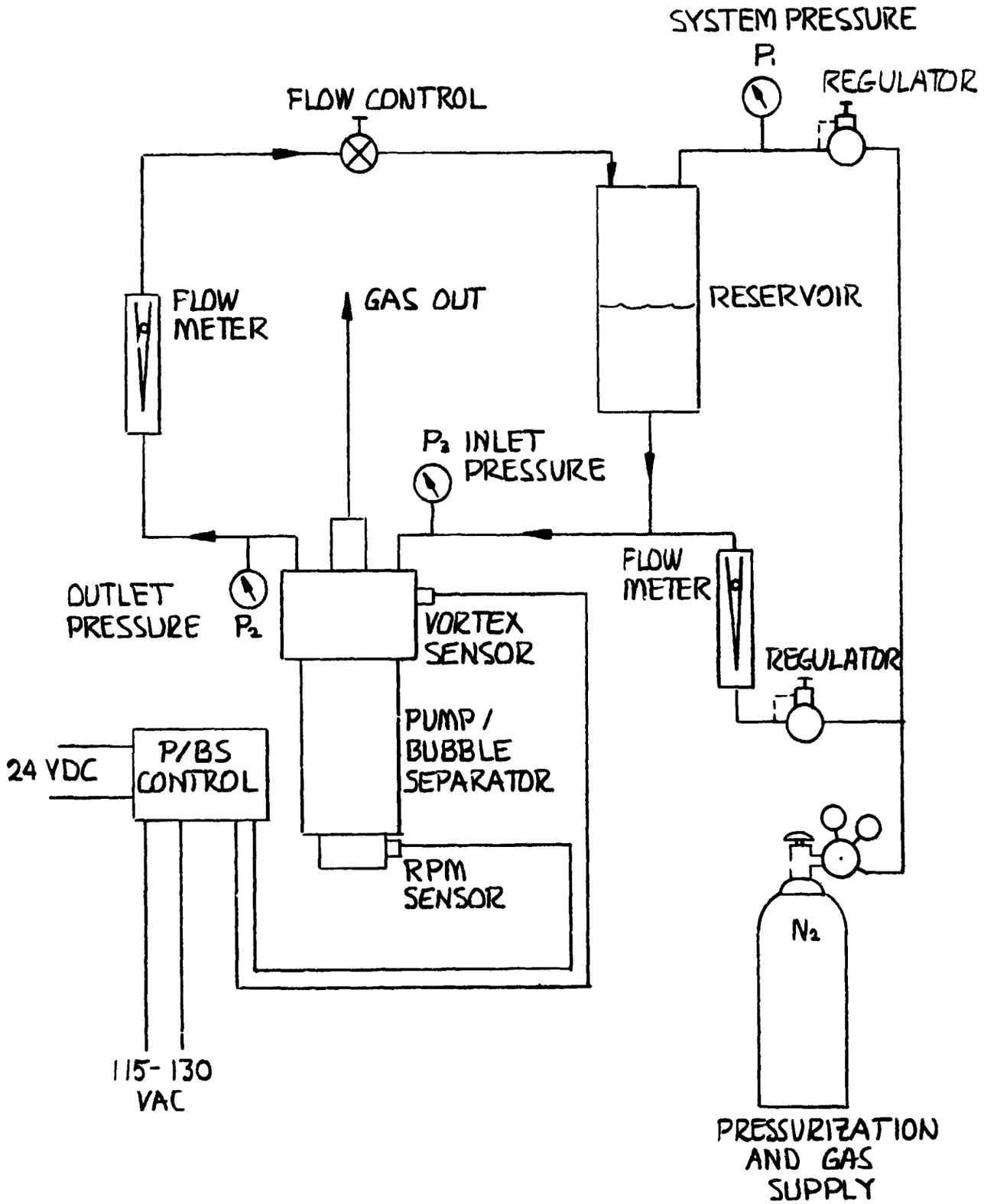

FIGURE 8 PUMP/BUBBLE SEPARATOR TEST SETUP

The test results are summarized in Figure 9. As shown here, the design performance requirements in all cases were met or exceeded. For example, blocked flow pressure averaged 46.19 kN/M^2 (6.7 PSIG) compared to the required 41.4 kN/M^2 (6.0 PSIG) minimum. Head rise was only minimally affected by flow rate over a wide range of system pressures 32.4 - 73.8 kN/M^2 (4.1 - 10.7 PSIG). Gas introduction rates over a range from 1.3 to 13.6 cc/min (0.08 = 0.83 in^3/min) showed no detrimental effect on performance. Insensitivity to orientation is shown by a negligible effect of attitude of the device on its performance characteristics.

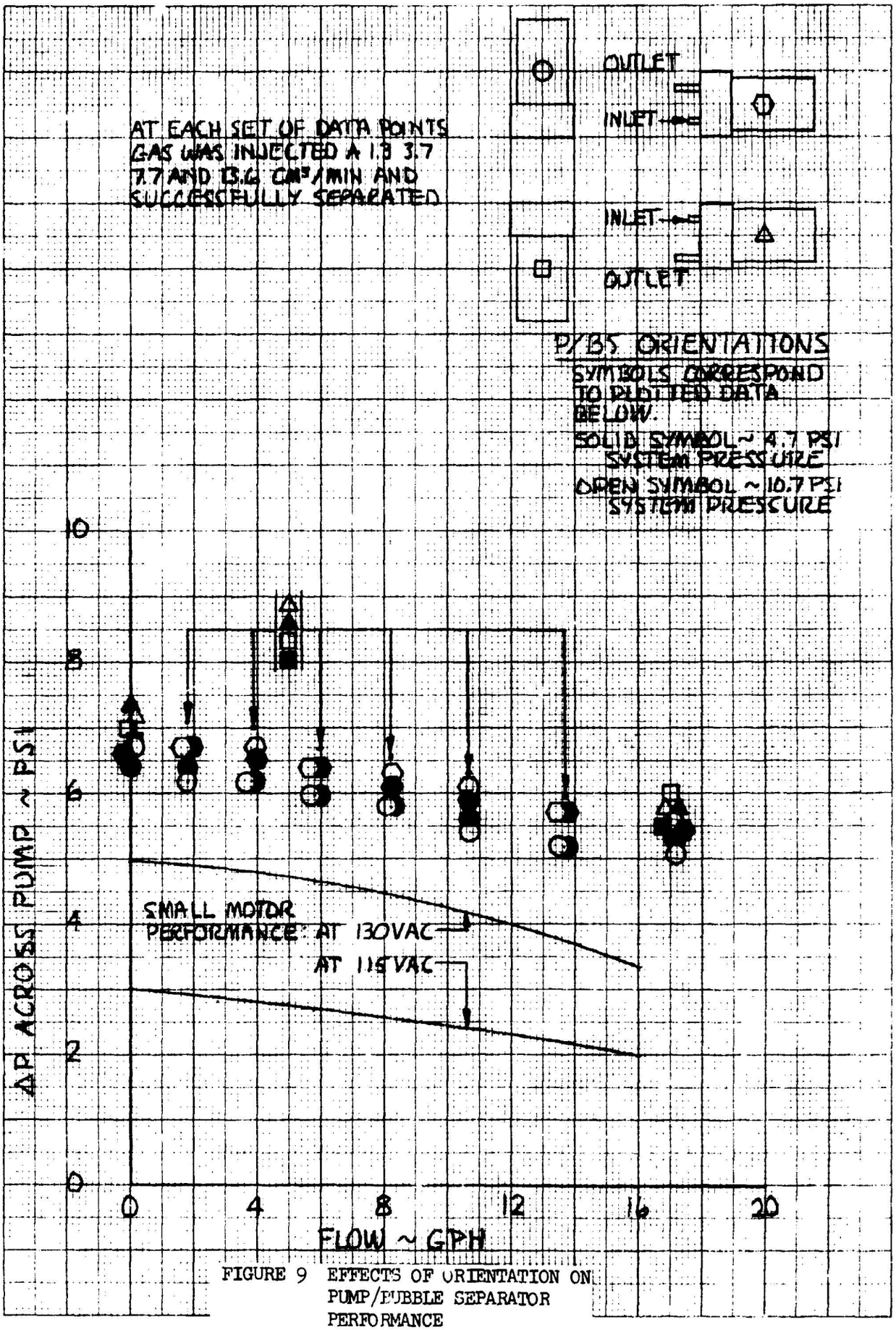

FIGURE 9 EFFECTS OF ORIENTATION ON PUMP/BUBBLE SEPARATOR PERFORMANCE

2.2 2 Reservoir

Mechanical Design Requirements

The reservoir provides, in one component, two basic functions: (1) it controls the system pressure and (2) it supplies the high/low electrolyte safety shutdown signals, the hydrazine and water feed lockout signals and the water feed signals. The system pressure control is designed to satisfy the following simple equation: electrolyte pressure + spring pressure = gas pressure.

The electrolyte/gas interface is provided by a piston utilizing a rolling diaphram (Bellofram) seal. The rolling diaphram is used to achieve minimum sticking and friction. This is an essential feature since the piston will translate at very low rates (on the order of 0.036 cm/min (0.014 in/min)) and must do so smoothly. The Bellofram is to be made of ethylene propylene reinforced with woven nylon so as to be compatible with KOH and N_2H_4. The guide bushings for the piston and the surface finish of the piston support also have a large effect on smoothness. Therefore the brushings are to be of the split ring type, made of glass reinforced teflon. Unfilled teflon may not be used since it has very low resistance to cold flow under load. The surface finish of the piston support is to be at least 8 microinches and buffed.

A single, 17-4 PH stainless steel spring is to be used. It should have a spring rate of 3.53 N/cm (2 lbs./in), provide a nominal load of 56±2.2N (12.7±0.5 lbs) at 4.19 cm (1.65 in) length and provide maximum load at solid height. It is further important that the ends be squared and ground.

Torque generated by the compression or release of the spring is to be isolated from the Bellofram by means of a ball radial/thrust bearing. Torque applied to a Bellofram will cause it to roll improperly and greatly increase the force required to move the piston. The upper spring seat is to be incorporated in the bearing support and must be adjustable to allow minor adjustments to spring load.

Since the nominal electrolyte working pressure is to be 103.4 kN/M^3 (15 psi), the gas side of the reservoir will "see" approximately 117.2kN/M (17 psi). The design pressure should be 1.5 times this or 172.4 kN/M^2 (25 psi). The complete unit will be leak checked to 258.6 kN/M^2 (37.5 psi).

The position transducer is to be a differential transformer type and will be immersed in gaseous nitrogen at 117.2 kN/M^2 (17 psi). All metal parts are 316 stainless steel except the electrical connector/feed through. The connector is a bulkhead type and self sealing. All seals and o-rings are ethylene propylene. Maximum electrolyte volume within the reservoir is 274 cc (16.62 $in.^3$), minimum volume is 71.28 cc (4.35 $in.^3$).

Fabrication and Assembly

The reservoir was fabricated and assembled per drawings BEH 20020 through BEH 20031. Figure 10 shows the completed reservoir while Figure 11 shows it with the pressure cover removed. The "window" in the transducer support can is to facilitate spring adjustment without further disassembly of the unit.

The fixed portion of the piston position transducer is supported by a moveable clamp. This allows the transducer to be positioned properly in relation to the moveable core which is attached to the reservoir piston. Necessary transducer adjustments are made during assembly and need not be changed thereafter.

FIGURE 10 ASSEMBLED RESERVOIR

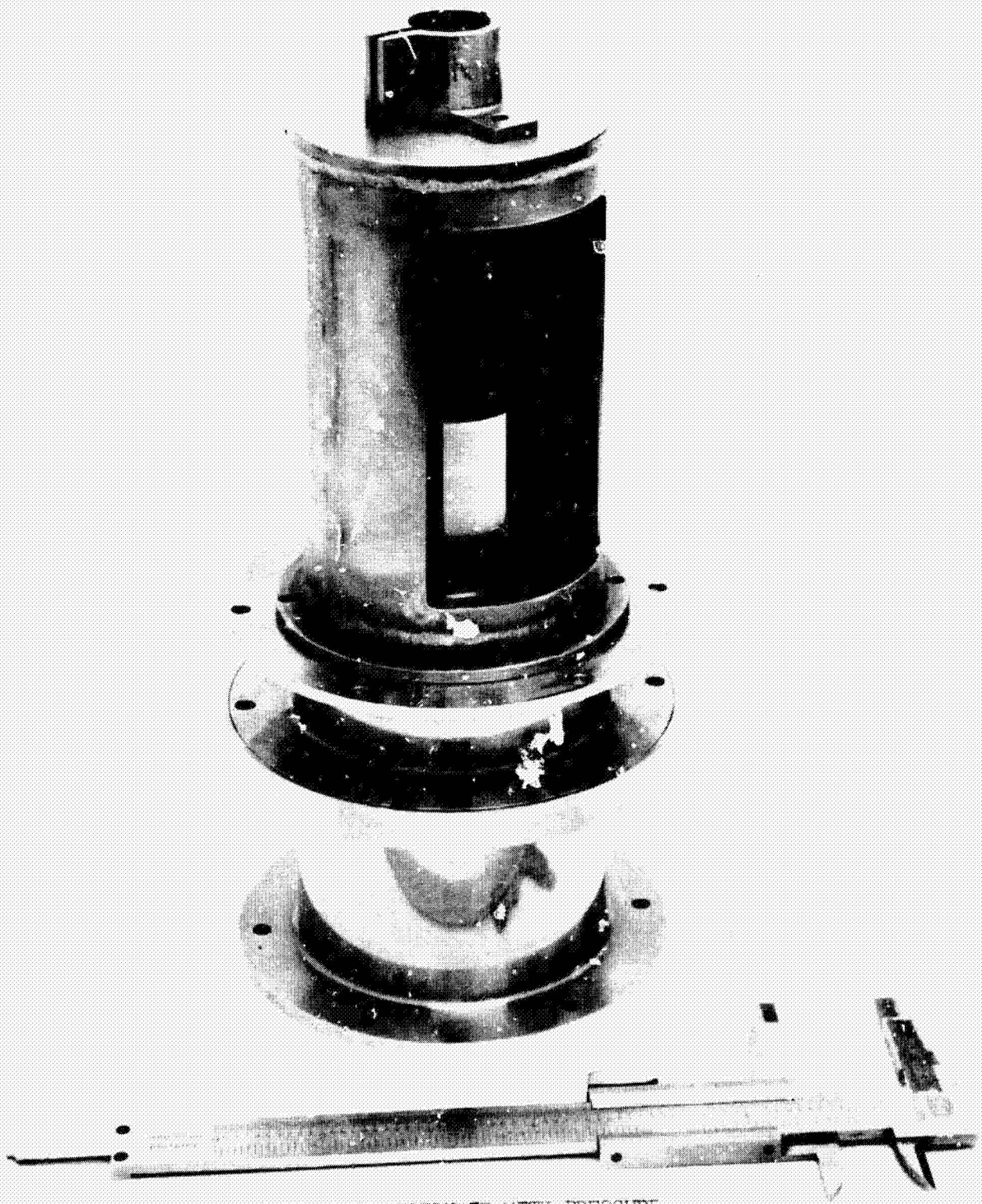

FIGURE 11 RESERVOIR WITH PRESSURE
COVER REMOVED

No problems were encountered during the fabrication of any of the reservoir parts. During assembly, however, a minor problem did rise in that no sealant or locking agent was applied to the three screws that hold the piston cap, Bellofram and piston together. During pressure testing a leak developed across the Bellofram via these screws. The unit was disassembled and reassembled using epoxy (Epon 828) to lock and seal the screws; thereafter the unit did not leak.

The assembly or disassembly of the reservoir requires a definite sequence which is shown in Table 1. It is particularly important that the sequence be followed in the area of the piston/Bellofram/piston support and transducer moveable core. Care must be taken with respect to the transducer core as it is easily bent. A special tool is required to assemble the piston support to the piston cap. It is a hex drive screw driver which measures 0.24 cm (3/32 in.) across the flats and has a 15.24 cm (6 in.) reach.

Table 1

Reservoir Assembly Sequence

To be used in conjunction
with Drawing No. BEH 20020 -
See also Figure 12, and appendix

	Assemble Item(s)	To	Item(s)	Note
Sub-assembly I	18(B-11 core only) and 24		12	B-11 core may be removed from Item 18.
	15		12	Item 15 is not retained on Item 12 except by spring pressure (later).
	6		15	Item 6 is not retained on Item 15 except by spring pressure (later).
	8 and 7		6	Item 8 goes on first. Position both rings at mid-point of threads and lock.
Sub-assembly II	14 (2 places)		3	Care must be exercised not to break plastic bushings (Item 14).
	Subassembly I		Subassembly II	Item 12 slides through Items 14 (2 ea.) - use care. Insure that item 1 is seated in Item 7 and 3, compress spring and hold.
	10 and 20 (3 ea.)		12	Put small amount of epoxy (Epon 828) on each Item 20 before assembly. Release spring slowly until Item 10 bottoms against Item 3
	1, 9 and 19 (3 ea.)		10	Insure that Item 1 is oriented as shown. Put small amount of Epoxy (Epon [illegible]) on each Item 19 before assembly.
	2, 22 and 23		3	Use care when sliding Item 2 over Item 1
	4 and 19 (6 ea.)		3	Insure that Item 4 is centered.

Table 1 (continued)

Assemble Item(s)	To Item(s)	Note
11, 21, 23, 25 and 18	4	Item 16 already wired to Item 18. Center Item 18 over Item 18 (B-11 core).
16	5	
17	5	Rubber cement may be used to retain Item 17.
5, 21 and 23	3	Insure that wires of Items 16 and 18 are on side of Item 4 opposite "window".

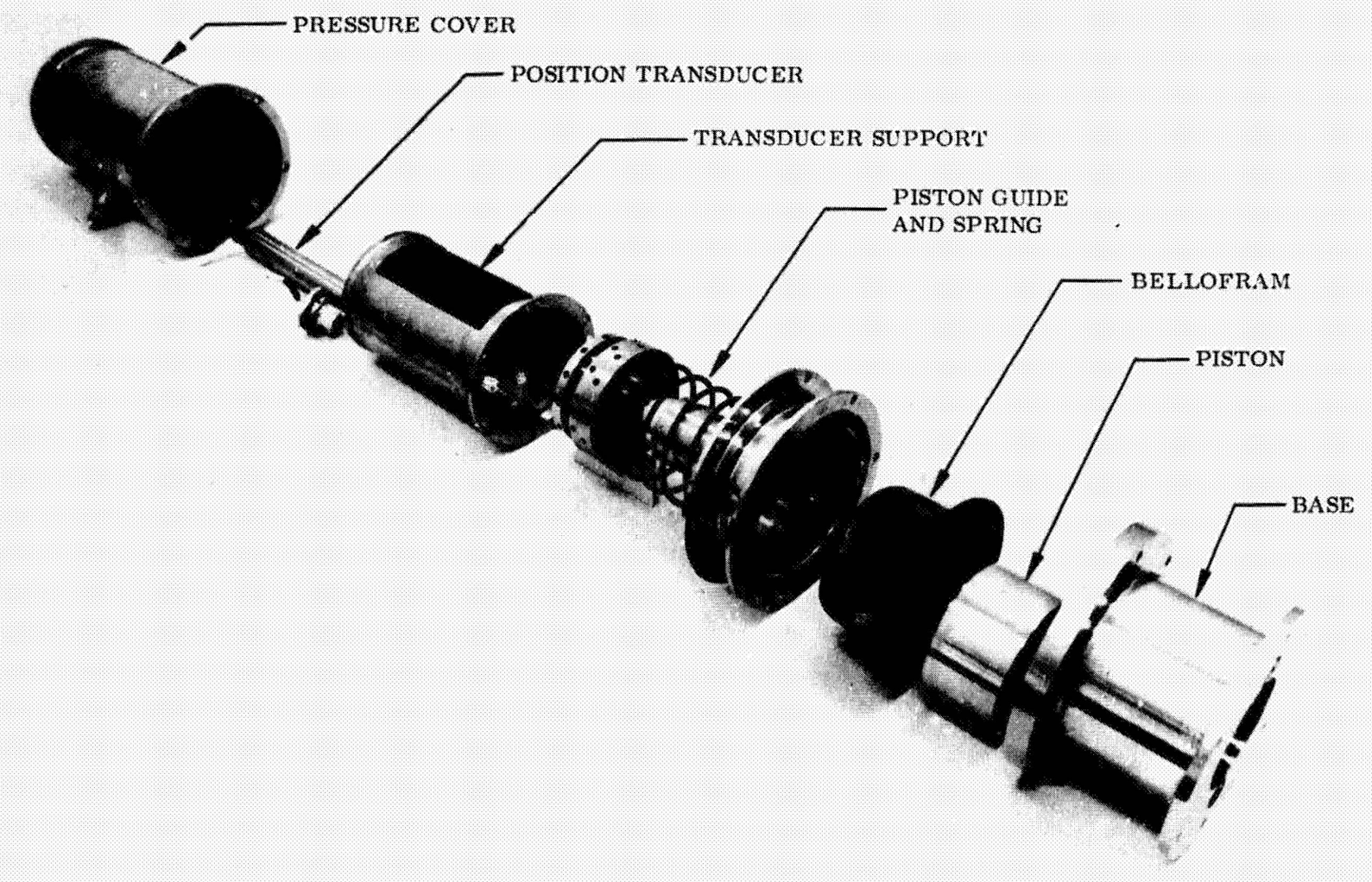

FIGURE 12 DISASSEMBLED RESERVOIR

Reservoir Control

The control unit of the reservoir (Figure 13) provides transducer excitation depending on piston position, and conditions the transducer output to be used for the control of various safety shutdown and operational functions. A D.C. voltage is sent to the control unit which varies as the reservoir piston moves from minimum volume position to maximum volume position. The piston position is a measure of the electrolyte volume. Voltage output vs piston position is shown in Figure 14. Water and hydrazine feed control are functions primarily of cabin pO_2, and anode pO_2, but certain reservoir volume "set points" serve to enable or inhibit these signals. The "set points" are identified in Figure 15. The high and low limits are safety shut down points. If electrolyte volume exceeds the high or falls below the low limit, the reservoir control calls for the shut down of the entire module. If the electrolyte volume exceeds the N_2H_4 feed off point any hydrazine feed commands, whether manual or automatic, are blocked out. Hydrazine may again be fed once the electrolyte volume falls below this point. Water consumed in the electrolysis process must be periodically replaced. This is accomplished by a pressurized water feed system which is controlled by the H_2O feed on and off set points. As water is consumed the electrolyte volume drops below the "H_2O feed on" point and the controller calls for a water feed. Feed continues until the electrolyte volume reaches the "H_2O feed off" point and the controller signals "feed off".

Two additional controls and two additional indicators are incorporated in the reservoir control. See Figure 16. Both controls are timing circuits. The first limits the time a given water feed may remain on and precludes the feeding of a large leak. This timer may be set (by a digiswitch) for any time 0 and 99 seconds. The second timer imposes a finite time between water feeds. This keeps the system from feeding a small leak. It too is set with a digiswitch and will provide times between 0 and 99 minutes. Digital readouts are included and show at a glance whether or not a water feed can be accomplished.

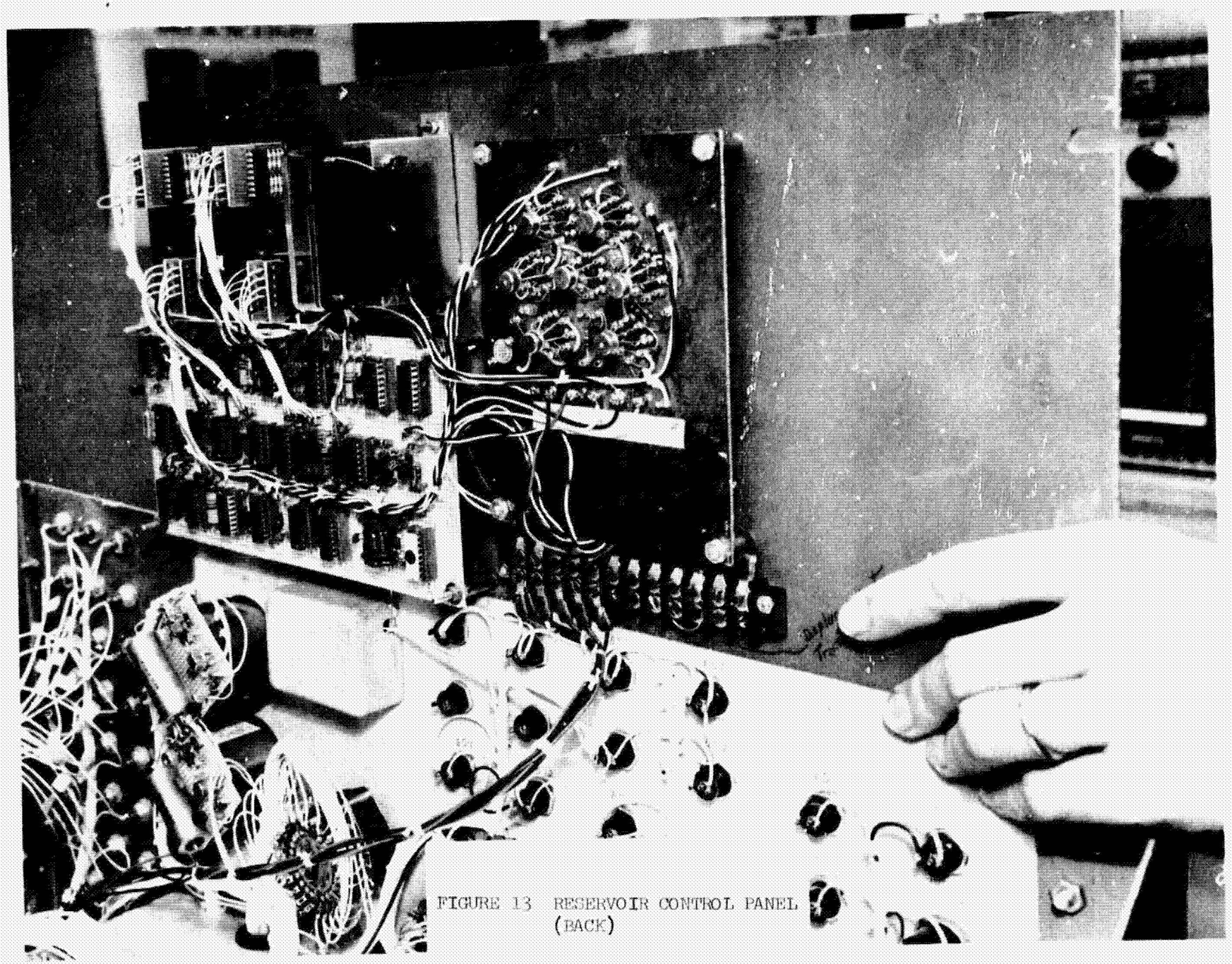

FIGURE 13 RESERVOIR CONTROL PANEL (BACK)

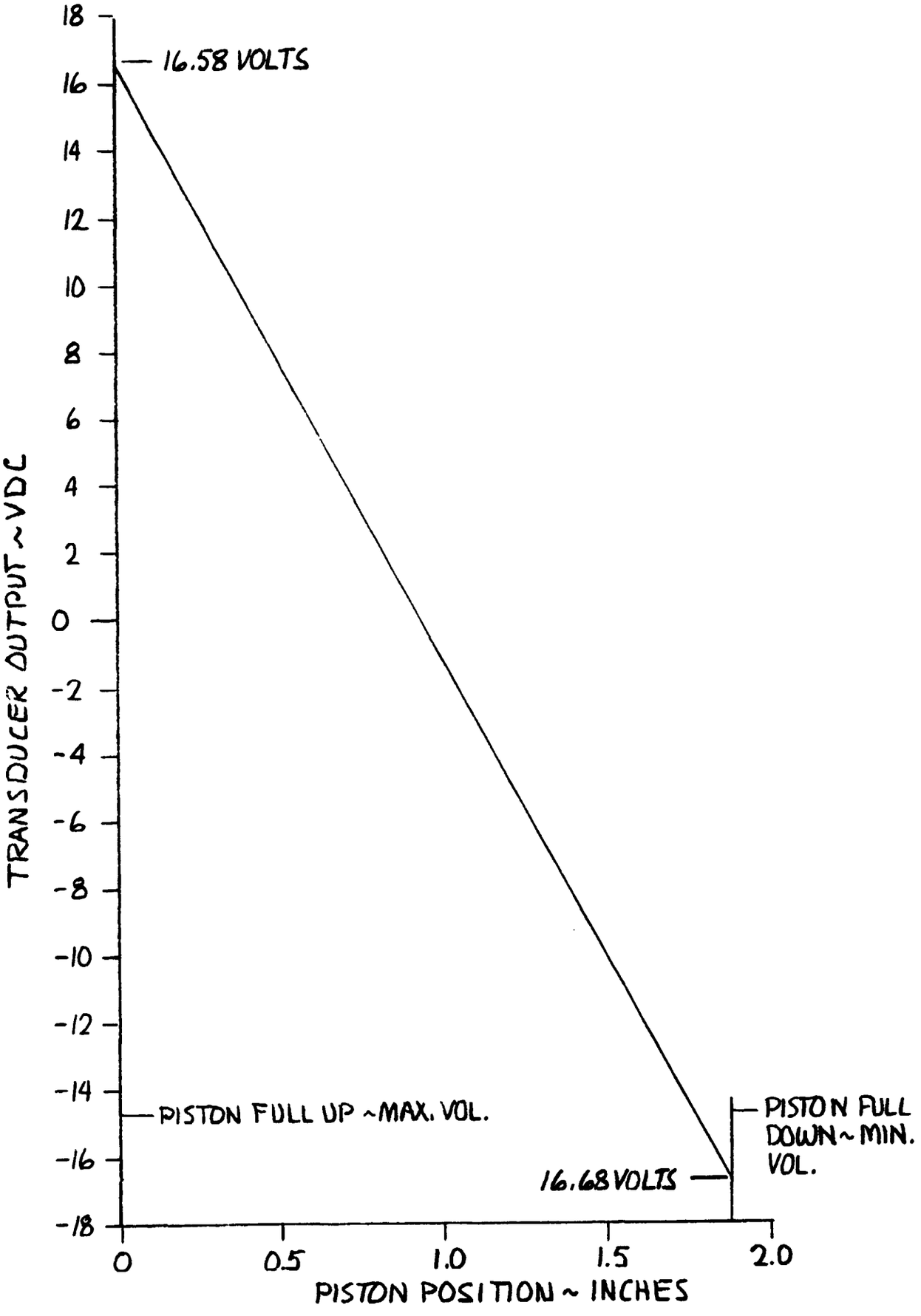

FIGURE 14 RESERVOIR PISTON POSITION VS. POSITION TRANSDUCER OUTPUT

NOMINAL RESERVOIR CONTROL SET POINTS

(Including Nominal Position, Volume)

	Transducer Output Volts	Position cm(in)	Volume cc(in^3)
Upper Mechanical Limit	+16.58		
		0.32 (0.125)	11.6 (0.71)
High Limit	+14.4		
		0.71 (0.28)	26 (1.59)
N_2H_4 Feed Off	+ 9.4		
		2.01 (0.79)	76.8 (4.69)
H_2O Feed Off	- 4.4		
		0.71 (0.28)	26 (1.59)
H_2O Feed On	- 9.4		
		0.71 (0.28)	26 (1.59)
Low Limit	-14.4		
		0.32 (0.125)	11.6 (0.71)
Lower Mechanical Limit	-16.68		

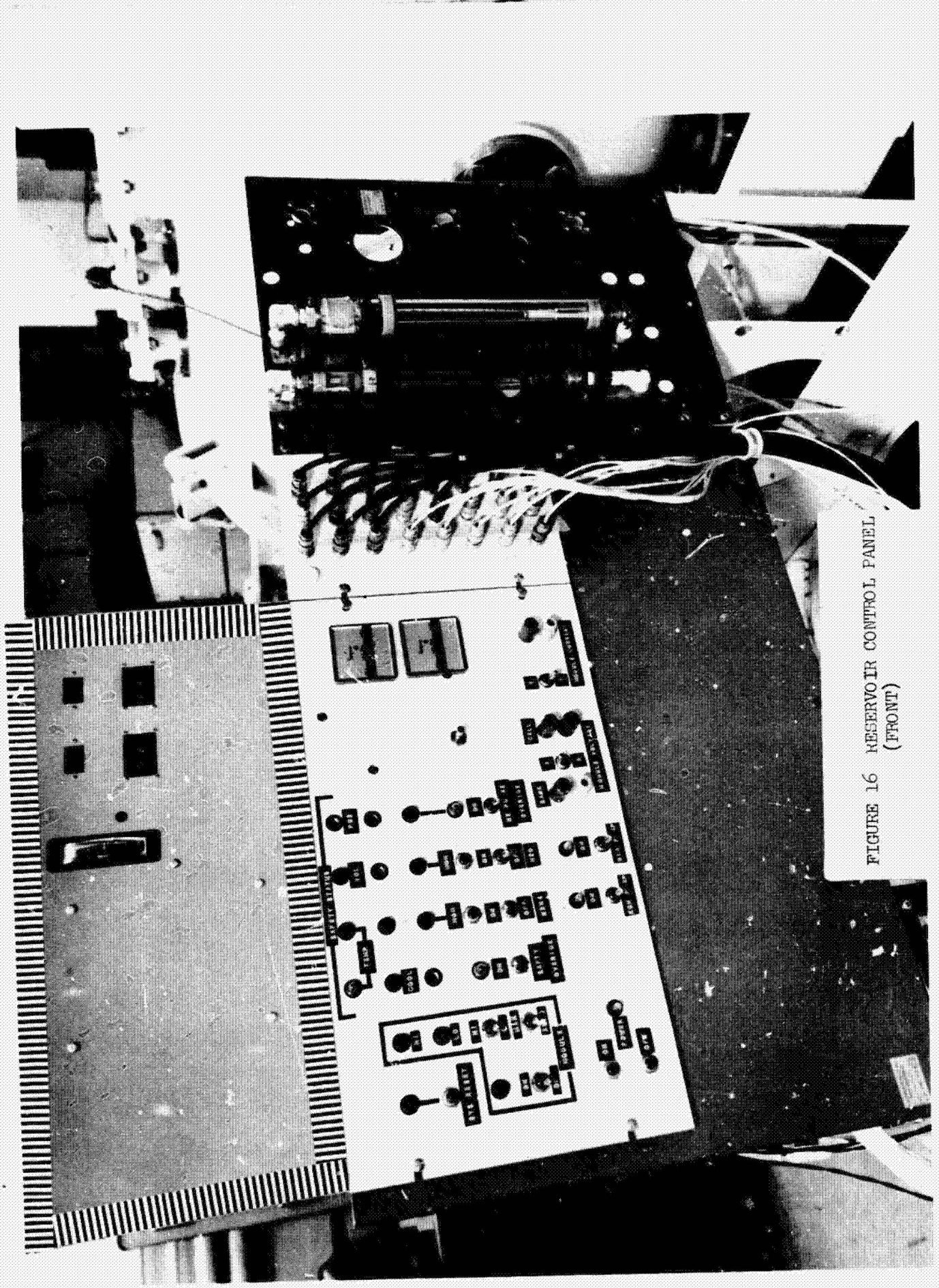

FIGURE 16 RESERVOIR CONTROL PANEL
(FRONT)

Both indicators relate to reservoir piston position. One, an edge meter, shows piston position directly in non dimensional units from -10 (minimum volume) to +10 (maximum volume). The other, which is an indicator light (LED), is off only when reservoir volume is within the water feed band.

Fabrication

Fabrication of the reservoir controller was accomplished without problems. Components used which deserve mention are integrated circuits, light emitting diode digital readouts and indicator and digiswitch time set switches. Bench check out of the unit proved satisfactory.

Testing

Leak Checks

The reservoir was pressure tested for internal and external leaks as follows. A gaseous nitrogen supply was attached to the gas side of the reservoir but with no pressure applied. This allows the spring to drive the piston to its maximum volume position. The reservoir was then inverted and the electrolyte side of the Bellofram filled with water via the inlet, outlet ports. The nitrogen pressure was then slowly raised until the piston started to move, displacing water out of the electrolyte side. Bubbles were observed in the water indicating a leak across the Bellofram. As pointed out under "Fabrication", the leak was found to be across the piston assembly screws and was corrected. The test was repeated verifying that there was no longer an internal leak. The electrolyte volume was again filled with water and the inlet outlet ports sealed. The reservoir was then completely immersed in water and the nitrogen pressure slowly raised to approximately 172 kN/M^2 (25 psi). No bubbles appeared and the test was terminated after one half hour.

Performance Characteristics

In order to test the reservoir for its volume and pressure characteristics and to verify its limits and set points, the test setup shown schematically in Figure 17 and pictured in Figure 18 was made.

With zero pressure on the gas side of the reservoir, the spring moves the piston to its maximum volume position. The pressurized water supply was then allowed to fill the electrolyte side of the reservoir and overflow into the graduated cylinder. The water supply valve and the reservoir outlet valve were closed and the amount of water in the graduated cylinder was noted. Next, 117.2 kN/M^2 (17 psi) gas pressure (regulated) was applied and the test was ready to proceed. Discrete amounts of water were allowed to bleed into the graduated cylinder. Water pressure, gas pressure, transducer output and water volume were read at each point. Figure 19 shows liquid pressure vs output signal, spring and Bellofram hysteresis and effective spring pressure. Total hysteresis averages ± 0.51 kN/M^2 (0.15 in. HG). The average equivalent

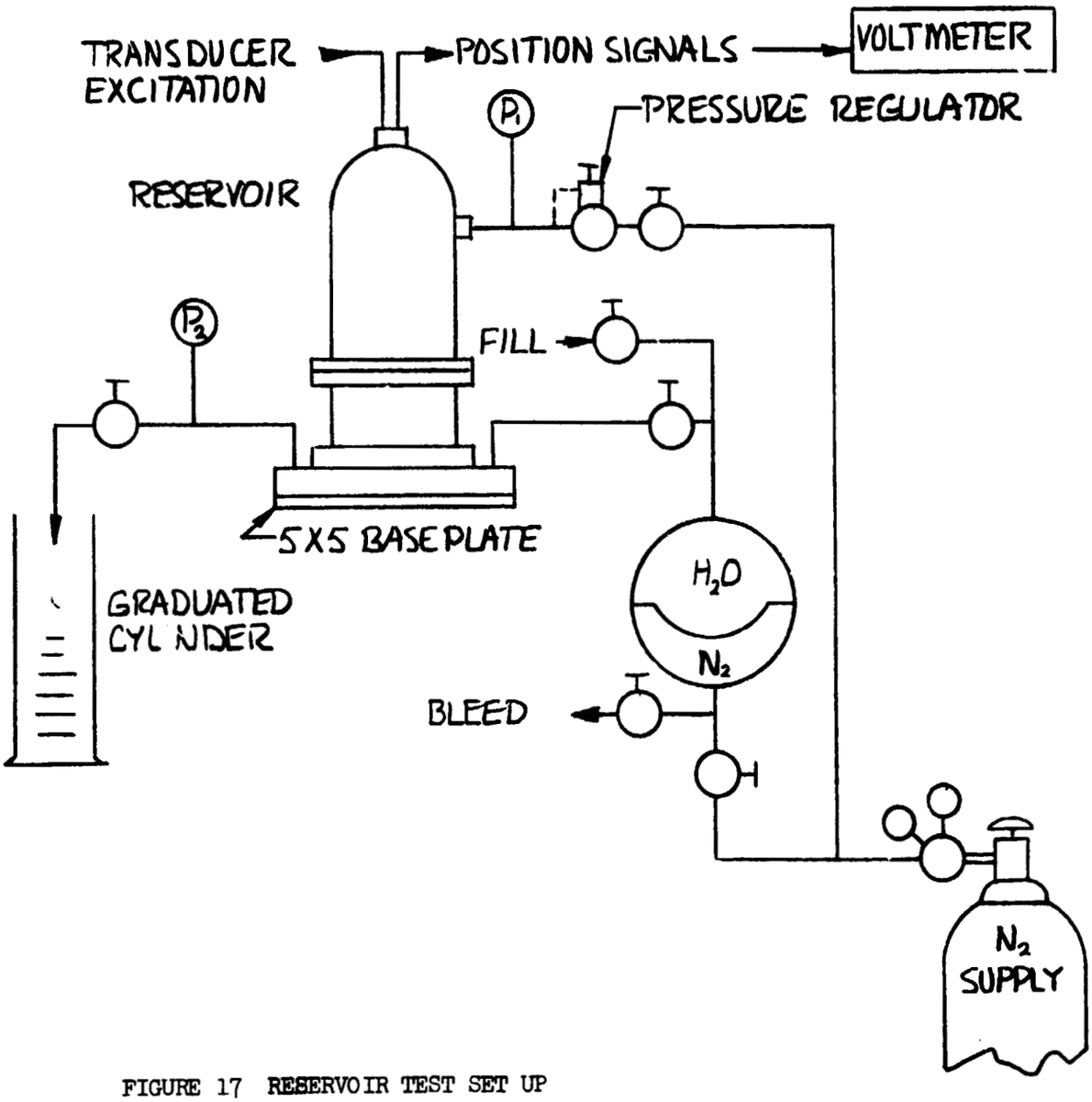

FIGURE 17 RESERVOIR TEST SET UP

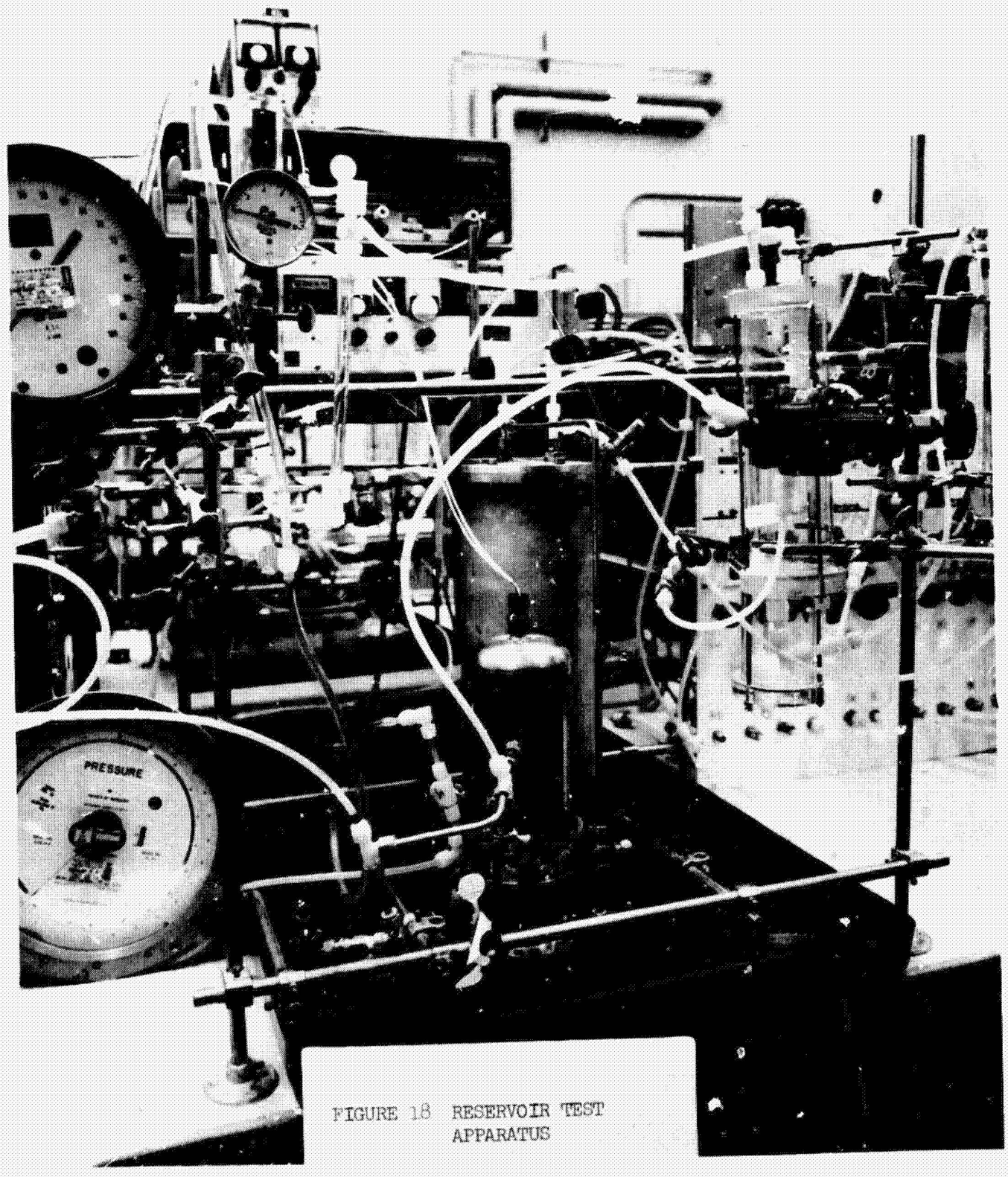

FIGURE 18 RESERVOIR TEST APPARATUS

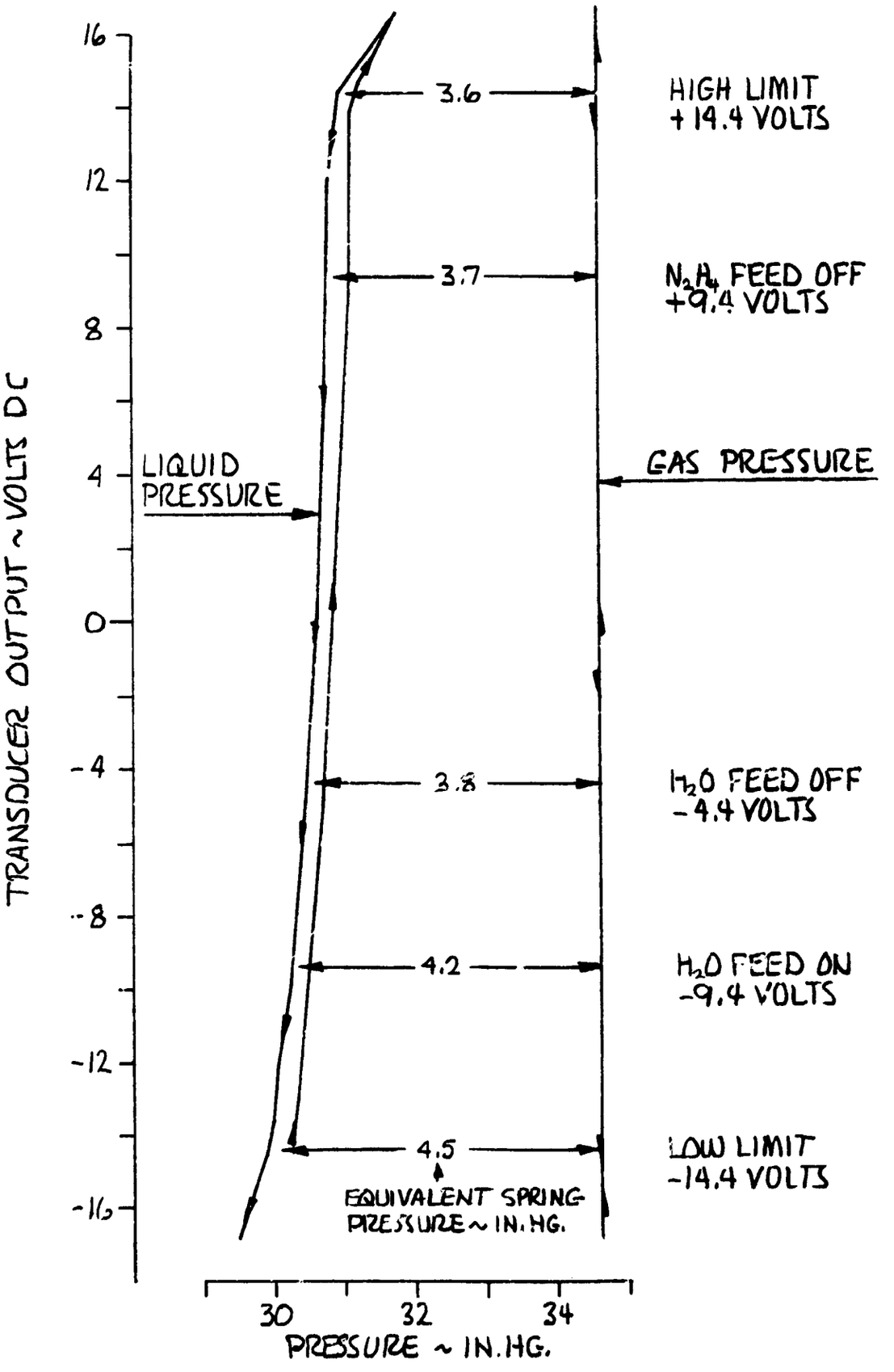

FIGURE 19 RESERVOIR PERFORMANCE CHARACTERISTICS

spring pressure between this high and low limit is 13.51 kN/M^2 (4.0 IN. HG). The spring was designed to provide an average of 13.75 kN/M^2 (4.07 IN. HG). Figure 20 presents the liquid volume vs output signal.

The overall performance of the reservoir and its control is excellent.

2.2.3 Integral Baseplate

Design Requirements

The full scale baseplate must satisfy two basic requirements. First, it is the primary structure of the prototype module. All components (valves, cell stack, reservoir, pump/bubble separator, cover and external gas and fluid lines) are mounted to or pass through the baseplate. Second, the baseplate is to contain, with one exception, all of the electrolyte lines or passages needed to interconnect the various module components (see Figure 21 and 22). The one exception is the external line which connects the reservoir "out" port to the cell stack "in" port. To have contained this line within the baseplate would have required a right angle baseplate, which would have increased considerably the complexity of an already complicated part. Also, the external line provides a desirable location for the module fill valve. The following summarizes the development and design requirements for the baseplate.

1. Baseplate material: Polysulfone was selected as a result of materials investigation done under NAS 9-10405.
2. Gas passages should be enclosed within the baseplate to the extent possible.
3. Baseplate may be laminated. Steps in the development of a lamination technique should as a minimum include:
   a. Screen all feasible candidate adhesives.
   b. Pressure test two or more candidate adhesives with an appropriate test size baseplate.
   c. Test the baseplate mounting and passage design with both the reservoir and pump/separator.
   d. All machined parts should be subjected to an annealing procedure.

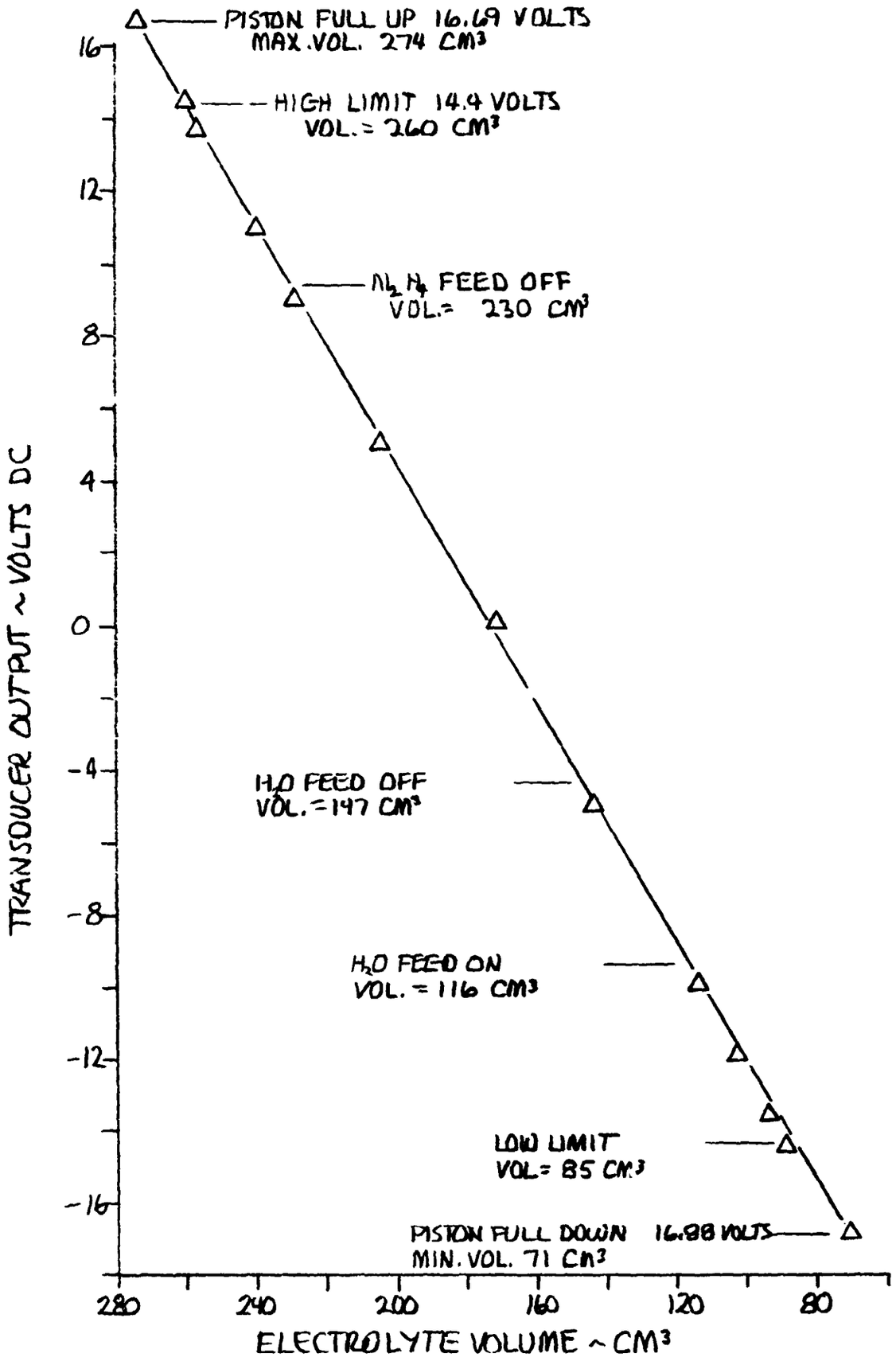

FIGURE 20 RESERVOIR PERFORMANCE CHARACTERISTICS

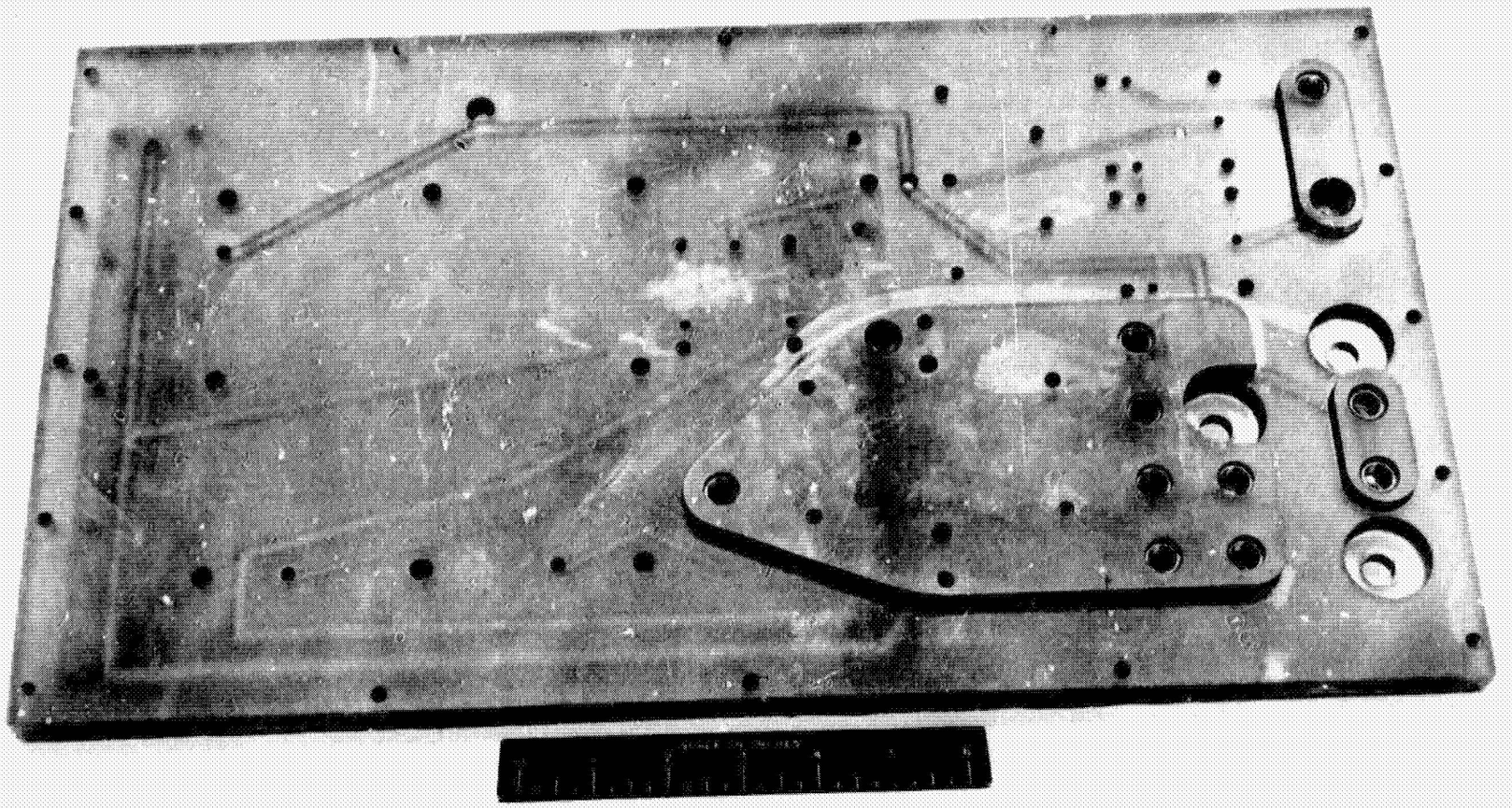

FIGURE 21 ASSEMBLED BASEPLATE
(TOP)

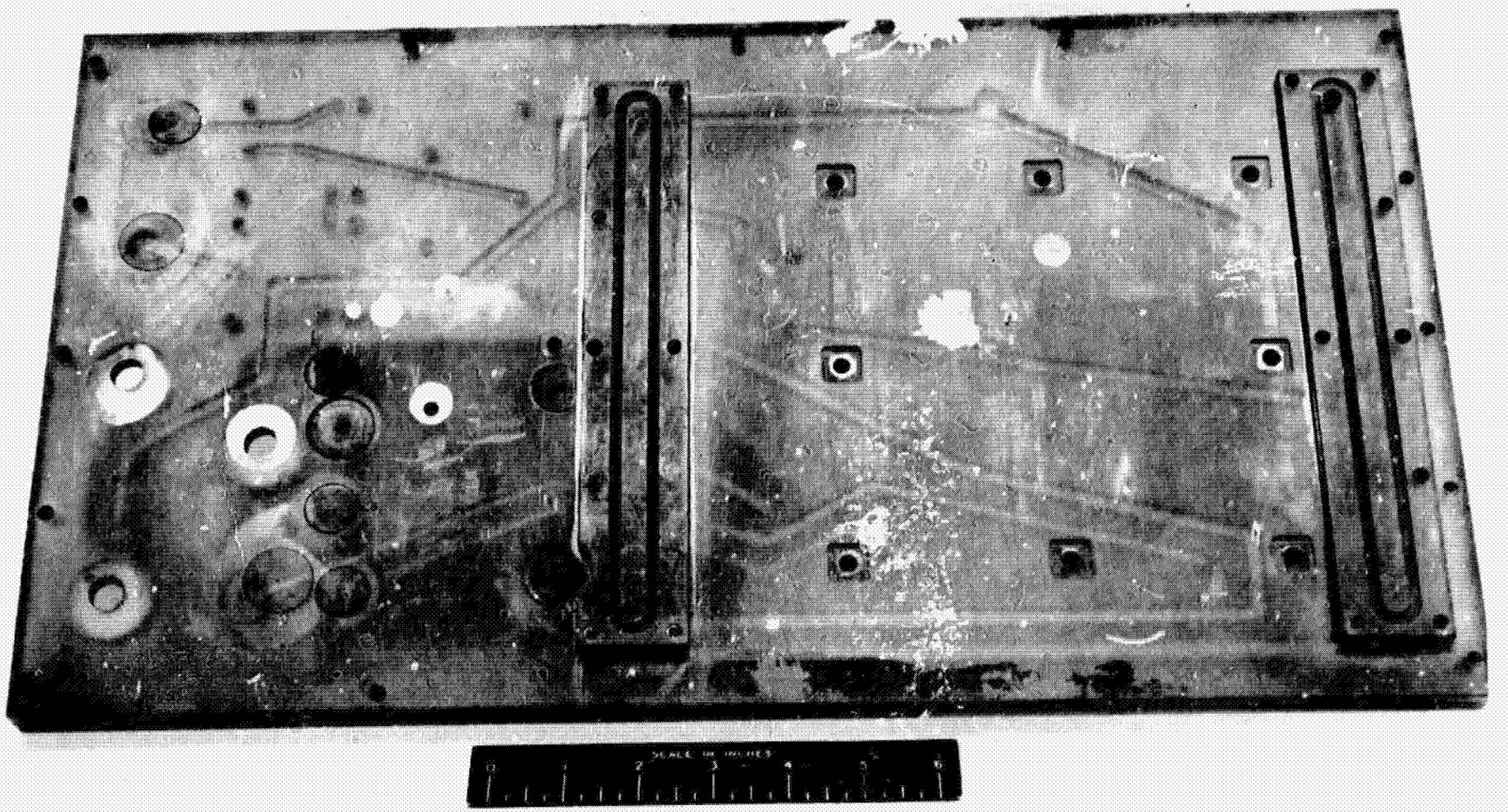

FIGURE 22 ASSEMBLED BASEPLATE
(BOTTOM)

Design Features

In order to ensure that the structural integrity of the baseplate was maintained, through-bolting of the total laminate was employed in several locations. A bolt pattern around the periphery of the baseplate provides two functions: (1) to prevent bond line failures of the "edge start" variety, and (2) to provide a large area for module and accessory mounting. Further, through-bolting is provided by three of the six reservoir mounting bolts, and two of the heat exchanger mounting bolts. These clamp the laminate roughly along its long dimension center line. See Figure 23. The result is that the primary function of the bonding agent is sealing.

In areas where it is not practical to through-bolt components onto the baseplate, tapped holes are provided with stainless steel helicoil inserts. Inserts are also used where threaded fittings enter the baseplate.

Bosses are used where necessary to provide adequate thread depth under threaded o-ring fittings.

Water, hydrazine and nitrogen feeds enter the module from the side opposite the cell stack as is the heat exchanger.

The outside of the baseplate is semi-transparent when wet and this allows visual inspection for gas in the electrolyte lines or liquid in the gas lines.

Adhesive Selection

Shell Epon 828, a two part, liquid epoxy was chosen as the adhesive to be used in bonding the baseplate. Table 3 shows a complete breakdown of the selection process. All adhesives investigated are listed.

Figure 24 illustrates the structural test setup. Test samples consisted of two, 1/4 inch x 1 inch x 2 inch, pieces of polysulfone bonded together

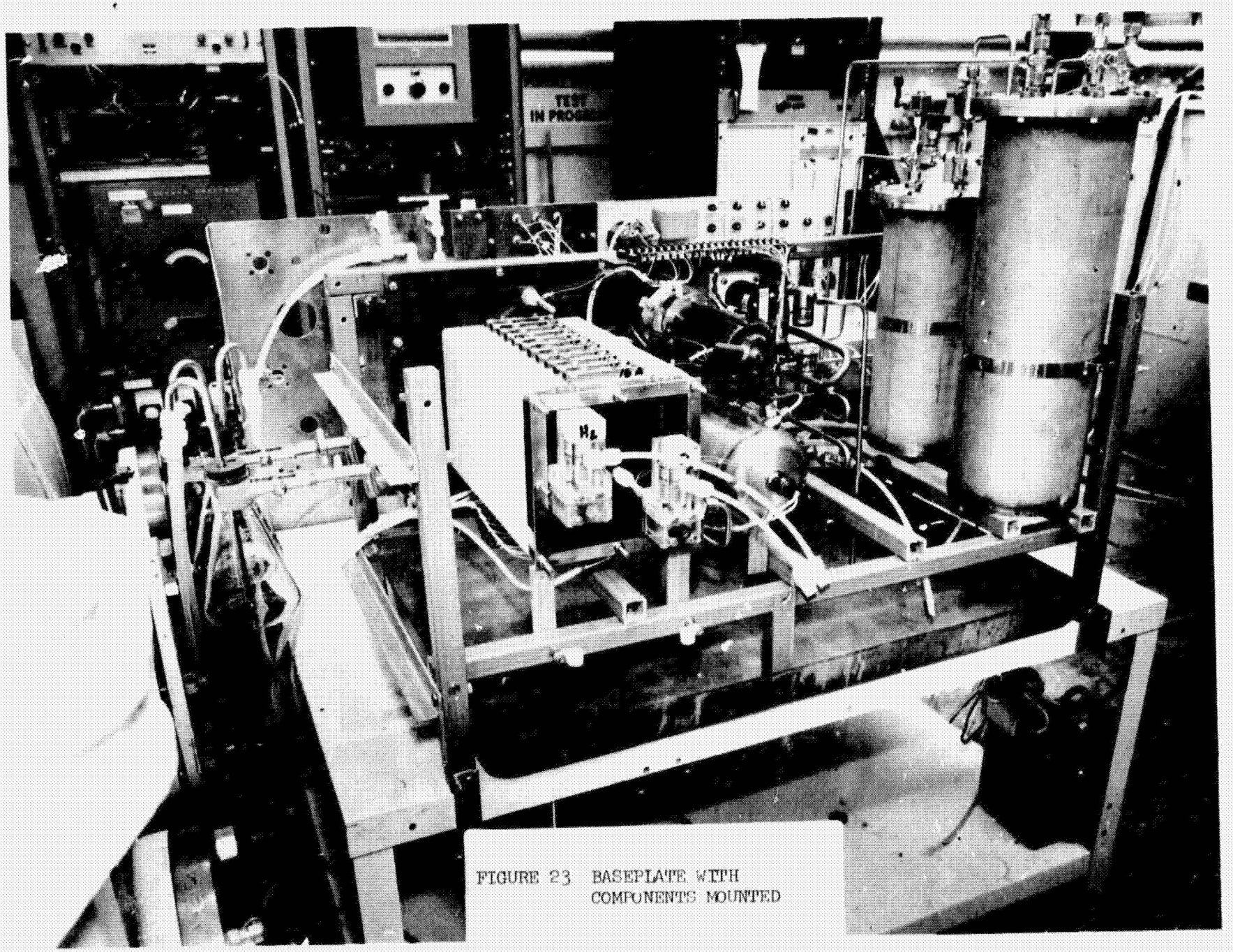

FIGURE 23 BASEPLATE WITH COMPONENTS MOUNTED

Table 2a

Adhesive Selection for Base Plate Bonding

Adhesives Evaluated			Type of Cure			Liquid Absorption Cured Bar of Adhesive Immersed in 30% KOH for 670 Hours			Appearance When Cured Between Two Glass Slides
Mfg.	Part No.	Description	Room Temp.	Bake	Air Dry	Appearance	Wt. Incr. ~%	Rejected	
3M	EC 1469	Single Part Refrigerated Epoxy	-	x	-	No apparent Deformation	5.2	x	-
3M	2216 B/A	2 Part Epoxy	x	-	-	Same	5.56	x	-
3M	1838 B/A	2 Part Epoxy	x	-	-	Same	3.46	x	-
3M	880	Rubber	-	-	x	Excessive Swelling	-	x	-
3M	AF 126	MOD. Epoxy Film	-	x	-	No Deformation	N/L	-	Few Bubbles
3M	AF 30		-	x	-	Much Deformation	3.46	x	-
3M	AF 64	MOD. Epoxy	-	x	-	No Deformation	0.30	-	
Shell	828	2 Part Epoxy	x	-	-	No Deformation	3.08	-	No Bubbles
Furane	220	2 Part Epoxy	x	-	-	No Deformation	2.85	-	-
Amer. Cyan	BR-89	MOD. Epoxy Paste	-	x	-	Attacked by KOH		x	-
Amer. Cyan	FM-123-4	MOD. Epoxy Film	-	x	-	-	-	-	Large Quantitie Interconnected Air Bubbles

Table 2b

Mfg. & Part #	Structural Test (See Fig. 24 for Test Set-up) KG at Failure	Rejected	Inter-passage and/or External Leak Tests Test Press = 37.5 PSI Duration = 360 Hours (Water) Nitrogen	H_2O Ending PSI	Rejected	Adhesive Chosen Reason
3MAF126	77.16	-	No Leak	34.5	-	-
-	-	-	-	-	-	-
3MAF64	27.43	-	Inter-Passage Leak at 25 PSI		x	-
Shell 828	9.5	-	No Leak	34.0	-	No Air Inclusions, Room Temperature Cure, Readily Applied in Even Coats, Satisfactory Structure Characteristics, Previous Experience in Its Utilization

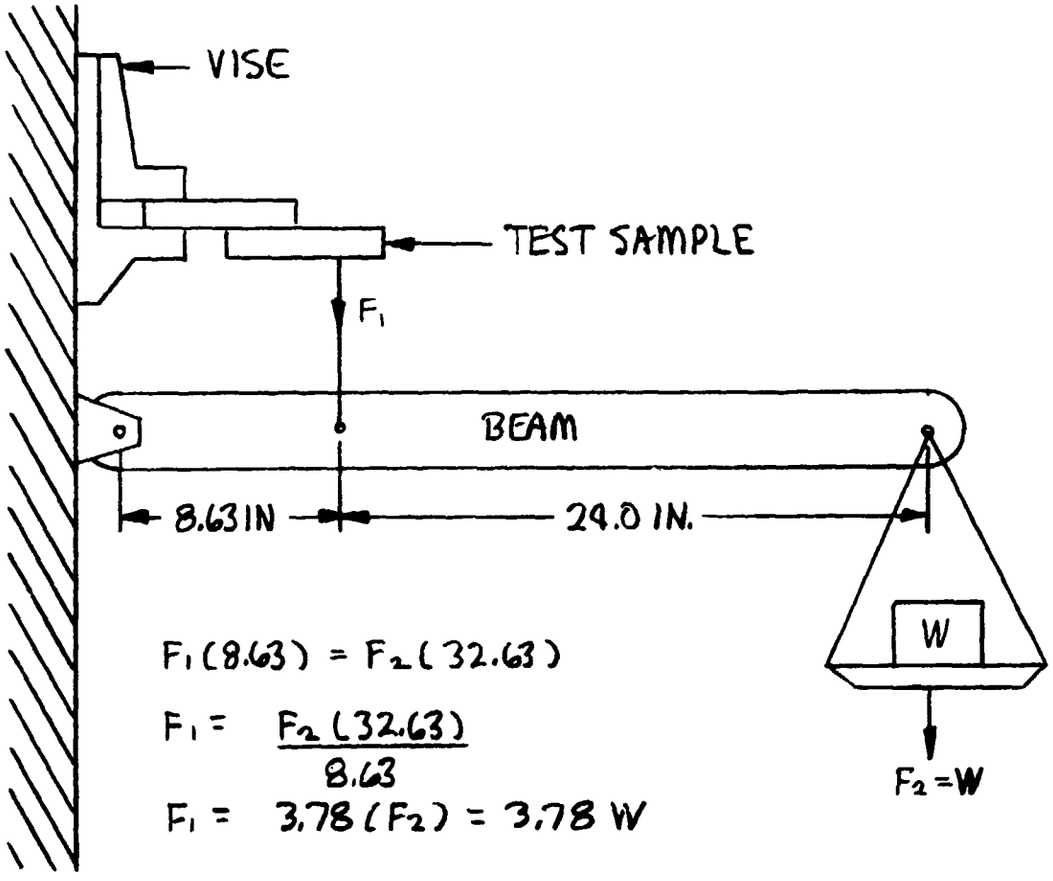

FIGURE 24 STRUCTURAL TEST SET UP, ADHESIVE SELECTION

so as to form a lap joint of 1 sq. inch area. The test piece was then loaded until the bond failed. All test samples were annealed prior to bonding and testing. Test results are shown in Table 3.

Six 5 inch square samples were made which were representative of two areas of the full scale baseplate. Three were designed to accept the reservoir and three the pump/bubble separator. At this point in time, all but three adhesives (AF64, AF126 and Epon 828) were used to make up three of the 5 x 5 baseplate samples. These were then subjected to a pressurization test using nitrogen only. Test pressure was raised to 37.5 psi in 5 psi increments. At 25 psi the sample bonded with AF64 showed a leak between two adjacent passages and was discarded. The two remaining samples were pressurized with water and allowed to stand for approximately 360 hours. Start and end pressures are shown in Table 2. The 3 psi drop noted for both samples is attributed to a drop in the average room temperature over the period of the test. It was concluded that either the AF126 or the Epon 828 would be suitable for bonding the baseplate. Epon 828 was chosen for the reasons noted in Table 3. The remaining 5 x 5 samples were bonded using the Epon 828.

Large Baseplate Samples

As described above, the 5 x 5 samples were made to simulate portions of the full scale baseplate. Passages were machined which were the same size and shape as those in the baseplate. Distances separating passages were representative of those in the baseplate.

The samples (as does the baseplate) consist of two basic pieces; a main body into which the passages are machined and the closure which is bonded to the machined side and so encloses the "D" shaped passages. See Figure 25. The 5 x 5 samples do not incorporate any bosses since they are made to accommodate only the reservoir or pump/bubble separator.

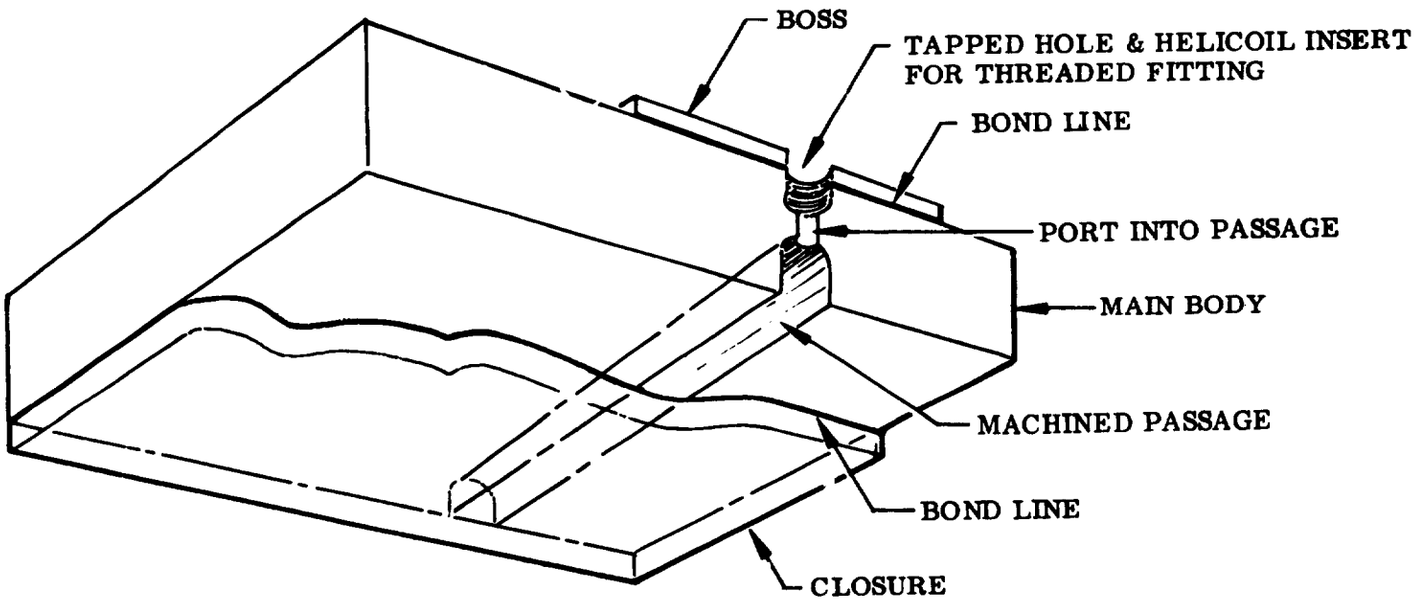

FIGURE 25 TYPICAL BASEPLATE CONSTRUCTION

Annealing of Polysulfone Samples

An undesirable characteristic of polysulfone is that it will stress crack (under certain conditions) if it has not been annealed (heat heated). A particularly dramatic demonstration of this can be accomplished by drilling a hole in a small piece of polysulfone and washing the machined part in a highly volatile solvent. As the part dries and cools, many small fractures will appear, usually starting at the machined surface. Parts that are machined too rapidly will usually show small cracks at the machined surface, even if heat treated immediately after machining. Annealing of the cracked part will usually prevent the further spread of the cracks.

Most of the useful information concerning the characteristics and uses of polysulfone were obtained from Union Carbide, one of the producers of this plastic.

None of the 5x5 samples was to be machined after being annealed or bonded. However, it was then realized that, in order to complete the full scale baseplate some tapped holes would have to be machined after it was bonded. It was therefore decided to re-anneal one of the 5x5 samples, whose separate parts had been annealed and then bonded. This was done with no adverse effect and the plan to bond, final machine and re-anneal the whole baseplate was continued.

Since the adhesive chosen was liquid, there was a need to develop a technique whereby a thin even coating of adhesive could be applied to one surface. This was accomplished by stretching and securing a .010 diameter wire as close as possible to each of two opposite edges of the part to which the adhesive was to be applied. An amount of adhesive, somewhat in excess of the amount required was then spread across one end of the part, between the wires. A stainless steel straight edge was laid across the two wires and the excess adhesive drawn slowly (with the straight edge) to the opposite end of the part. An even, bubble free, .010 thick coating thus results. Of course, the part must be flat and level for this operation to be successful. Removing the

the wires leave a slight depression down the edge of the part which is of no consequence since adhesive squeeze out fills it in.

Full Scale Baseplate

The baseplate was fabricated per drawings BEH20036, BEH20037, BEH20038, SKBEH008, SKBEH009, SKBEH010, SKBEH011. Unannealed polysulfone sheet was delivered to the shop with instructions to use only light oil or kerosene as a cutting fluid. Cleanup was to employ detergent and water only. The shop exercised considerable care in the machining of these parts and no problems were encountered. Since the baseplate required machining after bonding it was not annealed at this time.

Bonding required three days elapsed time. On the first day, the main body and closure were bonded together. The second day saw the bonding of all bosses on the component side of the plate. On the third day, the remaining bosses were added to the opposite side. A 24-hour curing period at room temperature was allowed between each bonding procedure. The baseplate was then returned to the shop for final machining which was uneventful.

The complete baseplate was next subjected to the annealing cycle detailed in Table 4.

Table 4

Oven Temp. °C/°F	Time Hours	
83/181	0830	
100/212	0850	
105/221	0910	
120/248	0930	Avg. Rate of Temp.
130/266	0945	Rise - 1.64°C (2.95°F)
140/284	0950	Per Min.
145/293	1005	
150/302	1020	
Hold for 5.5 hours		

Union Carbide data suggest a 5.5-6.0 hour soak at 150°C (320°F) - 165°C (329°F) for the thickness of material being annealed. The oven was shut down at 1635 and allowed to cool, along with the baseplate until the following morning.

Removal of the baseplate from the oven revealed it to have warped severely. The warpage is presumed to be due to the difference in thickness of the main body and the closure. Large areas of bond failure under all bosses as well as between the main body and closure rendered the part useless. Following a successful try at removing one of the basses, it was decided that all parts could be separated, cleaned of adhesive and rebonded. This was accomplished without further incident. The completed baseplate was not reannealed, the risk being considered too high.

Baseplate Pressure Tests

Two tests were employed to verify the pressure integrity of the baseplate. In the first, all internal passages were manifolded together, pressurized to 258.6 kN/M^2 (37.5 psig) as indicated by a manifold pressure gage with nitrogen and submerged in water. After 19 hours (overnight), the pressure had dropped approximately 20.7 kN/M^2 (3 psi). No bubbles were observed so the drop was attributed to a drop in water temperature. The second test was to determine if any leakage was occurring between internal passages. Again the liquid passages were manifolded together and filled with water. Gas passages were left open and filled with water after the baseplate was placed in a horizontal position. Liquid passages were then pressurized to 258.6 kN/M^2 (37.5 psi) and held for one week. During that time, no water was displaced from the gas passages. It was concluded that there were no internal leaks.

Liquid Passage Pressure Drop Test

The longest continuous liquid passage was chosen as the subject of this test. It is considered to be representative of all other liquid passages and was the only liquid line so tested. Figure 26 shows a schematic of the test setup. Pressure drop measurements were also made on a representative gas line. The same test set-up as above was used except that the reservoir was deleted.

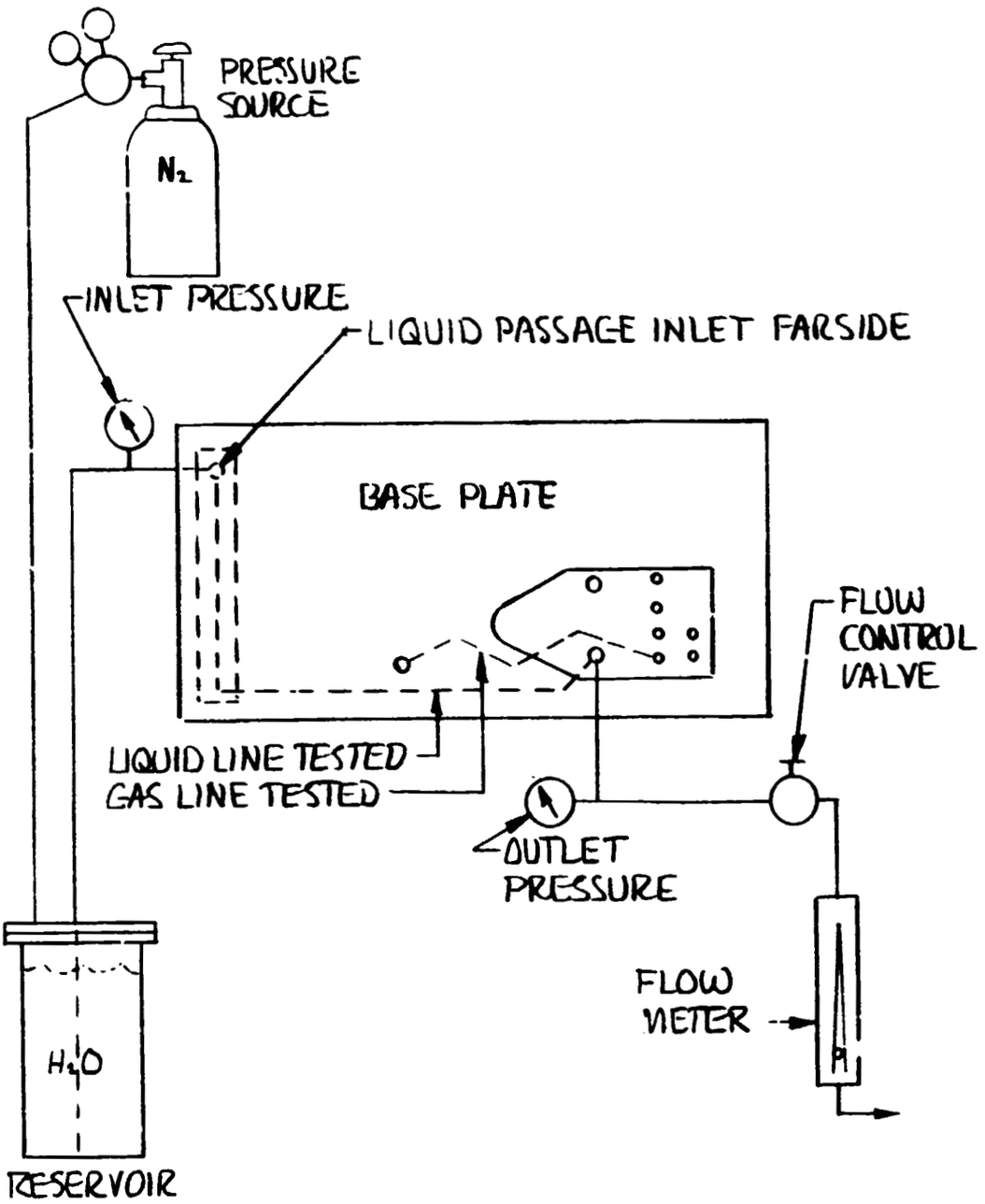

FIGURE 26 TEST SET UP FOR BASEPLATE PRESSURE DROP TESTS

Data from both tests are considered acceptable and are presented in Table 5.

Table 5

Medium	Flow Rate Liters/Min	(Gal/Min)	Inlet Press kN/M^2	(In. HG)	Outlet Press kN/M^2	(In. HG)	ΔP kN/M^2	(In. HG)
30% KOH	0.06	(0.02)	6.08	(1.80)	4.22	(1.25)	1.86	(0.55)
	0.12	(0.03)	6.42	(1.90)	4.46	(1.32)	1.96	(0.58)
	0.24	(0.06)	7.09	(2.10)	4.39	(1.30)	2.70	(0.80)
	0.37	(0.10)	7.09	(2.10)	4.56	(1.35)	2.53	(0.75)
	0.52	(0.14)	9.19	(2.72)	6.08	(1.80)	3.11	(0.92)
	0.68	(0.18)	11.99	(3.55)	8.61	(2.55)	3.38	(1.00)
Gaseous Nitrogen	M^3/Min	Ft^3/Min						
	0.002	(0.07)	0.68	(0.20)	0.54	(0.16)	0.14	(0.04)
	0.004	(0.14)	1.05	(0.31)	0.81	(0.24)	0.24	(0.07)
	0.010	(0.34)	2.53	(0.75)	1.59	(0.47)	0.94	(0.28)
	0.015	(0.53)	4.86	(1.44)	2.90	(0.86)	1.96	(0.58)
	0.020	(0.72)	8.10	(2.40)	4.90	(1.45)	3.20	(0.95)
	0.026	(0.92)	12.26	(3.63)	7.43	(2.20)	4.83	(1.43)
	0.032	(1.12)	17.90	(5.27)	10.74	(3.18)	7.06	(2.09)

2.2.4 Cell Stack

Design Requirements

The cell stack consists of 22 cells with 145 cm^2 active area on each electrode. The cells are connected hydraulically in parallel and electrically in series. The design maximum current to be applied to the stack is 21.75A (150 MA/cm^2 current density). This current is equivalent to approximately a 1.5-man rate of generation of oxygen and cabin leakage makeup of oxygen and nitrogen. The design goal for individual cell voltage is 2.00 volts at 75°F.

Design Features

The innovations in cell stack design which represent potential improvements over the design used in the breadboard system and which resulted from development activities in the previous contract are the following:

Injection-molded cell spacers (structural parts) with modified manifolding and electrolyte flow path to improve zero-g compatibility and producibility of parts.

Anode containing 5% iridium (5% of the platinum used) as an additive to the basic platinum catalyst to improve long-term performance stability.

Cathodes with reduced platinum catalyst loading to optimize hydrazine utilization efficiency at a minimum power penalty.

Slurried J-M asbestos to replace the use of sheet Acco asbestos to improve contact of the matrix with the electrodes.

Addition of a hydrophilic organic membrane (Gelman Acropor 1200) to reduce the sensitivity of the cells to gas breakthrough.

Single Cell Model Design Verification Testing

To pre-test the new design concepts for the cell stack, over 3000 hours of testing were conducted on a single-cell prototype. The results of this testing are described in the following sections, beginning with a chronological log of test results and design modifications resulting from the individual single cell tests, followed by a description of the final configuration and processing procedures for each element implemented in the buildup of the final cell stack.

Single Cell Testing

The first single cell assembly contained all of the design improvements outlined above. The cell spacers were machined to the configuration and dimensions planned for the injection-molded parts.

The anode was prepared according to the planned formulation and procedure described as follows.

The anode loading was a quantity scale-up of the previously successful 90 cm^2 electrodes except that it was to have iridium in addition to platinum as catalyst. The quantity of iridium was to be 5% of the scaled-up quantity of platinum. Accordingly, the makeup of the material applied to the anode screen was:

Platinum	-	6.32 grams
Iridium	-	0.33 grams
Teflon (trade name)	-	6.65 grams
Jaguar (trade name)	-	13.70 grams

As in the 90 cm^2 electrodes, the Teflon and Jaguar served as binder and extender respectively. Once weighed, the components were mixed thoroughly to insure even distribution of the Pt and Ir. throughout the material mass. The material was then trowelled onto the electrode screen which had been masked to fit the "window" in the electrode rim. Trowelling was continued until the material completely encapsulated the screen mesh and was distributed over the entire "window". The screen and material were lightly sprayed with mineral oil (to prevent sticking) and placed between two .010 thick sheets of clear polyester film. This "sandwich" was then lightly rolled until an even material distribution was obtained. The screen and material were then allowed to dry over-night in a low temperature oven.

Once dry the screen was subjected to a leaching procedure designed to remove all materials from the screen except the platinum, iridium and [illegible]. The screen was leached as shown in Table 6.

Table 6

Electrode Leaching Procedure

Solution	Time	Minutes	Ultrasonic Yes	Ultrasonic No
Hexane	15		x	
Propanol	15		x	
H_2O distilled	15		x	
Boiling, 30% KOH	120			x
H_2O distilled	15		x	
10% H_2SO_4	15		x	
H_2O distilled	15		x	
30% KOH	12	Hours		x
H_2O distilled	60			x

The screen was again dried and a sample scraping taken for analysis to determine residual impurities. These impurities should not and did not exceed 1%. The anode was completed (except for the addition of asbestos) by welding the catalyst screen into the electrode rim, then welding on the backup screen and applying the vinyl insulating tape.

The cathode was prepared (according to plan) is essentially the same manner as the cathode. Two basic differences do, however, exist. (1) The cathode contains no iridium and (2) its total loading is much lighter than the anode. The loading was applied to the screen in the same manner as the anode and consequently did not completely encapsulate the screen mesh; i.e screen mesh was visable. The leaching procedure of Table 6 was applied to the cathode screen with the result that noticably more material was shaken off the cathode (in the ultrasonic "baths") than the anode. The higher loss was attributed to incomplete incapsulation of the screen mesh and consequent decreased mechanical integrity. Nevertheless, the loading was judged to be satisfactory and the cathode was completed by adding asbestos.

The Johns-Manville, Fuel-Cell grade asbestos was applied to both electrodes by a process best described as slurrying. The asbestos is received from the vendor in .010 thick sheets and prepared and applied as described below.

A piece of the sheet material is cut to one-half the area of the electrode rim window. This amount of asbestos will be slurried over the entire catalyst loading. The asbestos was put into a breaker of hot KOH and pulverized until the fibers would remain in suspension in the KOH for a short time. This mixture was then put on a magnetic stirrer and agitated for approximately two hours. Excess KOH was removed by filtering with Acropor and the remaining asbestos fibers were rinsed thoroughly with distilled water. The asbestos was then remixed with water to a pouring consistancy.

A fixture was utilized which held the electrode horizontal and allowed the water-asbestos mixture to be poured on the catalyst loading while maintaining a slight vacuum on the opposite side of the electrode. The water was thus drawn slowly through the loading leaving the asbestos in intimate contact with the catalyst. Both electrodes were dried overnight in a low temperature oven and placed in plastic bags to await assembly into the single cell.

Gelman Acropor 1200 was bonded to two sides of the electrolyte spacer with Epon 828 epoxy.

The individual components were then assembled with test end plates (later used on the full cell stack) to form a complete single-cell assembly and installed in the bench test facility shown in Figure 27. The testing which followed is summarized in Table 7.

The first test was run for 330 hours with performance as shown in Figure 28. Two problems were identified as a result of this test: (1) external leakage of electrolyte from the electrolyte spacer was detected and (2) excessively high electrode voltages were observed. Cause of the poor performance was hypothesized to be either excessive gas pressure which tended to displace the gas liquid interface to the electrolyte side of the electrodes or poor performance of the new type of asbestos being used.

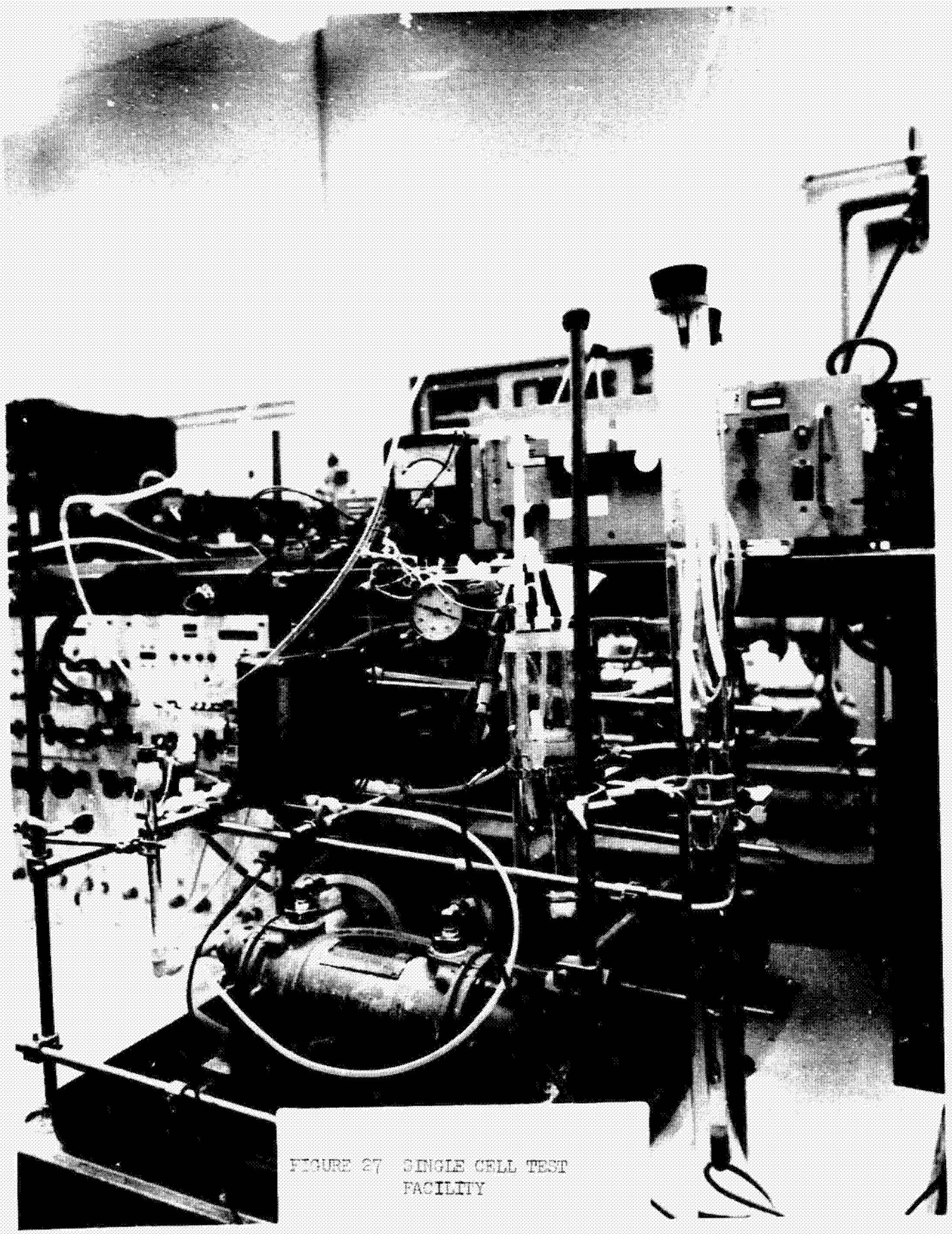

FIGURE 27 SINGLE CELL TEST FACILITY

TABLE 6 Test Log of Single Cell

Test Number	Test Time $t_o - t_f$ (Hours)	Test Objectives/Conditions	Reference	Results/Comments
1	0-330	Continuous 300-hour design checkout test	Fig. 28	External electrolyte leakage Excessive electrode voltage.
2	0-110	Determine effect of reduced electrolyte pressure drop on cell voltage	Fig. 28	No improvement in performance.
3	0-200	Determine effect of replacing J-M with Acco asbestos	Fig. 29	Stable electrical performance comparable to baseline requirements
4	0-350	Decreased o-ring groove depths to solve leakage problem.	Fig. 30	No external electrolyte leakage. Cathode unstable probably due to high carbonate concentration.
5	0-670	New electrodes, fresh electrolyte, fresh asbestos	Fig. 31	Stable performance Cathode voltage higher than desired.
6	700-780	Δ P gas over electrolyte vs voltage	Table 7	
7	780-784; 870-870-880	Hydrazine tests		See text p.62
8	0-330	New cathode, production anode, and injection molded electrolyte spacer	Fig. 33	Stable performance, voltage comparable to baseline.
9	0-500	Voltage vs current attitude tests sheet asbestos	Table 8	Sheet asbestos performance poorer than slurried. No effect of attitude on cell performance.

*An initial time of 0 indicates a change in the single cell configuration from the previous test. Otherwise only test conditions are changed and the test time is cumulative for consecutive tests.

The first step in determining the cause of the poor cell performance was to increase the cross-sectional area of the KOH inlet and outlet ports in the electrolyte spacer on the theory that the Δ P regulators for the generated gases (which sense liquid pressure in the inlet header) were not sensing the actual liquid pressure inside the cell; instead, they were sensing a higher pressure due to the pressure drop across the inlet electrolyte port. After enlarging the ports, the pressure drop across the electrolyte was measured and found to be negligible. With this modification the cell was reassembled and run for 110 hours in Test 2. The performance as shown in Figure 28 was essentially the same as in Test 1.

Continuing the investigation of cell performance, the new J-M asbestos was replaced with ACCO asbestos. In this configuration, Test 3 was run for 200 hours. Figure 29 shows that after approximately 35 hours the cell performance stabilized at a level comparable to that of the 18 cm^2 baseline cell performance established under Contract NAS 9-10405.

To correct the external leakage problem which was noted earlier, all o-ring groove dimensions on the cell spacers were re-examined. It was found that the large body o-ring groove depths were consistently on the high side of the tolerances of that dimension. The parts were then returned to shop, the grooves filled with epoxy and remachined to a depth 0.010 inches less than the original.

In Test 4, with the modified cell parts, the cell was operated for 350 hours with no evidence of leakage. Cell performance for this test is shown in Figure 30. After approximately 160 hours, the cathode performance began to degrade. At the end of the test, the electrolyte was analyzed and found to contain 0.8M carbonate; normal concentration is 0.1M. This excessive amount of carbonate probably was introduced by allowing the KOH saturated asbestos matrices to be exposed to room air for a long period of time between tests.

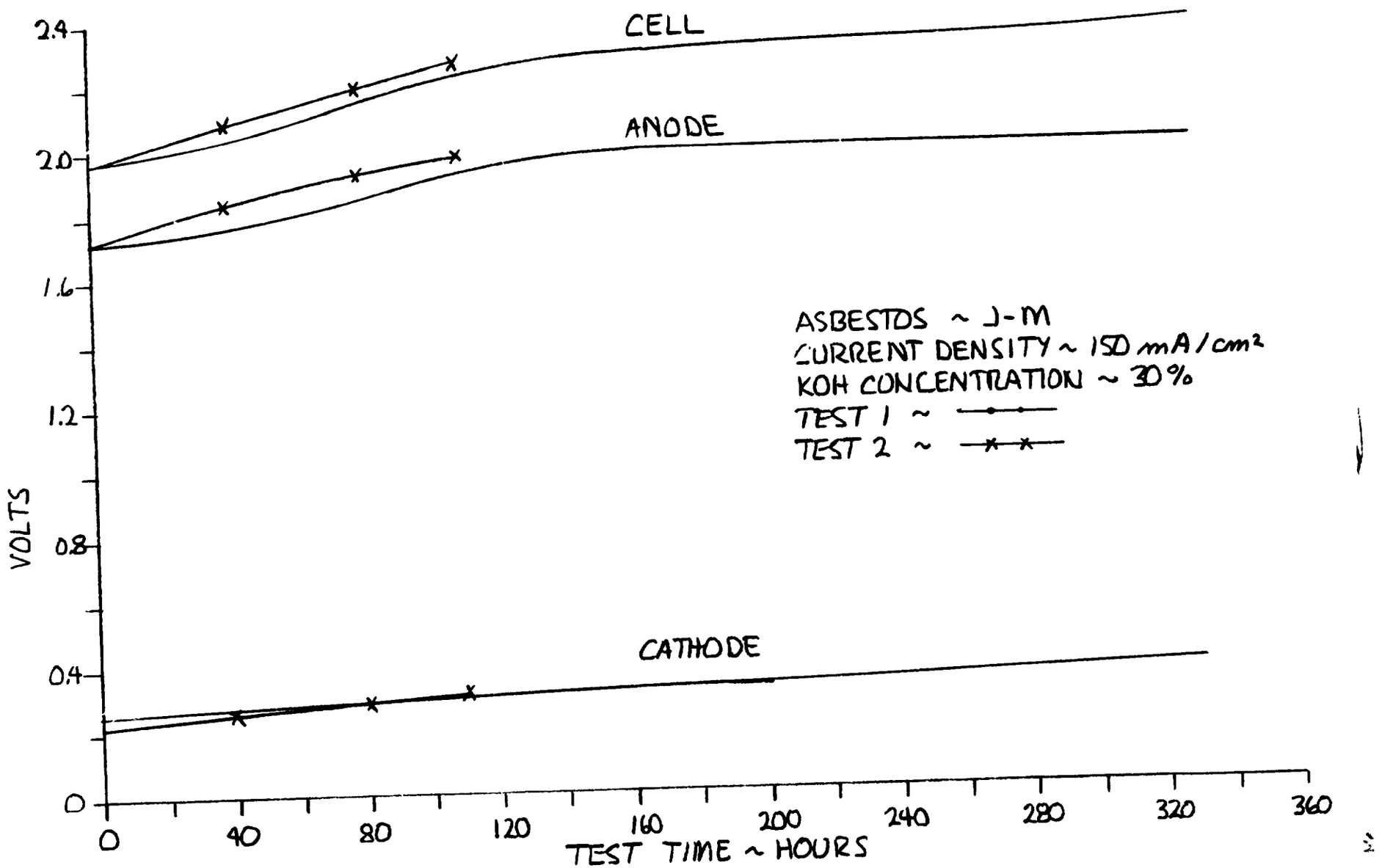

FIGURE 28 CELL CHECKOUT TEST

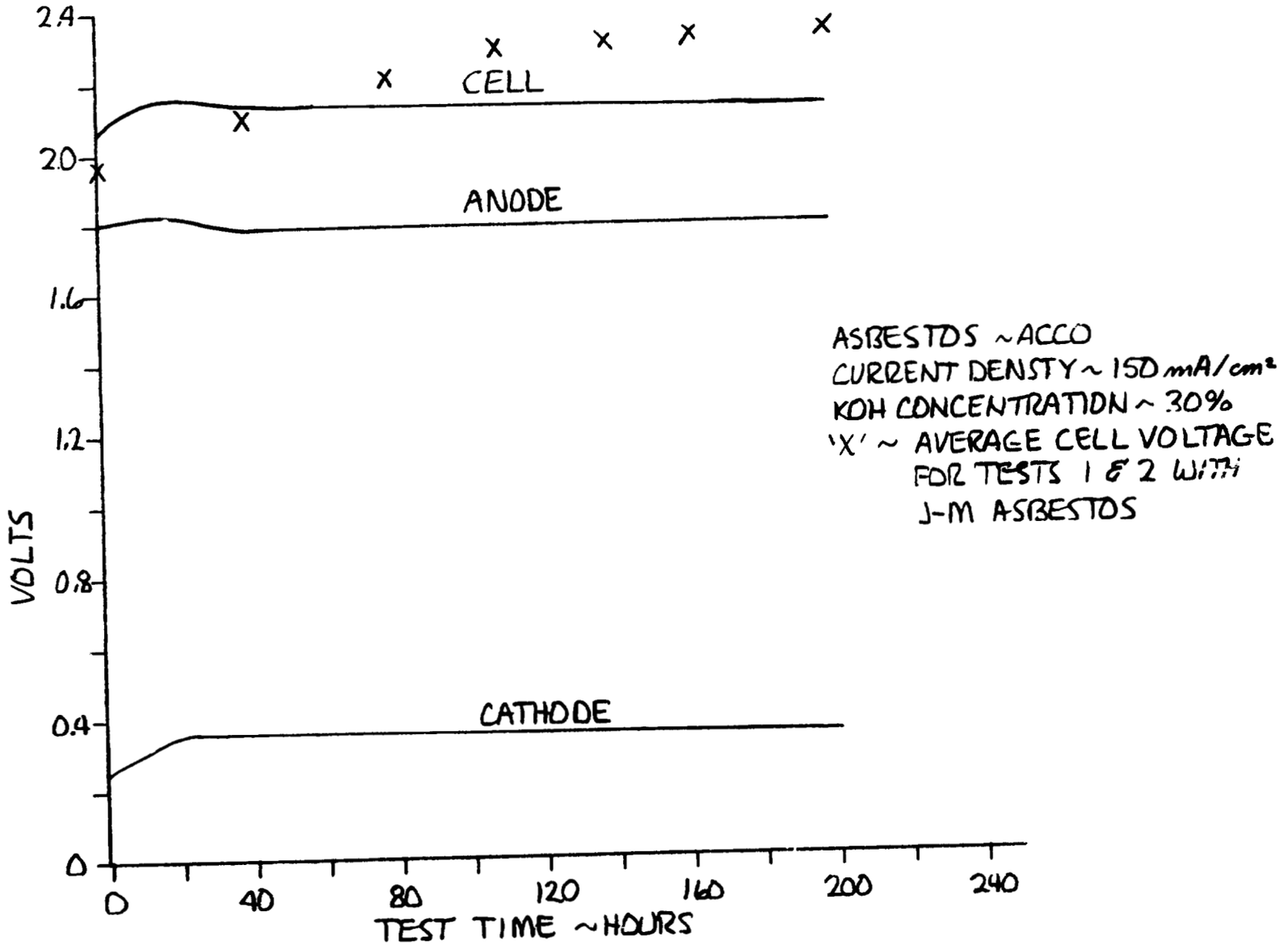

FIGURE 29 ACCO, J-M ASBESTOS PERFORMANCE COMPARISON

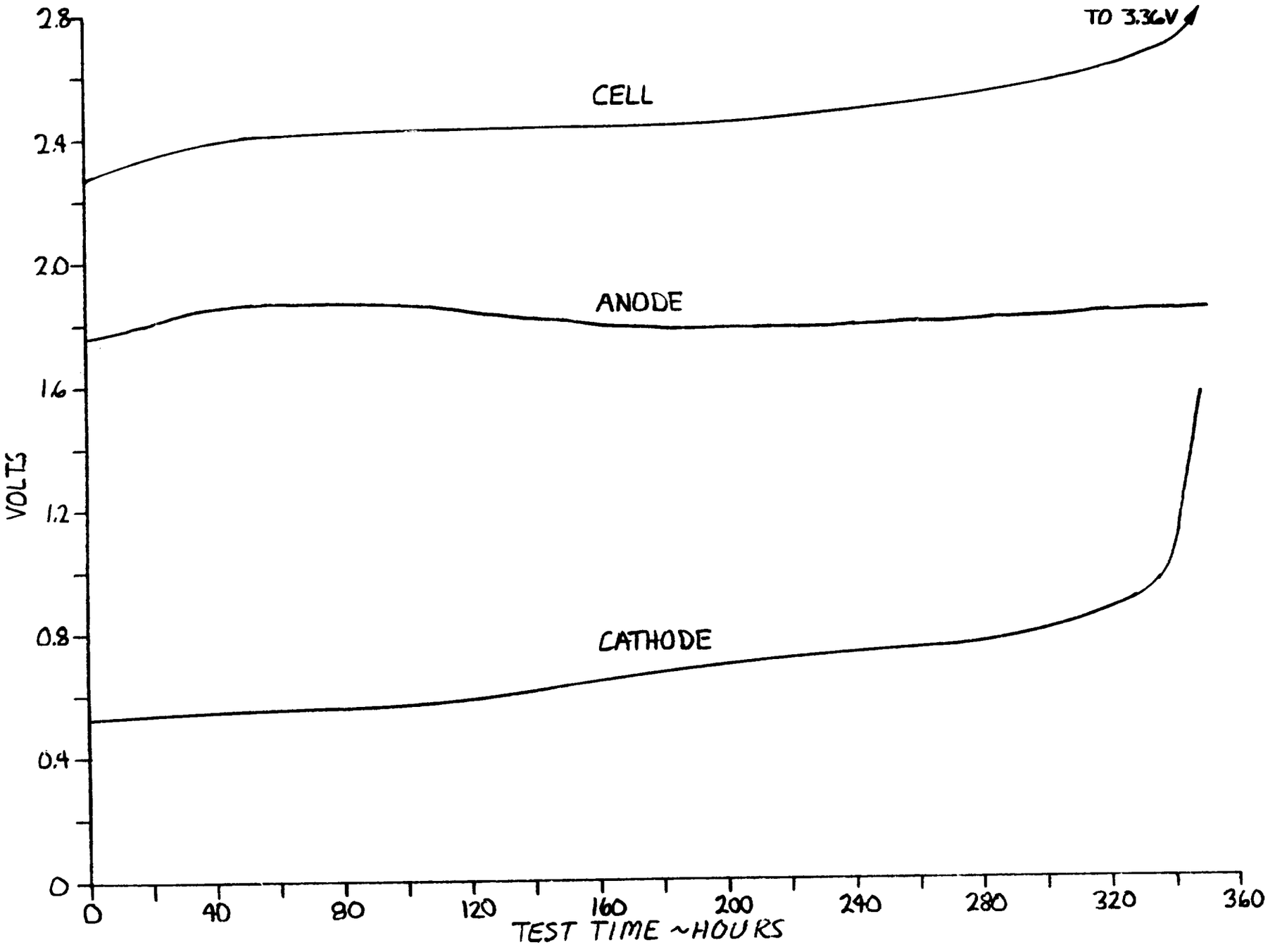

FIGURE 30 LEAKAGE CHECK

Two new electrodes were prepared with fresh asbestos. Fresh electrolyte was prepared and Test 5 was run for 670 hours. The performance, as shown in Figure 31, was stable, but with a cathode voltage somewhat higher than desired.

With the cell continuing to operate, Test 6 was initiated, at 700 hours elapsed time, to determine the voltage vs Δ P characteristics of the electrodes and the minimum Δ P to prevent liquid breakthrough. Cell gas pressure was decreased in approximately 26 mm Hg increments. Each pressure level was maintained for 6-7 hours to establish equilibrium conditions. Liquid breakthrough occurred at 63.5 mmHg on both sides. Table 8 shows the effect of gas pressure on electrode voltages. Electrolyte pressure was kept constant at 4.0 mmHg.

Table 8 - Voltage as a Function of O_2 and H_2 Pressure

	Cell Gas Pressure mm Hg		Voltage volts avg.		
	O_2	H_2	O_2	H_2	Cell
Initial	145.8	141.5	1.74	0.55	2.29
Run 1	116.8	117.0	1.64	0.47	2.11
Run 2	88.9	91.4	1.66	0.46	2.12
Run 3	78.0	78.0	1.65	0.43	2.08

At the conclusion of these Δ P tests, the cell had accumulated 780 hours of operation as shown in Figure 31.

With the cell continuing to run, Test 7 was initiated to evaluate the performance of the cell with hydrazine. For this purpose, the reference electrode was removed from the reservoir and a charge of hydrazine was added to achieve an initial hydrazine concentration of approximately 2.0 molar. Two events occurred almost immediately upon addition of the hydrazine: cell voltage started a rapid climb

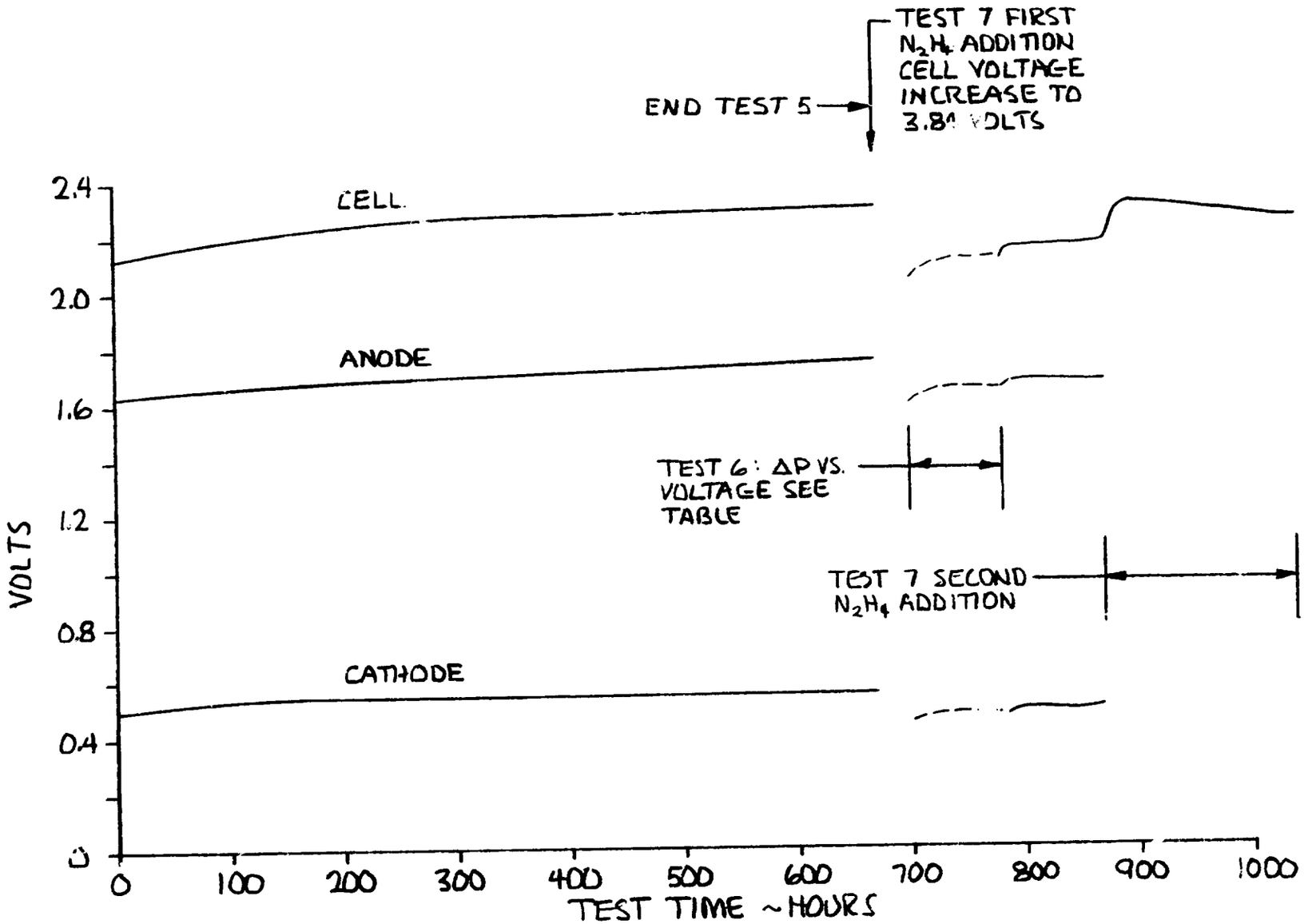

FIGURE 31 ELECTRODE, ASBESTOS, ΔP, HYDRAZINE CHECKOUT TESTS

(110 mV/hr) and gas bubbles appeared in the electrolyte. By the time the test was terminated (after four hours) the electrolyte in the reservoir appeared completely opaque due to the large quantity of very fine gas bubbles. In an attempt to determine the cause of this unexpected effect, the materials which were different in this cell from those used in previous successful hydrazine tests were selected for compatibility tests. The two selected materials, polysulfone and Aeropor, were tested in the apparatus shown in Figure 32.

The test consisted of immersing the sample in a hydrazine solution in a container which vented to an inverted graduated cylinder filled with water. Any gas generated as a result of hydrazine decomposition would then displace liquid in the cylinder. No hydrazine decomposition in contact with polysulfone was detected over a 72-hour period. Some gas was collected during the Aeropor tests but the quantity was too small to provide any conclusive evidence.

A second charge of hydrazine added at 870 hours to the cell electrolyte produced essentially the same effect as the first test, except that the amount of gas produced in the electrolyte was only about 20% of that observed previously, and secondly, the cell voltage increase was much less pronouced. (See Figure 31) These results point to the possibility of a contaminant in the cell which is being slowly consumed in its reaction with the hydrazine.

A new cathode, prepared by a different technique (described in a subsequent section) was used in Test 8. The anode was randomly selected from the production anodes being prepared for the full cell stack. The performance of these two "new" electrodes is shown in Figure 33. The run lasted 330 hours and the data show that both the cathode and anode performance were stable and at an acceptable level.

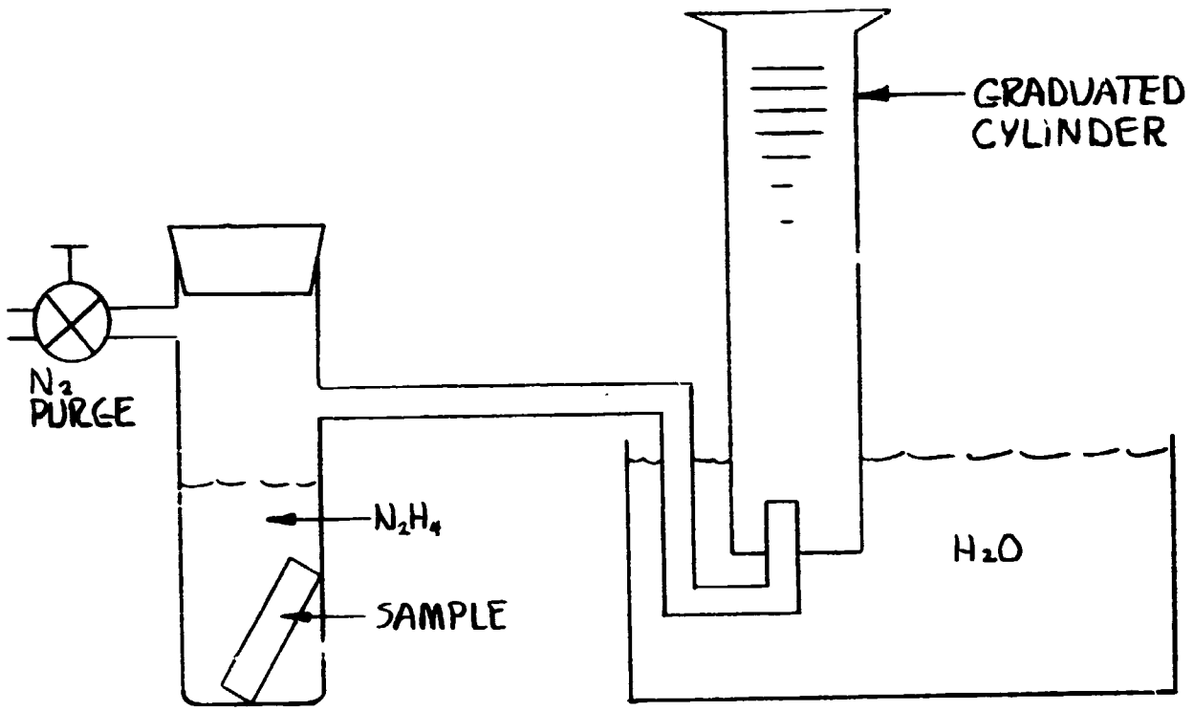

FIGURE 32 HYDRAZINE COMPATIBILITY TEST APPARATUS

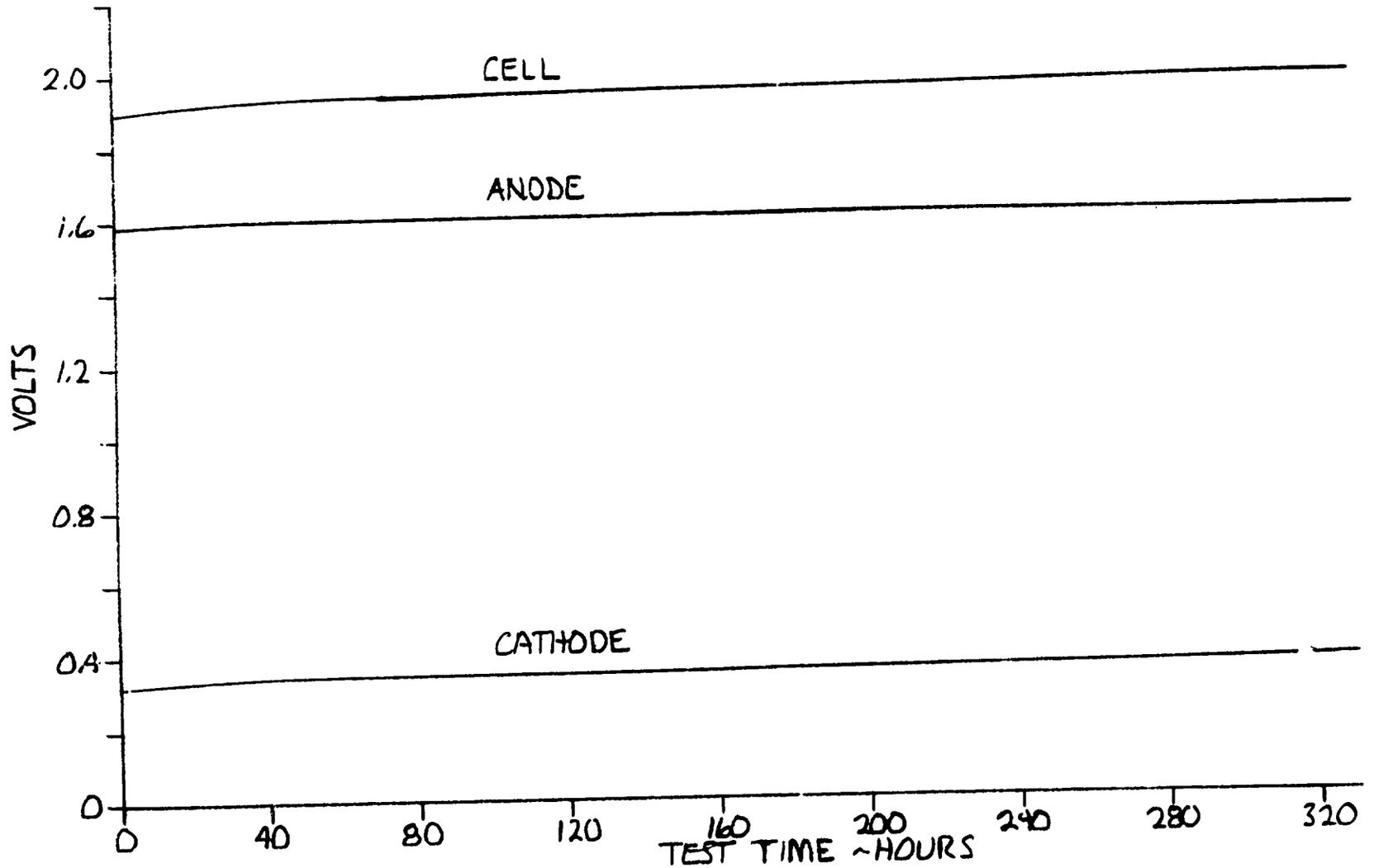

FIGURE 33 ELECTRODES WITH PRODUCTION CELL STRUCTURE TEST

Three of the sample (molded) spacers were used to build up the single cell of Test 8, and were subjected to approximately 800 hours (total of Tests 8 and 9) of running. The spacers performed well with no leaks or other undesirable traits. After the 330 hours of Test 8, the cell was disassembled and the spacers were carefully examined for any degradation in mechanical performance; none was found. The cell was then reassembled with the same three spacers for Test 9. Also the slurried ACCO asbestos was replaced with 20-mil sheet. As shown in Figure 34 the use of sheet asbestos in Test 9 increased the cathode voltage from 0.35 to 0.45 volts. A voltage-current profile was run on this cell configuration with the results shown in Table 9. This same cell was then operated in the following attitudes with no measurable change in performance.

Cell attitudes:
- Electrodes vertical - Anode down
- Electrodes vertical - Anode up
- Electrodes horizontal - Anode up
- Electrodes horizontal - Anode down

Table 9 Current Density vs Voltage

Current Amps	Current Density Ma/cm^2	Voltage Cell	Mean H_2	Mean O_2
10.9	75	1.827	.359	1.467
14.5	100	1.958	.451	1.487
18.1	125	2.051	.535	1.516
21.75	150	2.165	.607	1.557

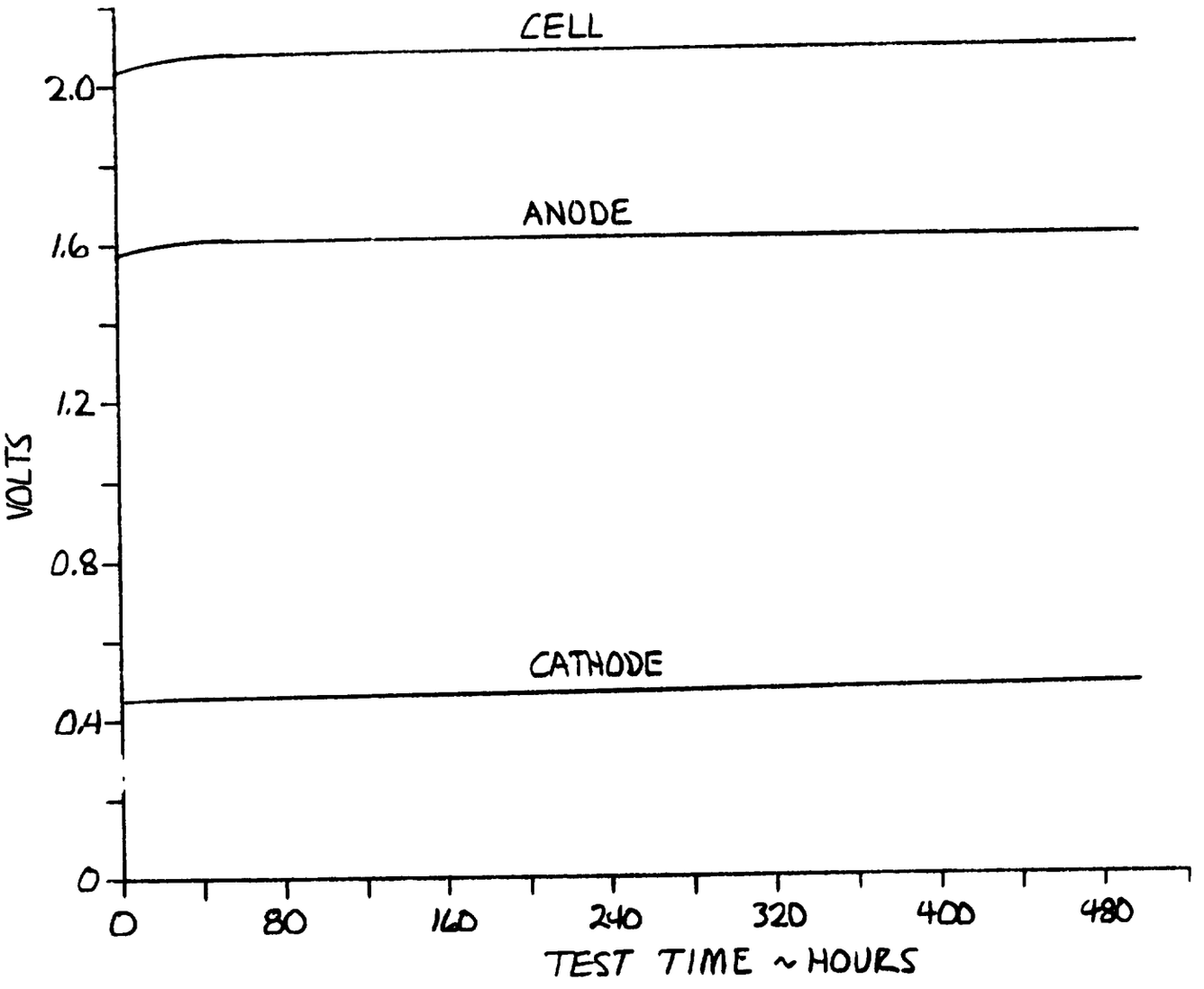

FIGURE 34 SHEET VS SLURRIED ASBESTOS TEST

Electrode Catalyst Loading

Prior to starting fabrication of electrodes for the full cell stack, it became evident that there was a need for a different procedure in applying the catalyst loading to the electrode screen. Trowelling the loading on wet produced electrodes which performed fairly well but lacked any mechanical integrity. During the welding of the screen to the rim, for example, significant quantities of catalyst would fall off the screen even with the screen being subjected to normal handling. Catalyst was also lost during leaching, particularly in the ultrasonic phases. Further, the loading had a dry, crazed appearance. While commercially purchased electrode material (used for reference electrodes) had a similar appearance, it was tacky in nature and did not tend to fall off the screen.

More material tended to be lost from the cathode since its smaller total quantity did not allow complete encapsulation of the screen mesh. Time required to apply the loading was a prohibitive 45 min.

It was therefore decided to try different formulation, mixing, and application techniques to get a more cohesive loading and which would allow shorter application times. Catalyst quantity was never changed. After determining that the iridium had no significant effect on the physical properties, test batches were made using only platinum in order to conserve iridium.

It had been previously noted that the formulation used on some of the single cell electrodes could be made into a chewing gum like consistancy if worked (kneaded) for periods of up to two hours or so. This time could be shortened by heating to drive off the volatiles of the extender and binder but produced a dry, crumbly mass. It was also noted that prolonged working apparently caused the teflon to encapsulate and insulate the particles of catalyst. The next logical step was to reduce the quantity of extender and/or binder. It was decided to remove some of the extender since it was to be removed during the leaching process any way. Several batches were made and worked, each successive batch containing less extender (Jaguar).

The final anode formulation reduced the original 13.70 grams of Jaguar to 8.90 grams and produced a material which could be worked into a cohesive, chewing gum like mass in under five minutes without heat. It could also be rolled into a 0.25 mm (0.010 in.) thick sheet, cut in half, applied to both sides of the masked electrode screen and rerolled. The resulting anode lost very little of its loading during leaching and performed quite well in the single cell (1.61 - 1.63 volts at 21.75 amps). The preceeding formulation and technique were used in making all the anodes for the full cell stack.

The same approach was tried unsuccessfully for the cathode. Several test batches later, it was discovered that the loadings are batch size sensitive with respect to workability and physical properties. Thereafter, batches were sized for three cathodes, worked to the proper consistancy, pressed into a mold and cut into three equal volumes. Jaguar on the cathode was reduced from 5.30 grams to 2.47 grams. There remained an application problem with the cathode. Even before the reduction in Jaguar, there was insufficient material to completely encapsulate the entire cathode window. To completely encapsulate the cathode screen mesh required a reduction in areas, or window size. At this point, insufficient time and budget precluded the additional investigation of cathode catalyst application techniques or alternative formulations. The cathode catalyst area was reduced by approximately 30% and applied in the same manner as the anode. This reduction in area cost approximately 0.15 volts in performance. Final anode and cathode formulations are shown in the following table.

Table 10 Electrode Formulations

Component	Weight/Anode grams	Weight/Cathode grams
Platinum	6.32	1.76
Iridium	0.33	-0-
Teflon	6.65	1.85
Jaguar	8.90	2.47

Asbestos

As previously mentioned, the Johns-Manville fuel cell asbestos did not perform well and the switch was made back to the Acco asbestos which had performed well on the previous contract. Since the slurrying process for applying asbestos was some-what time consuming (45 min. to one hour in the slurrying fixture plus overnight oven dry), it was decided to run a cathode fitted with sheet Acco in addition to running it with slurried Acco. The result was that the slurried Acco cathode ran at 0.1 volts less than with the sheet Acco. The conclusion was that the slurried asbestos was in more intimate contact with the catalyst and so provided better wetting of the catalyst. Based on the fact that the catalyst matrix was stronger than it had been previously, it was concluded that more vacuum could be applied to the slurrying fixture and thus shorten the water removal cycle. Tests showed that electrode time in the slurrying fixture could be reduced to about ten minutes.

The 2200 or so hours of single cell testing provided design verification for the machined cell spacers. As a result, the decision was made to proceed with the molding of the gas and electrolyte spacers for the full cell stack. The contract for the spacer tooling and molding was awarded to Baumbach Engineering of Mountain View, California. The double cavity mold tooling, Figure 35, was subcontracted by Baumbach to Rodak Tool Co. of Hayward, California. After some trial runs to determine correct molding temperature and pressure, sample parts were delivered, inspected and accepted. Go ahead was given for the molding of 26 each of the gas and electrolyte spacers. The overall quality of the product of both companies was excellent.

A piece was cut from a broken molded electrolyte spacer to serve as the specimen for an eighteen day environmental soak in KOH. The original weight of the piece was 5.0147 grams. Final weight was 5.0229 grams for an increase of 0.0082 grams or 0.16%. No swelling, distortion or discoloration were noted and the parts were considered acceptable for long term exposure to KOH.

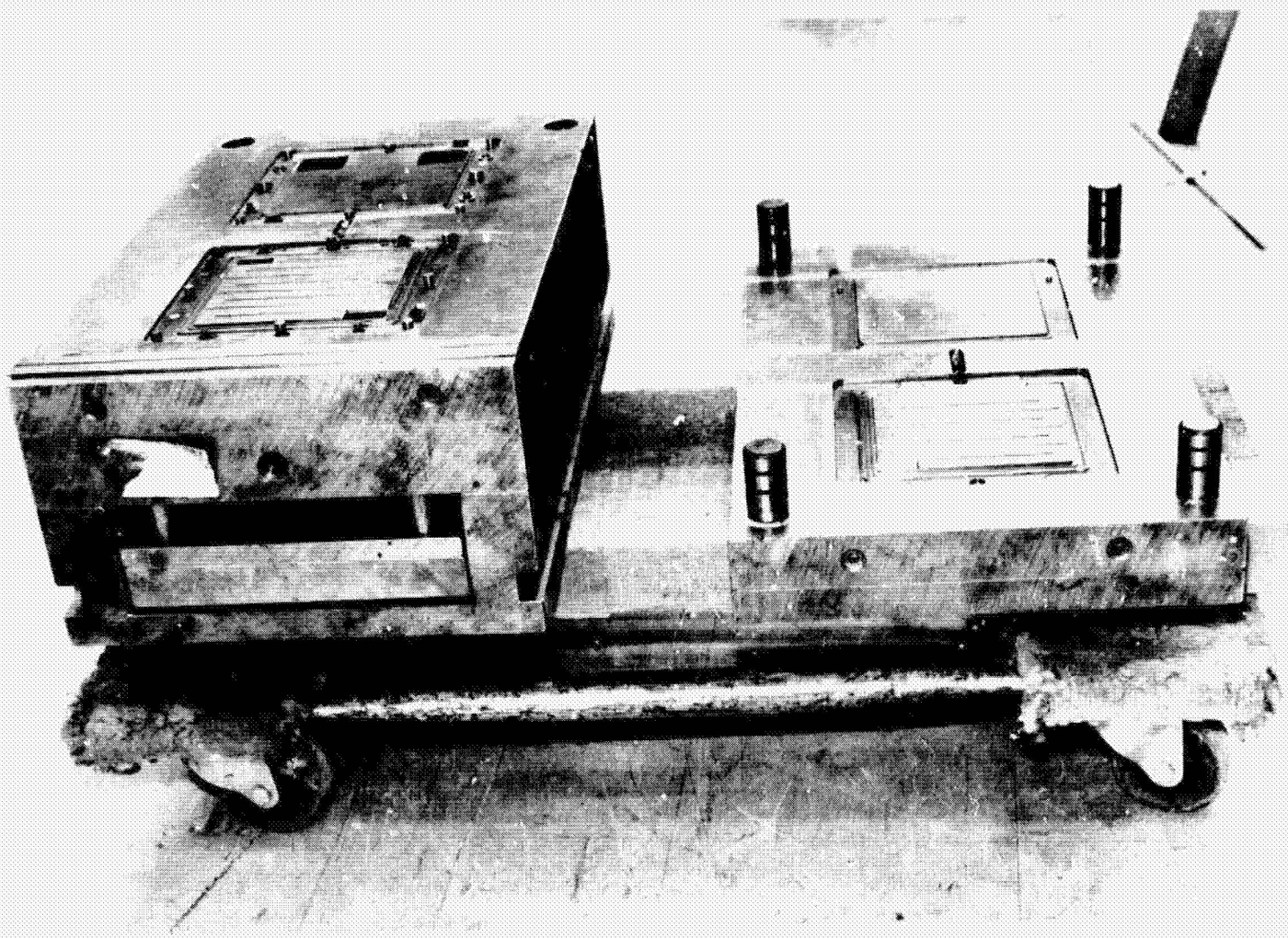

FIGURE 35 CELL SPACERS INJECTION MOLD

2.2.5 Power Controller

Tradeoff Study

A study was performed in order to select the type of control that should be used for energizing the electrolysis cell stack. Three types of control were considered: voltage control, current control, or current/voltage hybrid control.

Voltage regulation maintains a constant cell stack voltage. This technique automatically adjusts the current to compensate for variations in the individual cell potentials and the total stack internal resistance.

The current regulation technique provides a fixed constant current to the cell stack load. The output voltage of this type of regulator is solely dependent on the cell stack resistance.

Thirdly, a current/voltage hydrid regulator essentially provides constant power to a load. Voltage control is alternated with current control according to fluctuations in the characteristics of the cell stack.

This trade study was based on the average cell voltage vs current (VI) characteristics graphically illustrated in Figure 36. Points Q_1 & Q_2 designate the two quiescent operating points that the cell stack operates at during the high and low modes. Data for calculating the cell stack dynamic resistance, r, parameter at these two points was obtained from this graph. The dynamic resistance, r, is the slope of the curve at these points. Below is a tabulation of the results:

Qn	I	V/Cell	V/Stack	r
Q_1	7.25a	2.0V	44	.576r
Q_2	21.75a	2.175	47.850	.019r

Table 13 Quiescent Operating Point Characteristics

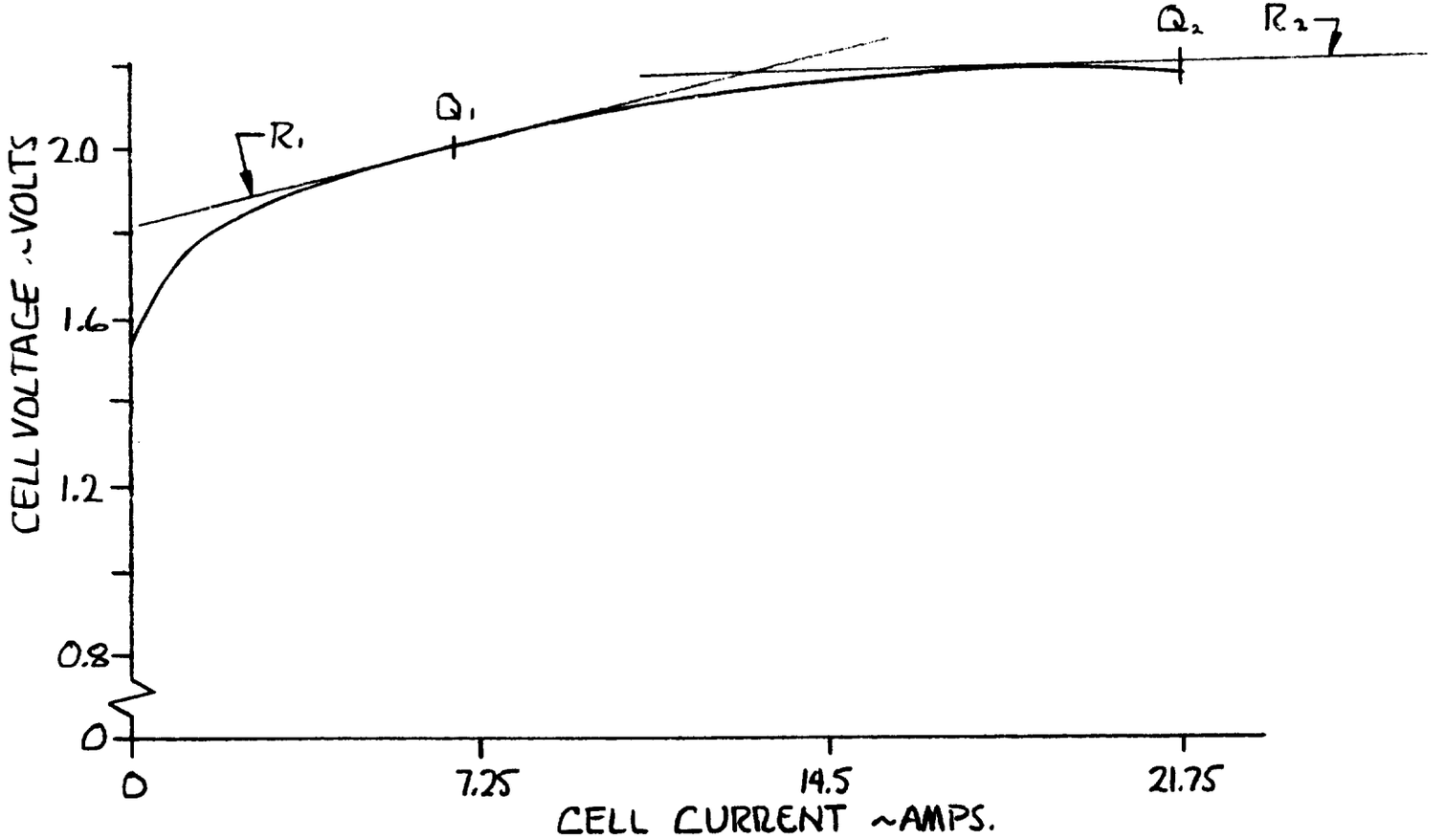

FIGURE 36 AVERAGE CELL VOLTAGE VS CURRENT CHARACTERISTIC

A pseudo current/voltage hybrid type of controller was selected for implementation in this application. However, instead of providing a constant power to the load it provides a constant current as the primary control as long as the cell stack voltage is below a fixed value. If the stack voltage exceeds this value, voltage control is switched in and limits the output current to maintain the voltage back within a normal operating condition. Thus, the primary control is current regulation and is backed up by a secondary control of voltage regulation.

Current control was selected as the primary control due to the low dynamic resistance of the cell stack at the high mode operating point, Q_2. If voltage control was employed at the high mode point, a ± 0.5% change in output voltage would cause a 26.25% change in the output current. Thus, an impractical burden would be placed on the controller in the form of component high precision tolerances which would exceed the financial scope of this contract. Also, since the quantity of output gas is directly proportional to cell current, a known input parameter (curve-t) would allow for an easier measurement of cell stack performance.

Power Controller

The power controller unit provides the necessary power conversion and control of electrical energy for electrolysis action in the cell stack. The unit is required to convert unregulated solar array power to a regulated constant current source with maximum efficiency. A brief summary of the requirements is as follows:

Input voltage 56 ± 10% VDC

Output current 21.75 amps high mode
7.25 amps low mode — Remotely selectable

Power conversion efficiency goal 90% or greater

On/off remotely controlled

Cell stack overvoltage protection

Cell stack overcurrent protection

.. switching type regulator was selected for implementation over a series pass dissipative type due to power conversion efficiency considerations. The maximum efficiency that could be expected from a series type regulator for this application is approximately 70%.

LMSC's initial state-of-the-art development of a switching regulated current source was performed under contract number NAS 9-11848. The design of the present controller utilizes the same basic switching theory technique employed in the former development, but the circuit has been completely redesigned to achieve better performance and allow incorporation of improved semiconductor devices. A block diagram of the resultant controller is illustrated in Figure 37.

Upon the application of an "ON" command, a current reference signal, IR, is emitted from the current reference amplifier and applied to one input of the error amplifier. The magnitude of this signal is dependent on the high/low mode select command and the respective settings of the high current or low current trimpot adjustments. These settings are now independent of each other whereas on the former units an adjustment of one mode changed the setting for the other mode.

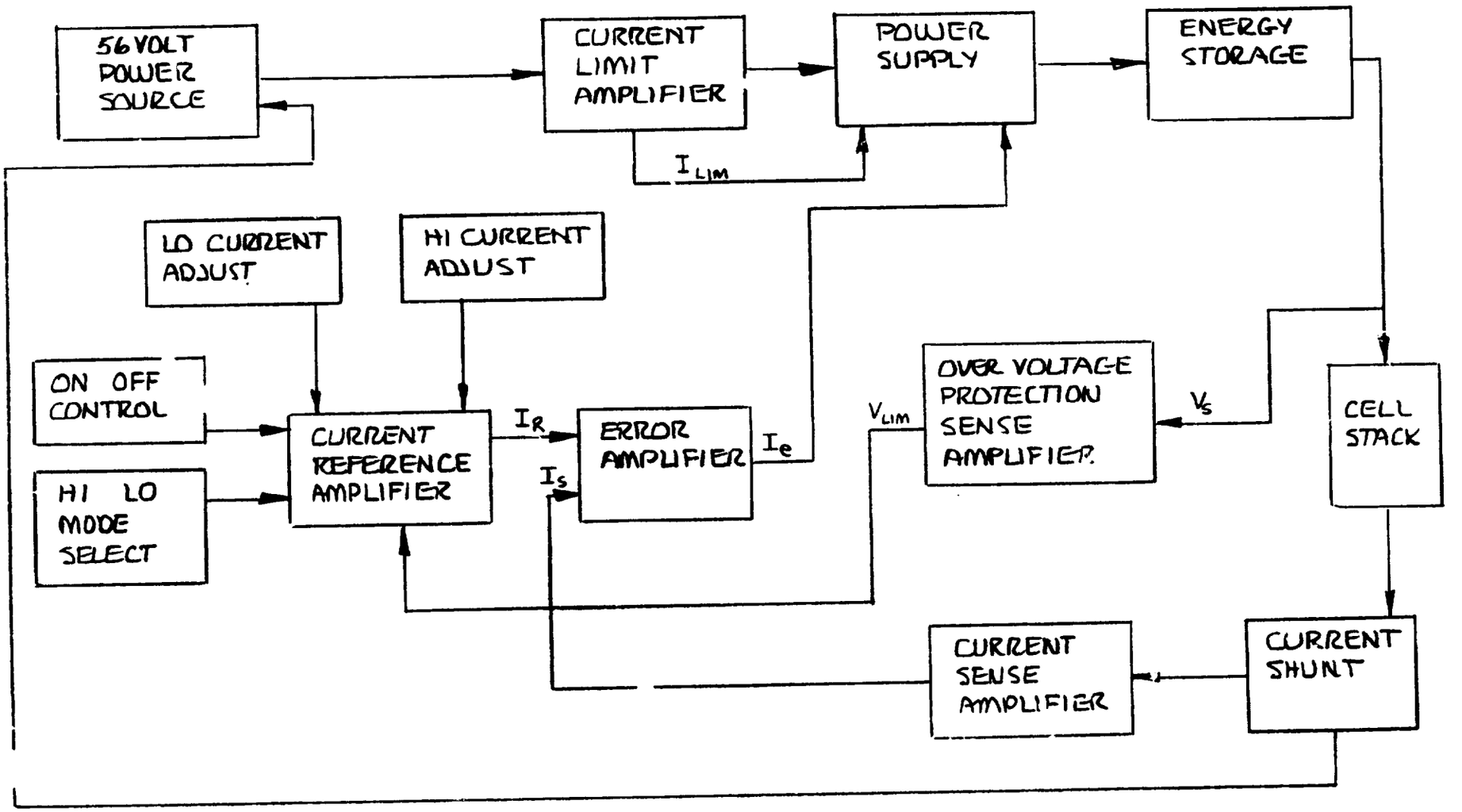

FIGURE 37 POWER CONTROLLER BLOCK DIAGRAM

The error amplifier is a circuit that compares two input signals and emits an output error signal proportional to the difference between the two inputs. In this case, current is sampled with the use of an in-line shunt. This signal is processed by a high common mode rejection configured sense amplifier whose output signal, I_s provides the 2nd input to the error amp. If the reference signal I_R, is larger than the sense signal, I_s, an error signal, I_e, is emitted which turns on the solid state power switch. Current is now allowed to flow into the energy storage network. This network controls the flow of current into the cell stack in that it allows the current to increase linearly. When the sense current signal, I_s, equals the reference signal, error signal, I_e, goes to zero and turns the power switch off. The energy storage network then releases its stored energy into the cell stack When the current falls below the reference signal level, the power switch is again turned on and this cycle continues to repeat. In summary, the cell stack current is continuously compared against a reference signal and the power switch is turned on and off to provide an average constant current to the cell stack.

Cell stack voltage is monitored by the overvoltage protection sense amplifier. If the stack voltage exceeds a fixed limit, a voltage limit signal, V_{lim}, is emitted and commands the current reference amplifier to lower the reference signal to a value as required to force the stack voltage below the maximum permitted value.

Test Results

Following fabrication of the power controller, the unit was bench tested and then installed into the cell stack test station. Due to an extremely tight schedule, complete development performance testing of the unit was not performed.

The bench test was performed using a resistive/capacitive load which electrically simulated the cell stack load. Several minor problems were encountered but were immediately corrected. The unit responded correctly to on/off and hi/lo commands. The power conversion efficiency of the unit was obtained from direct electrical measurements of load voltage and current vs supply voltage and current. The results of those tests are tabulated below:

Mode	Source	I	V	Power	Eff
High	Output	14.8a	45.5v	672w	92%
	Input	13a	56v	730w	
Low	Output	7.5a	39.2v	295w	94%
	Input	5.6a	56v	314w	

Table 11 Bench Test Power Conversion Efficiency

The high mode current of 21.75 amps was not attempted due to the use of a 56 VDC, 15 amp power supply. A 25 amp power source was not available at the time. The controller was then installed into the cell stack test station.

Power was applied to the system. The low mode current was adjusted to a nominal 7.5 amps. A satisfactory adjustment of the high mode current of 21.75 amps was not obtained. A value of approximately 18 amps was the maximum that could be obtained while still maintaining moderate control. A higher setting adjustment on the trimpot caused eratic operation. The power conversion efficiency measurements also indicated submarginal performance. These values are illustrated in Table II below.

Mode	Source	I	V	Power	Eff
High	Output	18.6a	43.6v	810w	84%
	Input	17.25a	56v	960w	
	Output	7.5a	37.54v	282w	90%
	Input	5.8a	56v	325w	

Table 12 Test Station Power Conversion Efficiency

Since the symptoms indicated that an indepth trouble shooting procedure would be required to yield a diagnosis of the problem and since the abnormality did not exhibit a potential safety hazard, a decision to "Run-As-Is" was made.

2.2.6 Water and Hydrazine Feed Tanks

Design

The two feed tanks are part of the special laboratory support equipment and are not intended as flight prototype hardware. Their purpose is to provide a feed capability for the prototype module. Analysis of the use of the feed tanks resulted in the following design.

All the metallic parts of both tanks are 304 stainless steel. Cover o-rings are ethylene propylene. Nominal liquid capacity of the $N_2H_4 \cdot H_2O$ tank is 3.79L (1 gal) plus a 1.4L (.3 gal) gas space above the liquid. The water tank has a nominal volume of 6.62L (1.75 gal) plus a .95L (.25 gal) gas space. The gas space is to preclude the possibility of liquid being drawn out the vent line should overpressure cause the relief valves to operate.

Both tanks are pressure vessels whose design and maximum working pressures are 172 kN/M^2 (25 psi). Both tanks are to be proof tested to 1.5 times the working pressure, 259 kN/M^2 (37.5 psi). Nominal working pressure is 138 kN/M^2 (20 psi).

The body of the tanks could have been made of either seamless or welded tube with the cover flange and bottom closure being welded on. Any welds which "show" on the inside of the N_2H_4 tank should be cleaned and polished to remove all oxides.

The cover for each tank must be removable. The inlet and outlet of each tank will be in the cover with the outlet incorporating a dip tube. Any fittings installed in the cover will be either o-ring seal type or welded. The cover is sealed with an o-ring.

The tanks will be used with the cylindrical axis vertical and the cover end up.

Fabrication

No problems were encountered during fabrication although one design change was made before fabrication was complete. The cover seal o-ring groove was moved from the cover flange to the cover itself. This was done to remove the discontinuity from the cover flange and to simplify machining.

Proof Testing

Both tanks were tested simultaneously. The test setup is shown in Figure 38.

The covers were secured in place and both tanks filled completely with water. They were then pressurized with GN_2 to 259 kN/M^2 (37.5 psi) and allowed to sit pressurized over night. By morning the pressure had dropped to about 103 kN/M^2 (15 psi). A plumbing leak was found and corrected. The tanks were pressurized and allowed to sit for 6 hours. Proof testing was witnessed and signed off by Q.A.

The completed hydrazine tank is shown in Figure 39.

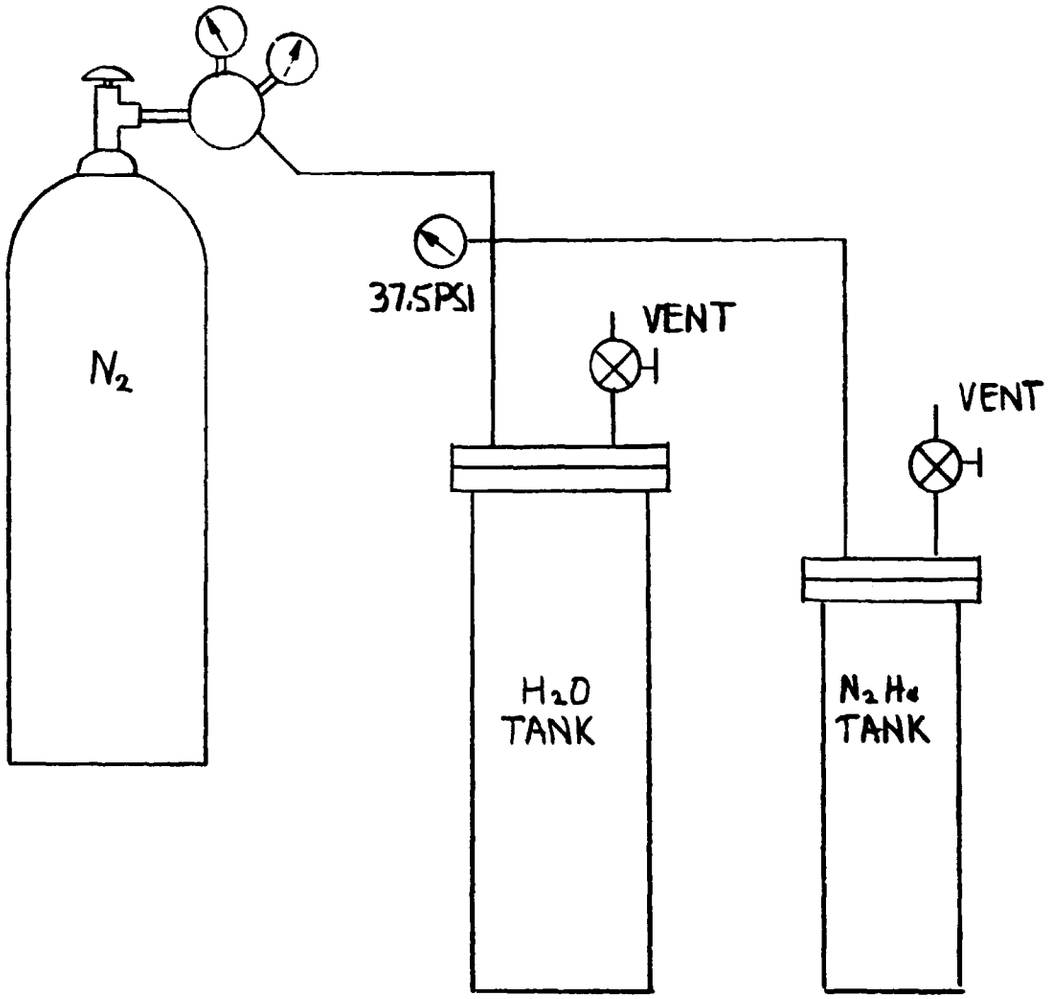

FIGURE 38 PROOF TEST, N_2H_4, H_2O FEED TANKS

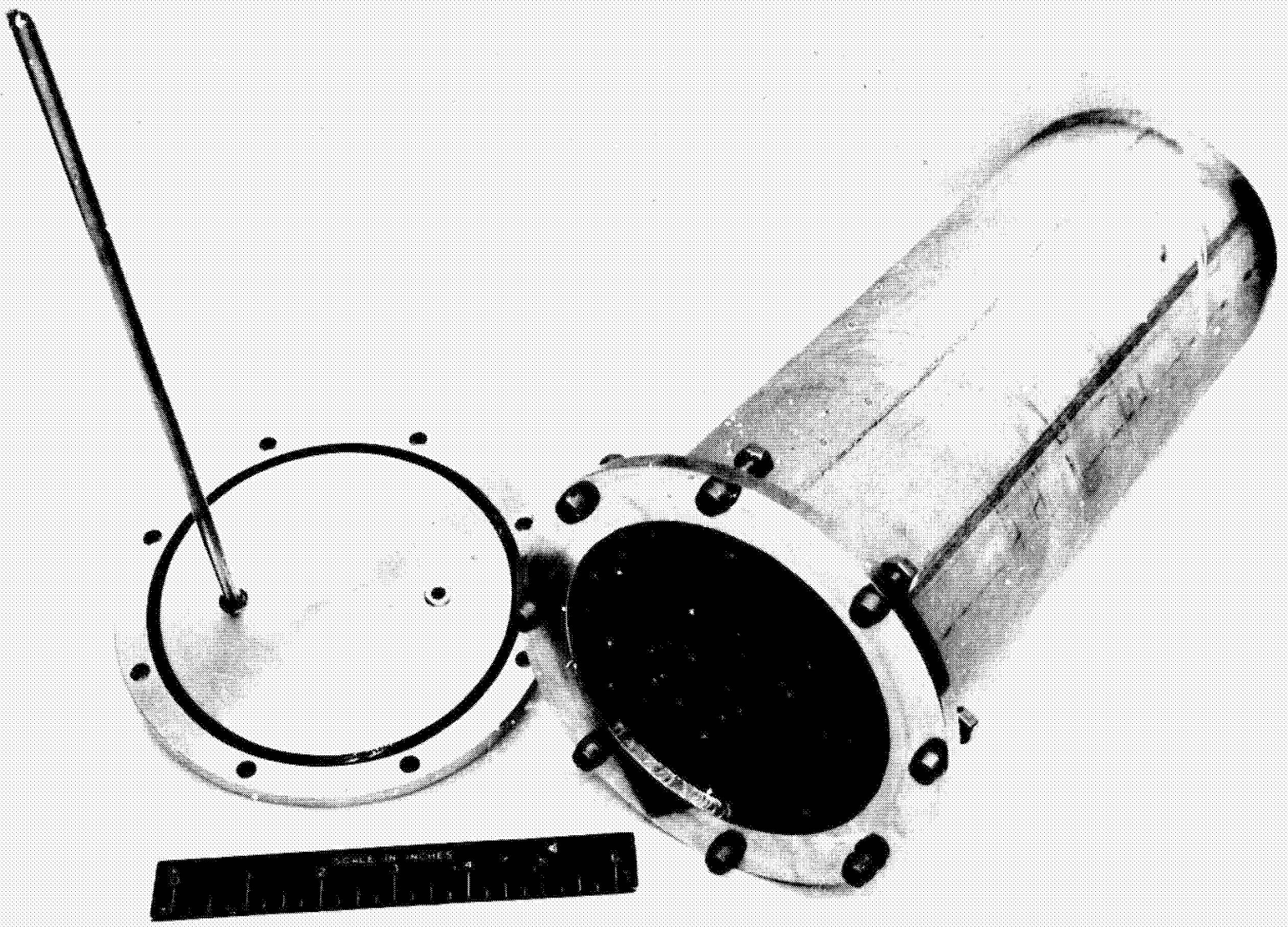

FIGURE 39 HYDRAZINE FEED TANK

2.3 Prototype Assembly and Testing

Module assembly started with the forming of the stainless steel N_2 purge lines, reservoir N_2 supply line, H_2O and N_2H_4 input lines, the "BURP" tank (3/8 in. 0.10 line) and the pump/bubble separator gas outlet line. The installation of the electrolyte drain valve (for test purposes only) and the seven Allied shut off valves was accomplished at the same time. The reservoir, pump/bubble separator and fluorocarbon 3-way valves were temporarily installed to insure that there was no interference between components. Next, all module internal wiring (except cell stack) was completed and all wires were terminated on two terminal strips mounted on what would be the upper edge of the baseplate. See Figure 40. At this point all solenoid valves were checked for proper operation and that the "power off" position of each valve was correct.

A cross-sectional sketch of the assembled cell stack was made for and used as an aid in the assembly of the cell stack (Figure 41). This sketch is further useful in that it lists all cell stack parts, the number of each part required and defines the electrical path through the stack. Cell stack assembly, although not particularly difficult, proved to be time consuming. Since no special clamping jigs were made for stack assembly, three people were required to implement the assembly procedure. Two performed the actual assembly and the third insured that no o-rings were left out. (Each of the 45 spacers has eight o-rings and the header has six.) This makes a total of 366 o-rings in the cell stack. As might be expected, a missing o-ring may be easily overlooked by those assembling the stack.

Once the stack assembly was completed, the stack was moved to the test station. The test station structure was modified to accept the module.

FIGURE 40 MODULE EXTERNAL LINES

N = Nº OF CELLS	22
2N = Nº OF ELECTRODES	44
N = Nº OF ANODES	22
N = Nº OF CATHODES	22
N+1 = Nº OF RIMS BENT OPPOSITE (O)	23
N-1 = Nº OF RIMS BENT SAME (S)	21
N÷2 = Nº OF CATHODES (O) = CATHODES (S)	11
N÷2+1 = Nº OF ANODES (O)	12
N÷2-1 = Nº OF ANODES (S)	10
N+1 = ELECTRODES WITH RUBBER BUMPERS	23
ALL ANODE (O) HAVE RUBBER BUMPERS	12
ALL CATHODE (O) HAVE RUBBER BUMPERS	11
N = Nº LIQUID SPACERS	22
N+1 = Nº GAS SPACERS	23

EVEN Nº OF CELLS PROVIDES SAME GAS AT BOTH ENDS OF STACK

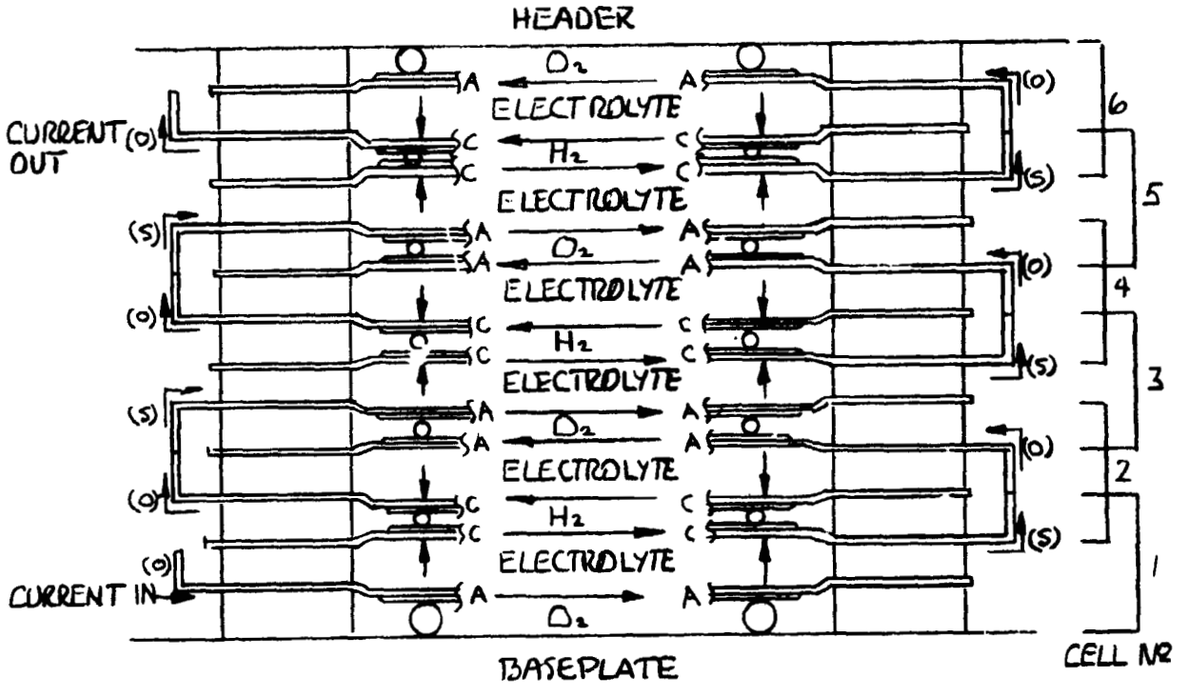

Figure 41 Cell Stack Build Up

The original intent had been to fill the module via the drain valve. However, the first filling attempt with water proved this approach impractical due to entrapped air. A second shut off valve was added to the electrolyte line between the reservoir outlet and the cell stack header inlet. At the same time a pressure gage was installed in the same line and was later used to verify the gas/electrolyte Δ P across the reservoir.

When filling the module via the cell stack header, most of the entrapped air can be bled off through the pump/bubble separator gas out valve. Since no purge is applied during the initial stages of module fill, the gas spacers flood. This insures thorough wetting of the Acropor membrane, asbestos and catalyst. Further, it places an excess of fluid in the system which allows any remaining entrapped air to be removed as follows (item numbers in text refer to circled numbers on diagram Figure 42):

(1) Activate system power, Figure 43 but insure safety override, N_2H_4, H_2O, N_2 purge are module and all off.

(2) Set P/Bs motor and valve control switches (Fig. 6) to "Auto". Leave power off.

(3) Note that the reservoir position indicator (Fig. 43) show maximum volume position and the control panel shows a high volume shutdown light.

(4) Move safety override switch to on and note yellow light.

(5) Apply 20.68-27.58 kN/M^2 (3-4 PSI) nitrogen pressure to the module (item 10). This pressurizes the reservoir and starts the purge of the gas spacers.

(6) Apply power to the pump/bubble separator. Trapped gas in the electrolyte loop will be removed and dumped as long as the blue indicator light under "Valve Control", Fig. 6 is on. Once the light goes out or cycles infrequently, fill procedure may continue. During this procedure, the reservoir level indicator may or may not drop. It should return to maximum volume when the P/Bs stops dumping gas.

(7) Excess liquid being held in the gas spacers must now be removed. This is accomplished by draining liquid out of the module via the drain valve (Item 19). Drain liquid slowly until the reservoir indicator reads approximately zero. Close the drain valve and observe the reservoir indicator. If it rises, let it do so until it stops or shows maximum volume. Repeat this procedure until the reservoir indicator no longer rises when the drain valve is closed. The module is now full and contains approximately 1.4 liters of liquid.

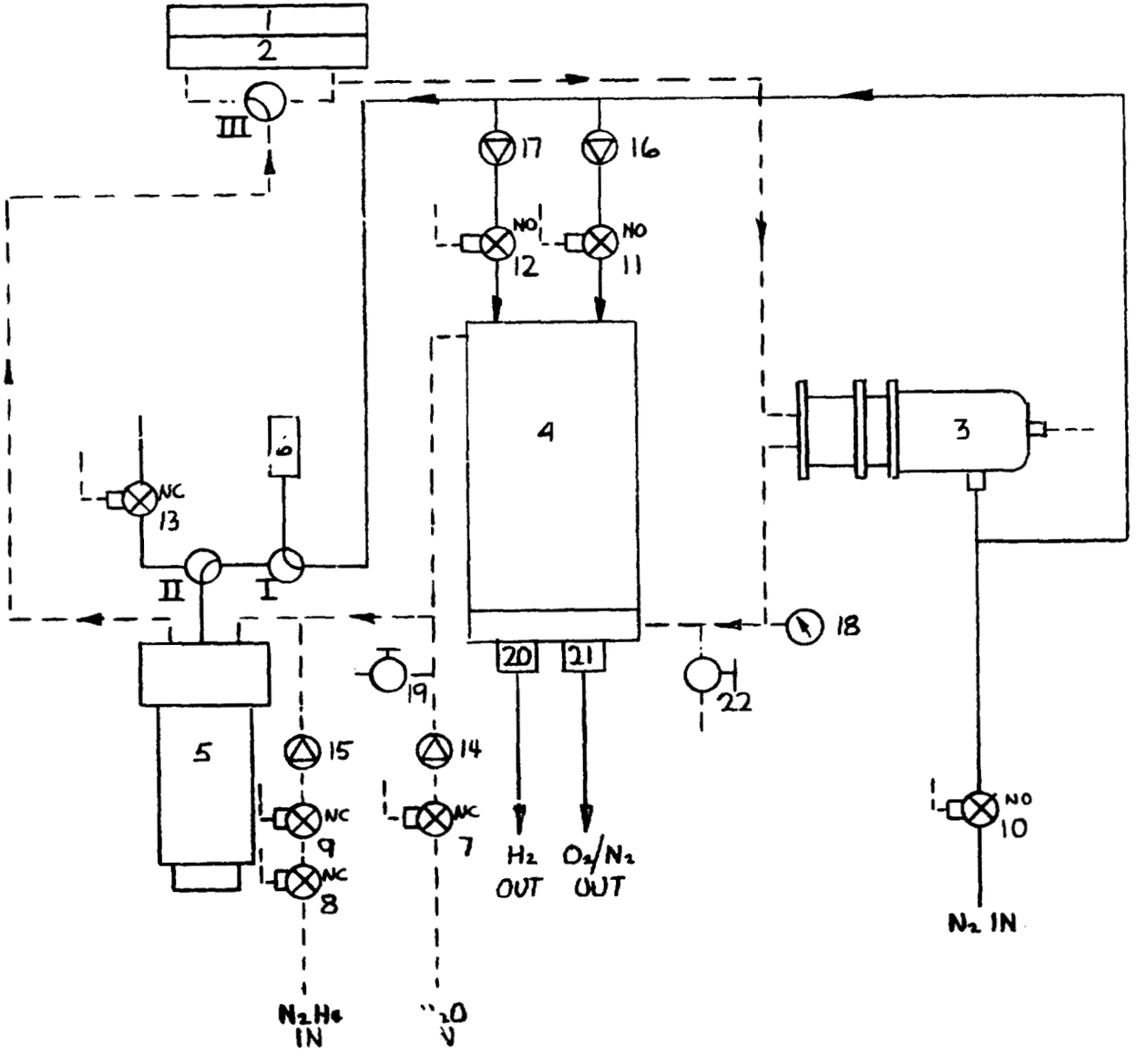

1 COOLER
2 HX
3 RESERVOIR
4 CELL STACK
5 P/BS
6 "BURP TANK"
I 3 WAY SOLENOID
II " "
III " "
7 H_2O FEED SHUT OFF
8 N_2H_4 FEED SHUT OFF
9 " " " "
10 N_2 SUPPLY SHUT OFF
11 N_2 PURGE SHUT OFF
12 " " " "
13 GAS OUT, P/BS CONTROL
14 CHECK VALVE
15 " "
16 " "
17 " "
18 PRESS. GAGE. STACK INLET
19 DRAIN & C.O. VALVE
20 ΔP REGULATOR
21 " "
22 FILL VALVE

Figure 42 "As Built" Hydraulic and Gas Schematic

Figure 43 System Test Control Panel

Upon filling the module with water and raising the N_2 control pressure to about 68.95 kN/M^2 (10 PSI), it became obvious that there was an internal gas leak. Close inspection of the baseplate indicated that the leak was within the cell stack. Also a liquid leak was discovered which suggested that the bond had failed between a heat exchanger mounting boss and the baseplate.

The module was removed from the test stand in order to make repairs.

Both heat exchanger mounting bosses showed bond failures. This was corrected by removing both bosses, machining o-ring grooves around the boss ports and bolting the cold plate - heat exchanger - boss assembly through the baseplate, using existing bolt holes.

The hunt for and correction of the leak in the cell stack was not so simple. The cell stack was carefully diassembled piece by piece to determine if any o-rings were missing or improperly positioned. Such was not the case.

It was eventually determined that there were two modes of gas leakage through the Acropor: (1) the Acropor had been punctured in two places. These punctures were plugged with epoxy resin. (2) The Acropor itself was leaking because it was not being wetted thoroughly. (Acropor does not act as a gas barrier unless it is wetted.) New Acropor samples were immersed in water and 30% KOH and found to wet unevenly as evidenced by a chalky appearance where wetting was incomplete. The Acropor was cleaned with propanol rinsed with water, but then it was impossible to wet the Acropor again after it was allowed to dry. At this point Gelman Instrument was contacted and it was learned that new Acropor contains a wetting agent which was removed by the propanol, but that the propanol had no effect on the Acropor performance, once it was wet.

In the mean time a system and procedure had been developed to inspect for and locate any Acropor associated leaks in the electrolyte spacer assemblies. All electrolyte spacers were inspected and found to be free of any leaks when thoroughly wet.

Two things should be pointed out here: (1) There must be no residual propanol left in the Aeropor since it will burn if it comes in contact with the catalyst. Once cleaned with propanol, which also acts as an excellent wetting agent, each electrolyte spacer must be thoroughly rinsed with distilled H_2O and kept wet to insure wetting within the stack. This of course means that the stack must be assembled wet.

The cell stack and module were reassembled and remounted in the test station. Test station modifications and wiring were completed and the module was again ready for pressure and leak checks. These tests showed no internal or external leaks. Checks were also made to verify the control and function of all components involved in the module and test setup except the power controller which had to await the addition of electrolyte to the systems. The module was drained of water and filled with 30% KOH.

Module Testing

All module and test functions except the power controller were activated and found to be operating properly. Power was applied to the power controller and the current level set procedure started, low mode first. Low mode level is one third the high mode level (21.75A) and equals 7.25A. These values produce a current density of 150 MA/cm^2 high mode and 50 MA/cm^2 low mode. Low mode was set and held successfully. High mode could not, however, be set above 19.5A. The power controller was shut down and an in-place circuit and component check was performed. The check revealed two minor problems which were corrected, but which should not have had any effect on the high mode performance. It was concluded that no damage to the power controller would result from setting it at 18.5A and running the module at that level. Upon receiving NASA approval to do so, the module test was started.

C - 2

As can be seen on Figures 44 and 45 the first 260 hours of testing were uneventful. Except for adding water to the feed tank, changing N_2 supply bottles as necessary and collecting and plotting data the system operated unattended. It should be noted that the total and cell voltages were essentially stable by ten hours and completely stable by 140 hours. At 260 hours (Saturday afternoon) a power controller malfunction placed the high mode current at about 25 amp. Between Saturday afternoon and Monday morning the cell stock accumulated a total of about 9 hours of running at 25 amps. Using the voltages acquired at 25 amps, a three point plot was made to predict the total stack voltage required had the stack run at 21.75 amps. The plot, Figure 46, indicates a voltage of about 46.3 volts. This is somewhat higher than desired, producing an average cell voltage of 2.1 volts. 1.95-2.0 volts per cell was the goal although 2.05 volts is considered acceptable. Although it cannot be proven, the higher voltages are attributed to the cathodes, based on single cell tests. Figure 47 shows a sample of the current data collected during the power controller malfunction. It will be noted that the low mode current continued to function normally. A section of the normal current trace is shown in Figure 48. The power supply was set to limit at 19.5 amps to preclude further operation at the high current.

At 496 hours it was noted that the P/Bs was dumping gas at a rate of 3 times per minute. Inspection of the P/Bs inlet passage showed large quantities of gas to be coming from the cell stack outlet. The gas being discharged was analyzed and found to be predominantly hydrogen. This suggested an Acropor leak. Although this leak effectively precluded any hydrazine testing, it was decided to allow the test to continue as long as the P/Bs could handle it. The P/Bs gas discharge was immediately connected through a liquid trap to the hood where it was discharged along with the rest of the hydrogen being generated. By 640 hours the leak had increased so that the P/Bs was discharging gas 12 times per minute.

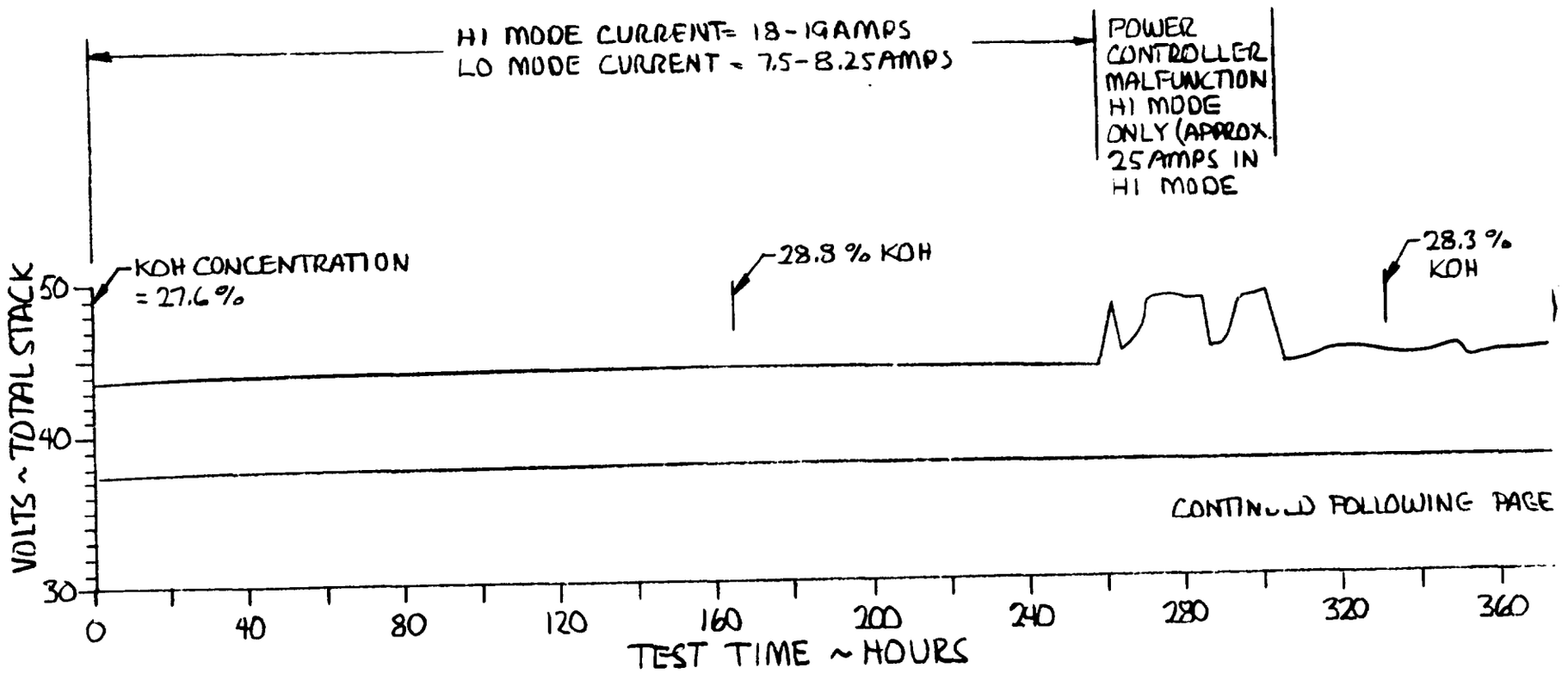

Figure 44 Prototype Module Test

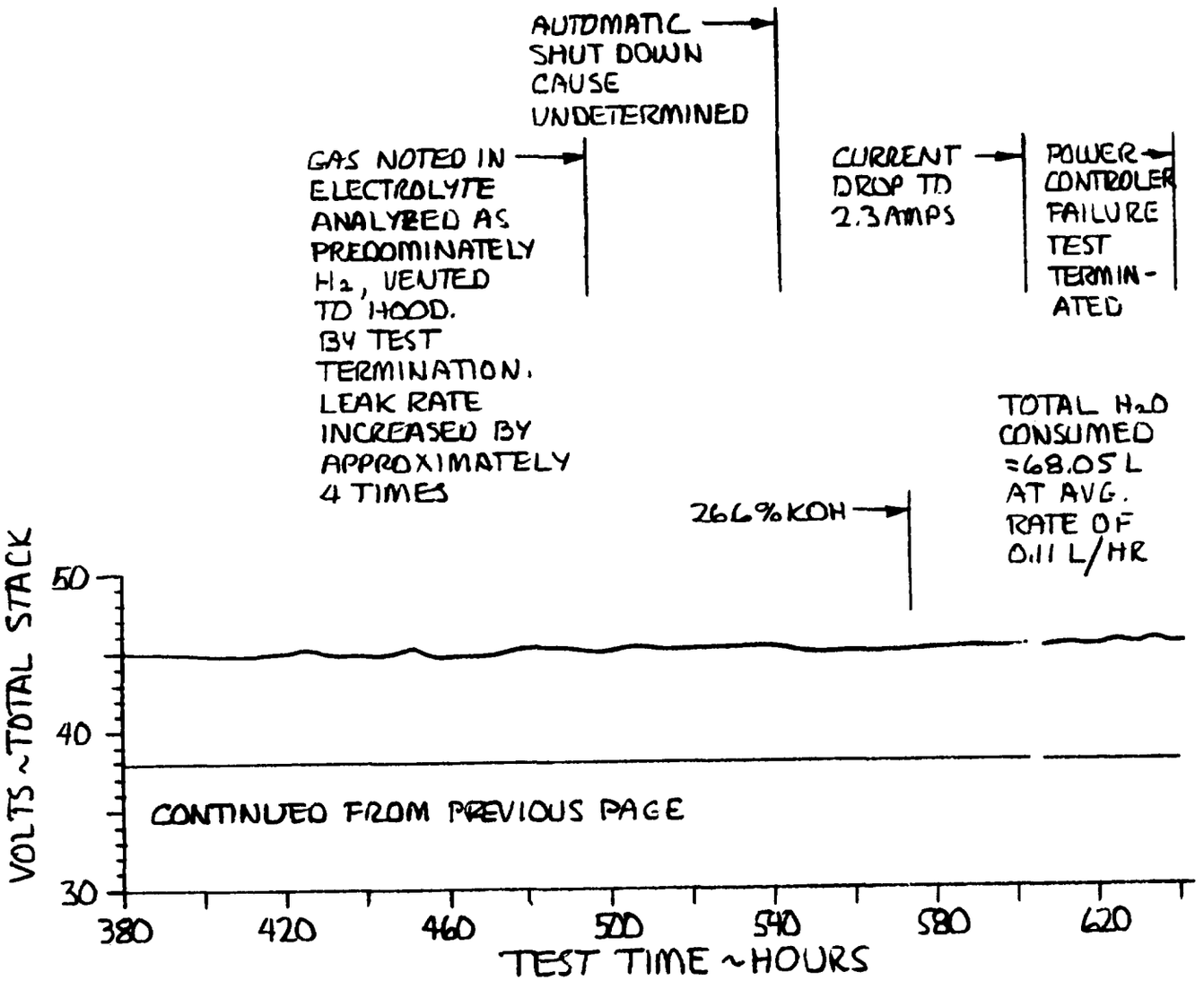

Figure 44a Prototype Module Test

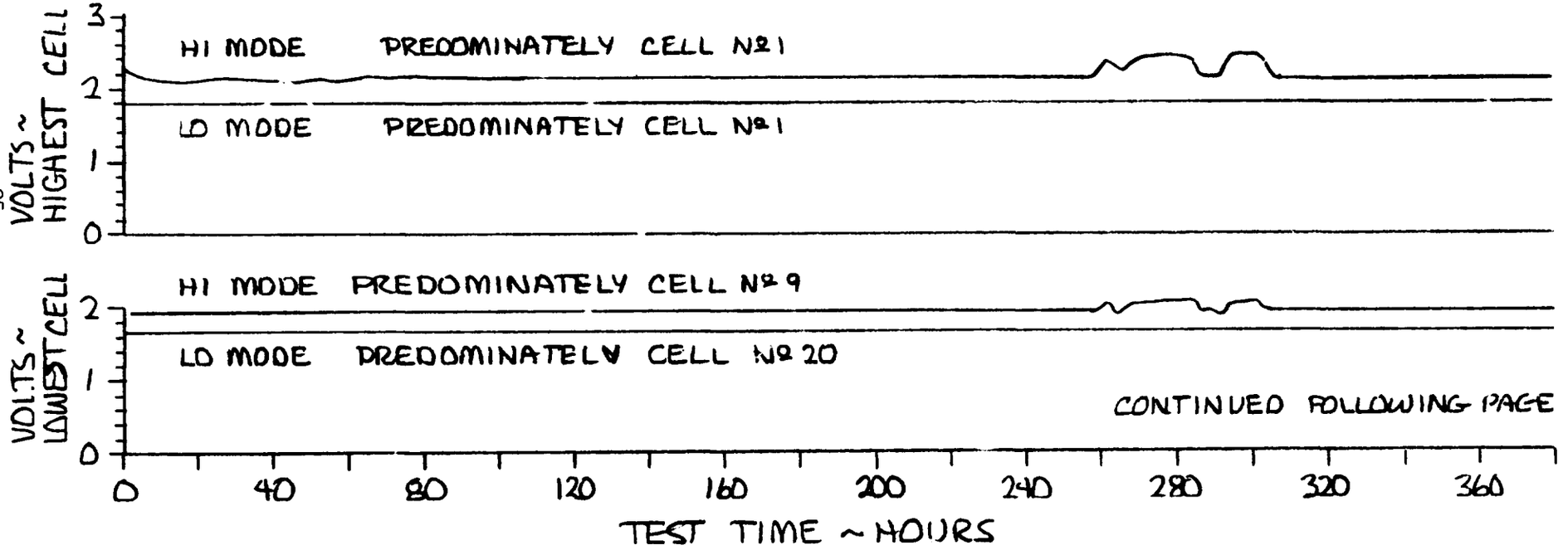

Figure 45 Hi and Lo Cell Performance Prototype Module Test

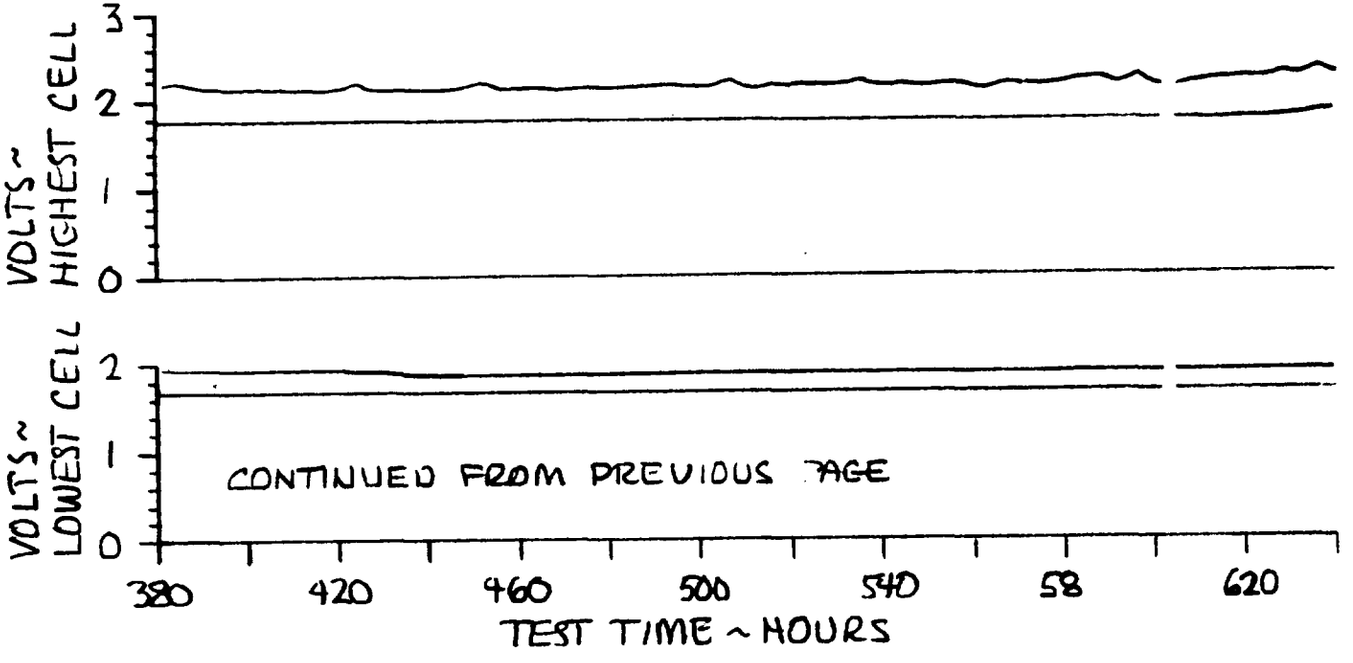

Figure 45a Hi and Lo Cell Performance, Prototype Module Test

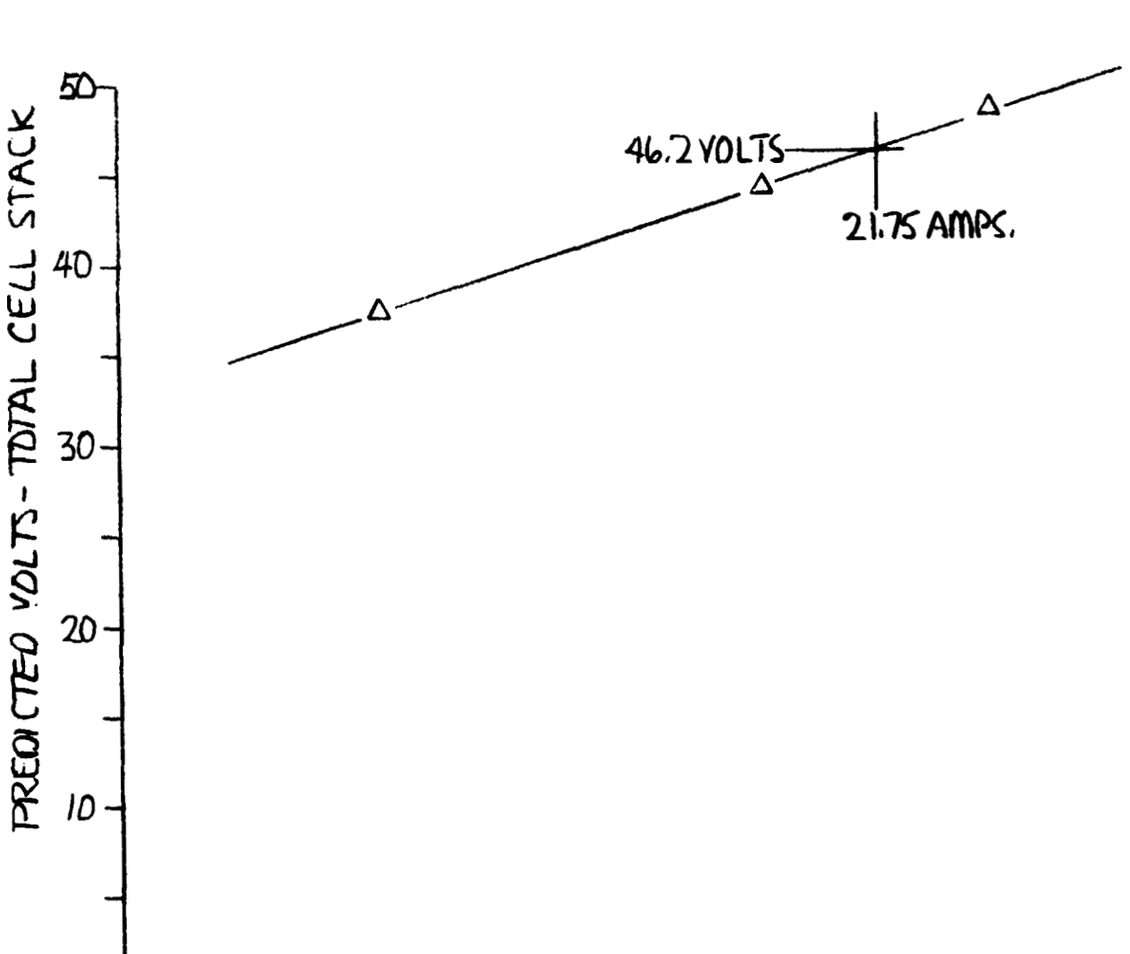

Figure 46 Predicted Cell Stack Voltage Hi Mode

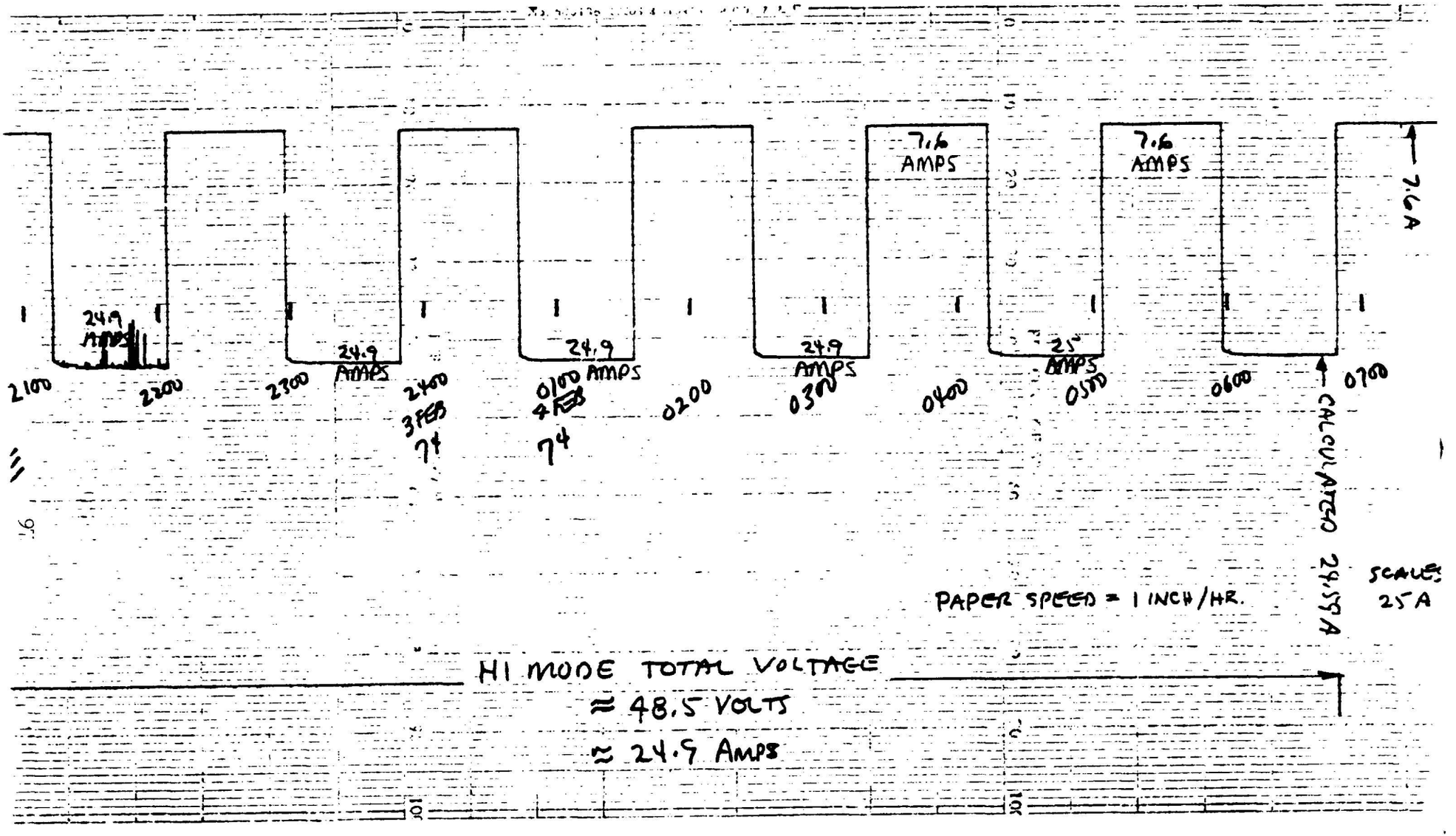

Figure 47 Cell Stack Current
During Power Controller
Malfunction

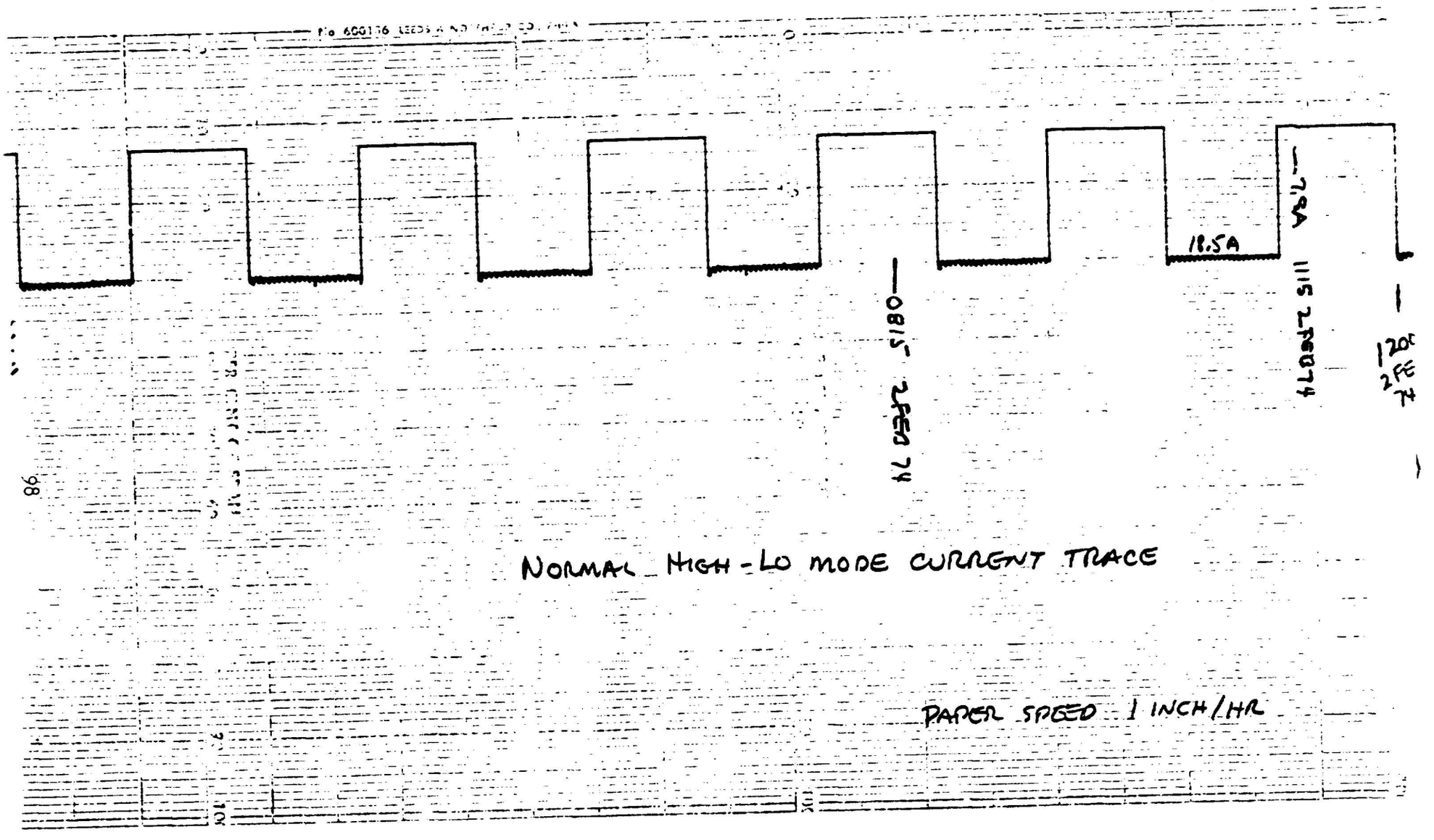

Figure 48 Cell Stack Current,
Normal Operation

The power controller malfunctioned again in the high mode at 543 hours with a resulting system shut down. The test was restarted approximately 25 minutes later and continued satisfactorily until at 641 hours the power controller failed completely and the test was terminated.

Except for the fact that no hydrazine testing was accomplished, the module generally performed well. A total of 68 liters (18 gallons) of H_2O was consumed at an almost constant high-low mode average rate of 0.11 liters per hour (0.03 gallons/hour).

COMPUTER MATH MODEL

A point steady state math model of the hydrazine electrolysis module was developed and is intended as a first step toward eventual simulation of real duty cycles. With this model overall heat and mass balances can be calculated. Certain dependent variables are predicted from empirical and theoretical data. The steps in the development of the model are discussed in this section. Use was made of experimental data obtained in previous hydrazine and water electrolysis programs and is so referenced in the text.

Reaction Mechanisms

The well-known half-cell reactions that occur in an alkaline electrolysis cell proceed according to:

$$\text{Anode: } 4OH \longrightarrow O_2 + 2H_2O + 4e^-$$
$$\text{Cathode: } 4H_2O + 4e^- \longrightarrow 2H_2 + 4OH$$

The overall cell reaction is then:

$$2H_2O \longrightarrow 2H_2 + O_2$$

With the addition of hydrazine to the alkaline electrolysis cell, the following reactions occur[1]:

$$\text{Cathode: } N_2H_4 \longrightarrow N_2 + 2H_2$$
$$\text{Anode: } N_2H_4 \longrightarrow N_2 + 2H_2 \xrightarrow{O_2} N_2 + 2H_2O$$
$$\text{or } N_2H_4 + 4OH^- \longrightarrow N_2 + 4H_2O + 4e^-$$

These equations show the hydrazine reaction to be simple autocatalytic decomposition in the absence of the electrolysis reaction.

When electrolysis current is applied, however, the anodic reaction is influenced by the presence of oxygen. This effect can be defined by using the parameters, "a" a function of current to describe the oxygen concentration and, "x", a function of bulk hydrazine concentration to describe the anodic hydrazine concentration. The physical situation is defined by the following three equations:

$$a > x: \quad xN_2H_4 \longrightarrow xN_2 + 2xH_2 \xrightarrow{aO_2} xN_2 + (a-x)O_2 + 2xH_2O \qquad (1)$$

$$a = x: \quad xN_2H_4 \longrightarrow xN_2 + 2xH_2 \xrightarrow{XO_2} xN_2 + 2xH_2O \qquad (2)$$

$$a < x: \quad xN_2H_4 \longrightarrow xN_2 + 2xH_2 \xrightarrow{aO_2} xN_2 + 2(x-a)H_2 + 2aH_2O \qquad (3)$$

When x = 0, pure oxygen is being generated at the anode, and when a = 0, the reaction is the same as the cathodic hydrazine reaction. The relationship described by this equation is shown graphically in Figure 49.

Combining the anodic and cathodic reactions for both electr and hydrazine decomposition (in the region where $a > x$), the overall cell reaction becomes:

$$(x+y)N_2H_4 + 2(a-x)H_2O \longrightarrow (a-x)O_2 + (x+y)N_2 + 2(a+y)H_2 \qquad (4)$$

where x = N_2H_4 reacting at the anode
y = N_2H_4 reacting at the cathode
a = function of electrolysis current

The overall reaction and electrode reactions are shown in Figure 50.

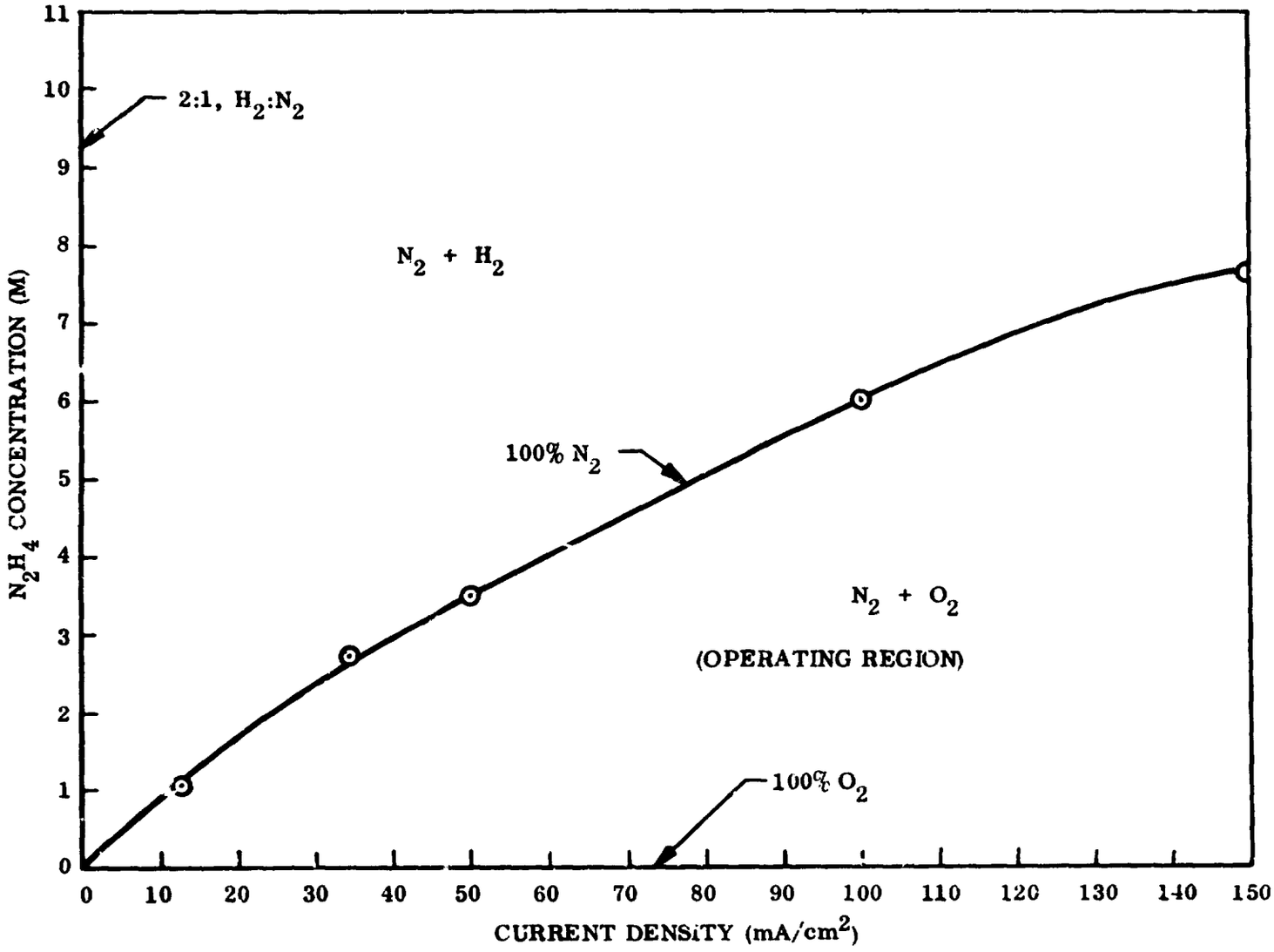

Figure 49 100% Nitrogen Equilibrium Curve

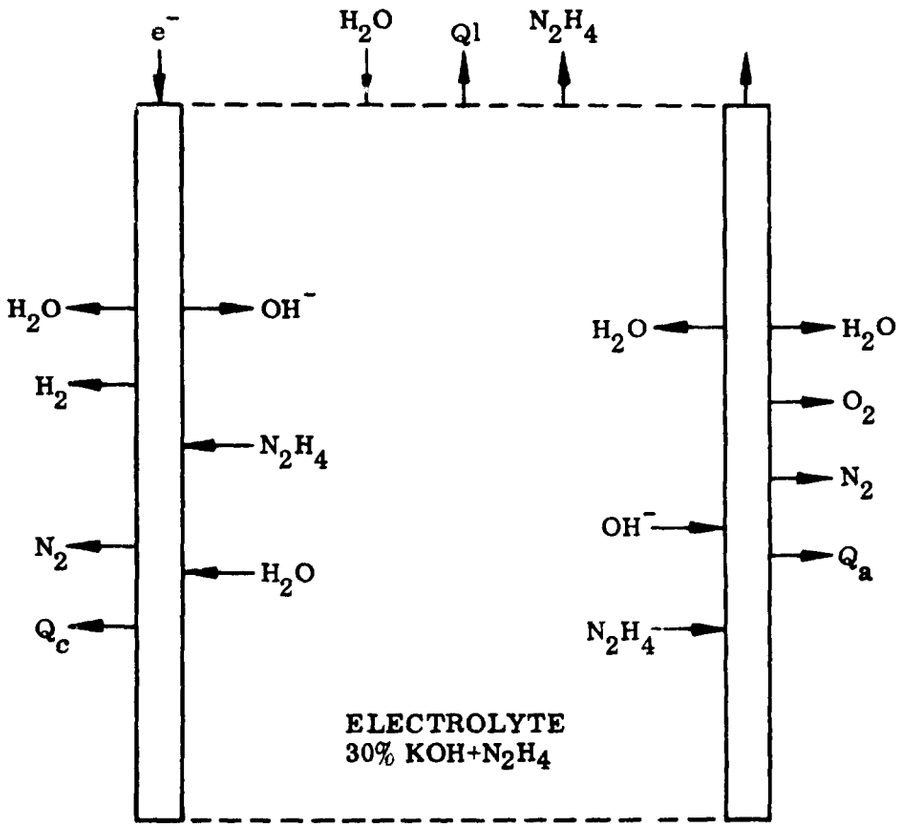

$4aH_2O+yN_2H_4+4ae^- \rightarrow ZaH_2+4aOH^-+yN_2+2yH_2$

$4aOH^-+xN_2H_4 \rightarrow (a-x)O_2+xN_2+2(a+x)H_2O+4ae^-$

OVERALL REACTION:

$(x+y)N_2H_4+2(a-x)H_2O+\text{electrical energy} \rightarrow (a-x)O_2\ (x+y)N_2+2(a+y)H_2+\text{heat}$

Figure 50 Overall and Electrode Reactions

For the purpose of developing the math model, the assumptions were made that (1) a x, i.e. operation in the region below the curve in Figure 49, and (2) x = 4y, i.e., 80% of the total hydrazine reacting at the anode. The limiting hydrazine concentration to maintain the condition of a x was experimentally determined to be[4]:

$$C_{max} = \frac{I}{A + I} \qquad (5)$$

where

C = hydrazine concentration (mols/liter)

I = applied current (mA/cm^2)

A = electrode area (cm^2)

and , . = experimentally determined constants.

The reaction rate of hydrazine is first order and follows:

$$\frac{dC}{dt} = Cm \qquad (6)$$

where, m, the rate constant, is a function of cell geometry, temperature, and operating current.

The variation in the rate constant with current density is shown in Figure 51.[4] The effect of temperature on the rate constant has not been well defined and for that reason will be considered negligible at this point in the model development.

The concentration of hydrazine in the cell at any point in time is defined by:

$$C = \frac{x}{m} + \left(C_o - \frac{x}{m}\right) \exp(-mnt/v)$$

where x = hydrazine feed rate

C_o = initial hydrazine concentration

n = number of cells

t = elapsed time

v = volume of electrolyte

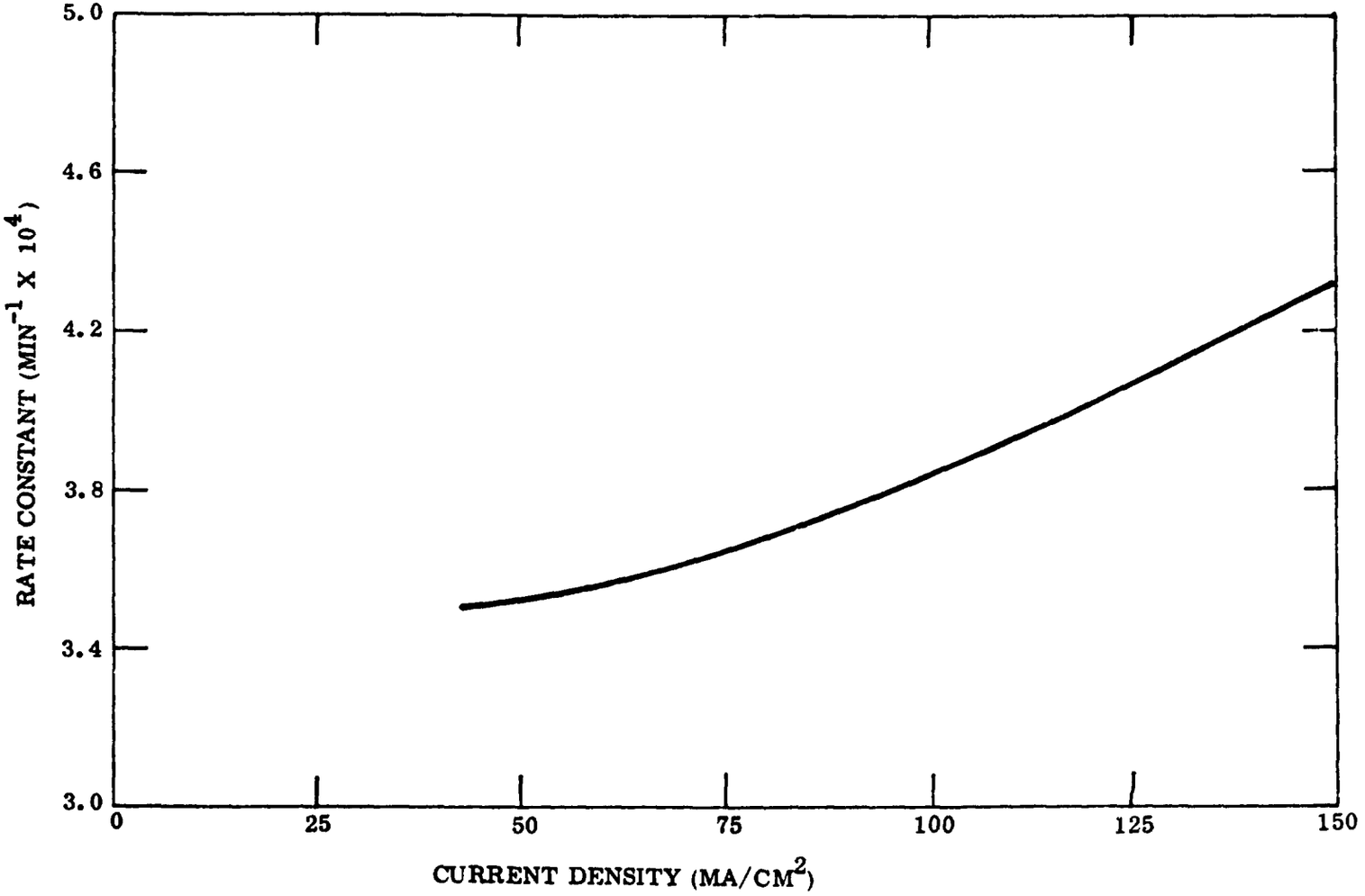

Fig. 51 Reaction Rate Constant vs. Current Density

Operating Variables

The controllable variables in the cell are the following:

a) hydrazine feed rate (X) which is a system control variable to affect the rate of nitrogen production.

b) electrolysis current density (I/A) which is a system control variable to affect the total gas production rate and the proportion of N_2/O_2.

c) temperature (T) which is a system design variable to optimize efficiency and electrical performance.

d) pressure (P) which is a system design variable to optimize system weight and interface compatibility.

e) electrolyte concentration (C_{KOH}) which is a system design variable to optimize electrical performance.

The dependent variables include:

a) hydrazine concentration in the cell

b) gas composition (% nitrogen and water vapor)

c) water consumption

d) cell voltage

e) cell electrical resistance

Hydrazine Concentration

Hydrazine concentration in the cell was shown earlier to be a complex function. For steady state conditions, however, it can be approximated by considering the exponential term to be negligible when t is very large. This leads to the simple relationship that $C = \frac{X}{m}$. While it is known to vary with cell geometry, temperature and current density, the total variation over the range of interest is less than a factor of two. Because of this the rate constant will be considered invariable except with respect to current density in developing the math model.

Gas Composition

The anodic gas composition is a function of several variables. The amount of nitrogen is determined by the hydrazine concentration and the current density and varies as:

$$\dot{U}_{N_2} = k_1 \, n \, C + k_2 \, n \, C \, \frac{I}{A} = \quad \text{gms/min}$$

The constants, k_1 and k_2 have been experimentally determined[5]; the equation then becomes:

$$\dot{U}_{N_2} = 4.8\ n\ C + 0.0134\ n\ C\ \frac{I}{A} = \text{gms/min} \qquad (8)$$

The total anodic gas generation rate is determined by Faraday's Law and can be expressed as

$$\dot{U}_T = knI = \text{gms/min} \qquad (9)$$

where $k = RT/FeP$

and F = Faraday's Constant

R = gas constant

T = temperature

P = pressure

The oxygen generation rate can be obtained by difference $\dot{U}_T - \dot{U}_{N_2} = \dot{U}_{O_2}$ (ignoring the water vapor contained with the mixture) or

$$\dot{U}_{O_2} = knI - 4.8nC - 0.0134nC\ \frac{I}{A} = \text{gms/min} \qquad (10)$$

The water vapor in the anodic gas can be expressed psychrometrically because the dewpoint of this gas is known[3]* to be equal to the operating cell temperature.

The nitrogen content of the cathodic gas will be 20 percent of the volumetric amount of nitrogen at the anode because of the earlier assumption of an 80% anodic hydrazine conversion efficiency. The amount of hydrogen will be, according to Faraday's Law and the above hydrazine conversion assumption.

$$\dot{U}_{H_2} = 2nkI + 0.4\ \dot{U}_{N_2} = \text{gms/min} \qquad (11)$$

---

*at KOH concentration of 30%

The first term is the electrochemically generated hydrogen. The second term is the hydrogen produced from the decomposition of hydrazine. Experimental dewpoint data, as shown in Figure 52, are used to determine the water vapor content of the cathodic gas.

Water Consumption

Water consumption consists of the net electrolyzed water and water lost in the generated gas streams. It will vary with hydrazine concentration, current density and temperature. On a molar basis it can be expressed as

$$\dot{U}_{H_2O} = 2\,\dot{U}_{O_2} + f(T_a) + f(T_c) = gms/min \qquad (12)$$

where the first term is the net water consumed by electrolysis, and the second and third terms are the evaporative losses in the generated gases.

Cell Voltage

The cell voltage is made up of several elements with several dependencies. The overall cell voltage is expressed as

$$V_c = V^o + {}_{O_2} + {}_{H_2} + IR = volts \qquad (13)$$

where

N_{O_2} = anode operating over potential (or voltage drop)

N_{H_2} = cathode operating over potential (or voltage drop)

IR = cell electrolyte voltage drop

The first term, V^o, is the theoretical potential of the cell and is described by the Nernst equation as

$$V^o = \frac{{}^2H_2O - O_2 - {}^2H_2}{4F} + \frac{RT}{4F} \ln \frac{a^2H_2O}{P_{O_2}\,P_{H_2}} = volts \qquad (14)$$

At standard conditions (25°C and 1 atm) this equation reduces to

$$V^o = +1.23 + 0 = volts$$

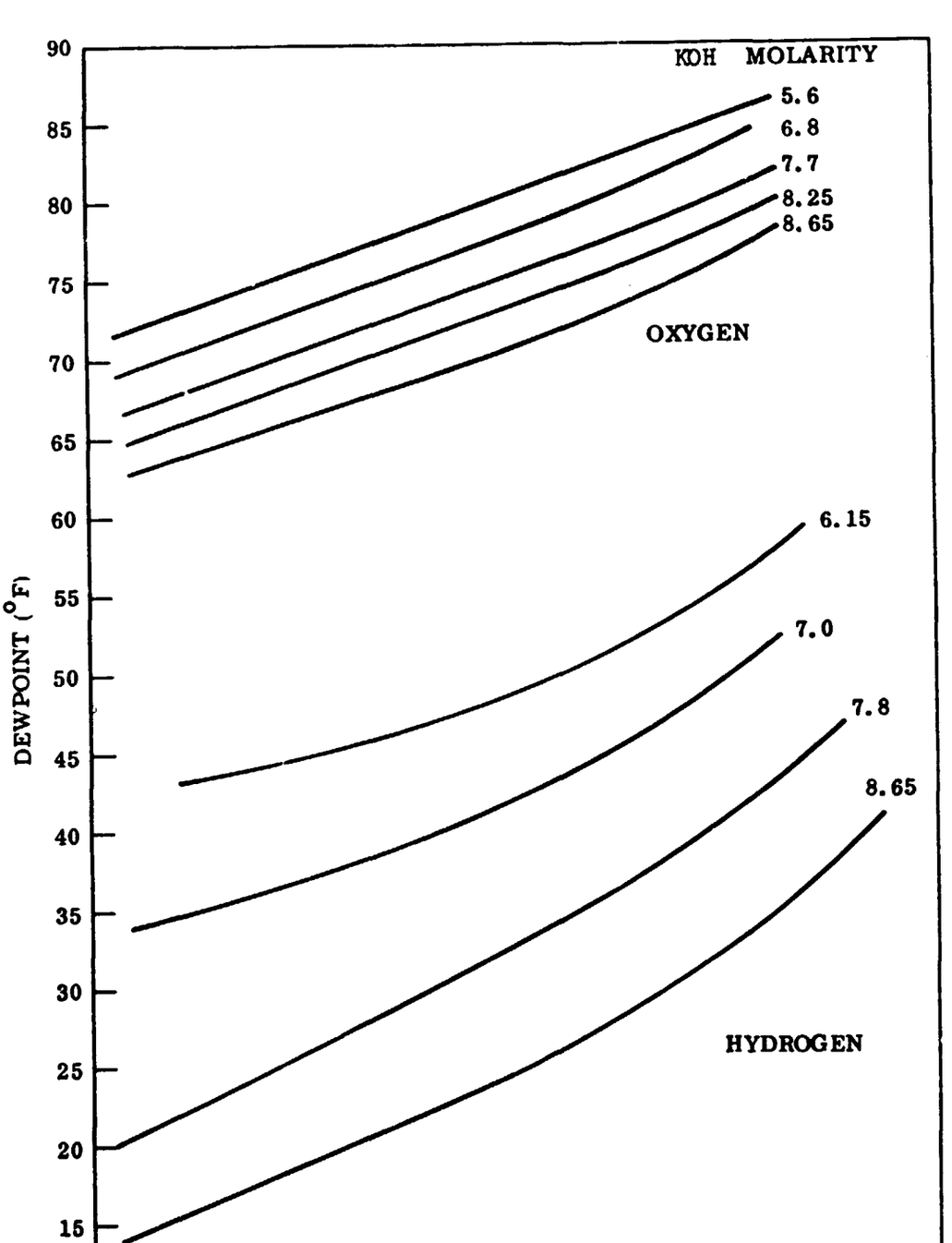

Figure 52 Effluent Gas Dewpoints

At other than standard conditions, e.g., at higher or lower pressures, the theoretical potential will vary according to the second term in the Nernst equation. An example Pourbaix[6] diagram is shown in Figure 53 to illustrate the pressure effect. Note that pH has no effect on V°. This follows since there is no pH term in the Nernst equation for this electrode pair.

The relationship between the theoretical reversible cell potential, temperature and heat of reaction can be obtained from the Gibbs-Helmholtz equation,

$$F - H = T \left[\partial(\Delta F)/\partial T\right]_P \tag{15}$$

Substituting for ΔF its equivalent, $-nFV^{\circ}$, we have under conditions of constant pressure

$$\Delta H = -nFV^{\circ} + nFT(\partial V^{\circ}/\partial T)_P \tag{16}$$

$$\text{and } (\partial V^{\circ}/\partial T)_P = (\Delta H/nFT) + (V^{\circ}/T) \tag{17}$$

The contributions of electrode overvoltages and cell IR to the total cell voltage cannot be predicted mathematically because they will vary with the nature and composition of the electrodes and the cell geometry. Their effects on the thermodynamics of the system can, however, be determined indirectly by voltage difference. A short derivation follows to explain the technique.

For a system at constant pressure with electrical work, the first law of thermodynamics can be written as

$$\Delta H = \Delta Q - \Delta WE \tag{18}$$

where ΔH = system enthalpy

ΔQ = heat added to the system

ΔWe = work done on the environment

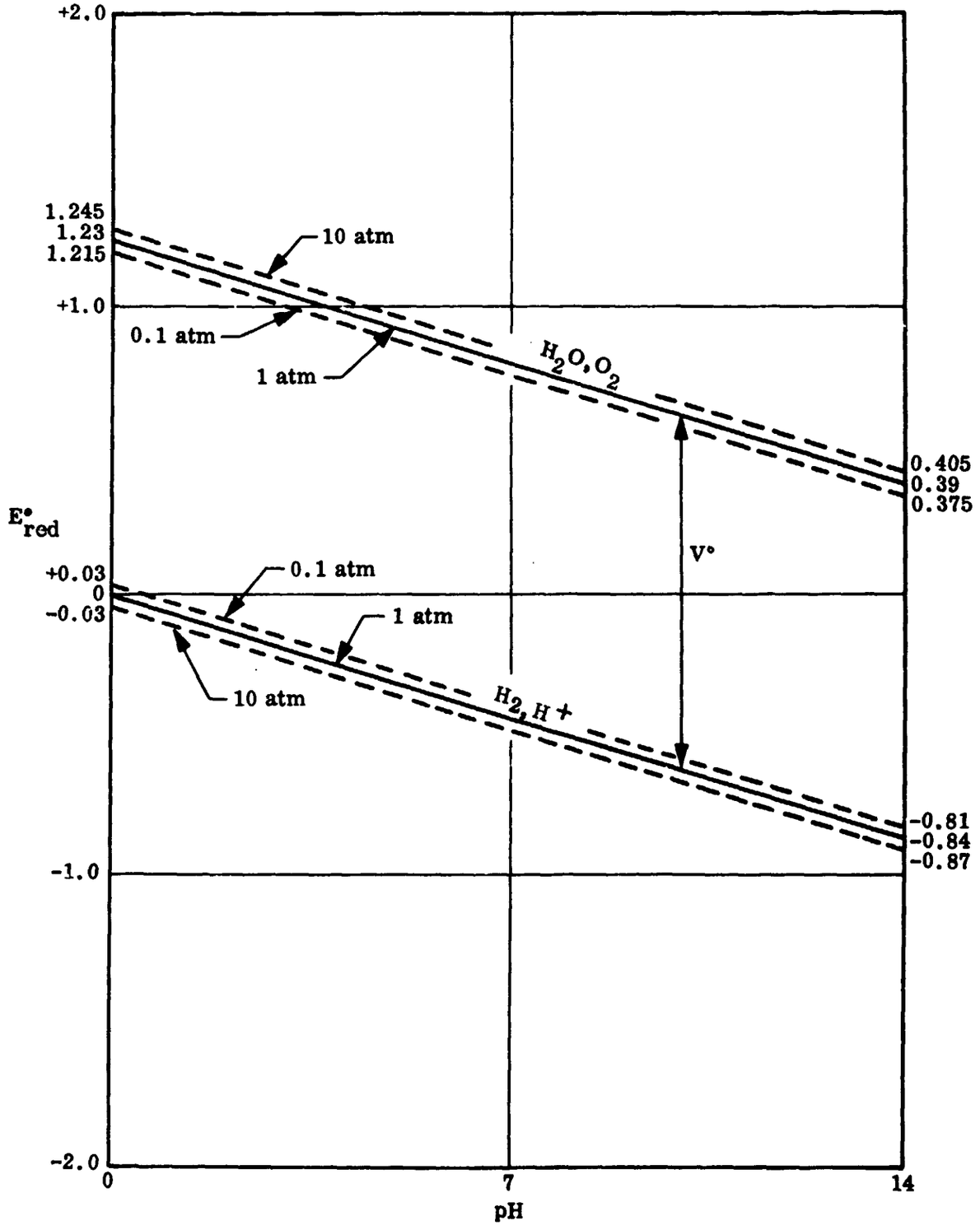

Figure 53 Pourbaix Diagram

The term ΔW_e is equivalent to n F(-Vc) where n and F are constants and V_c is the total cell voltage.

Combining this equation with the second law of thermodynamics, the expression can be written:

$$\Delta F = \Delta H - T \Delta S, \tag{19}$$

$$\Delta F = \Delta Q - nF (-V_c) - T\Delta S \tag{20}$$

where

ΔF = system free energy change

T = system temperature

ΔS = system entropy change

But we can also write

$$-nFV^{o} = \Delta F^{o} \text{ galvanic} = -\Delta F^{o} \text{ electrolysis} \tag{21}$$

where V^{o} is the theoretical potential of the cell and ΔF^{o} electrolysis is the free energy change of the system. By combining Equations 20 and 21, the following expression for the heat production of the system is obtained:

$$\text{heat output} = -\Delta Q$$
$$= nF (V_c - V^{o}) - T\Delta S$$
$$= nF \eta - T\Delta S$$

where $(V_c - V^{o}) = \eta^{o}_{O_2} + \eta^{o}_{H_2} + IR = n$ = total system overvoltage

If the net heating were zero, then $\Delta Q = 0$, and

$$nF\eta = T\Delta S$$

and $$\eta = \frac{T\Delta S}{nF}$$

The no-heat voltage of the cell is then

$$V_{Q-O} = V^{o} + \frac{T\Delta S}{nF}$$

Below this voltage, the cell will tend to be cooled by the reaction; above this voltage heat will be added to the environment.

Cell Resistance

The cell internal resistance is determined primarily by the electrolyte concentration and is influenced by the cell temperature as shown in Figure 54. The total cell resistance can only be determined experimentally because it is influenced by a myriad of variables such as electrode resistance, cell geometry, and concentration gradients in the cell matrix which vary with operating conditions. A simple model of a typical electrolyte concentration profile in a unit cell is shown in Figure 55.

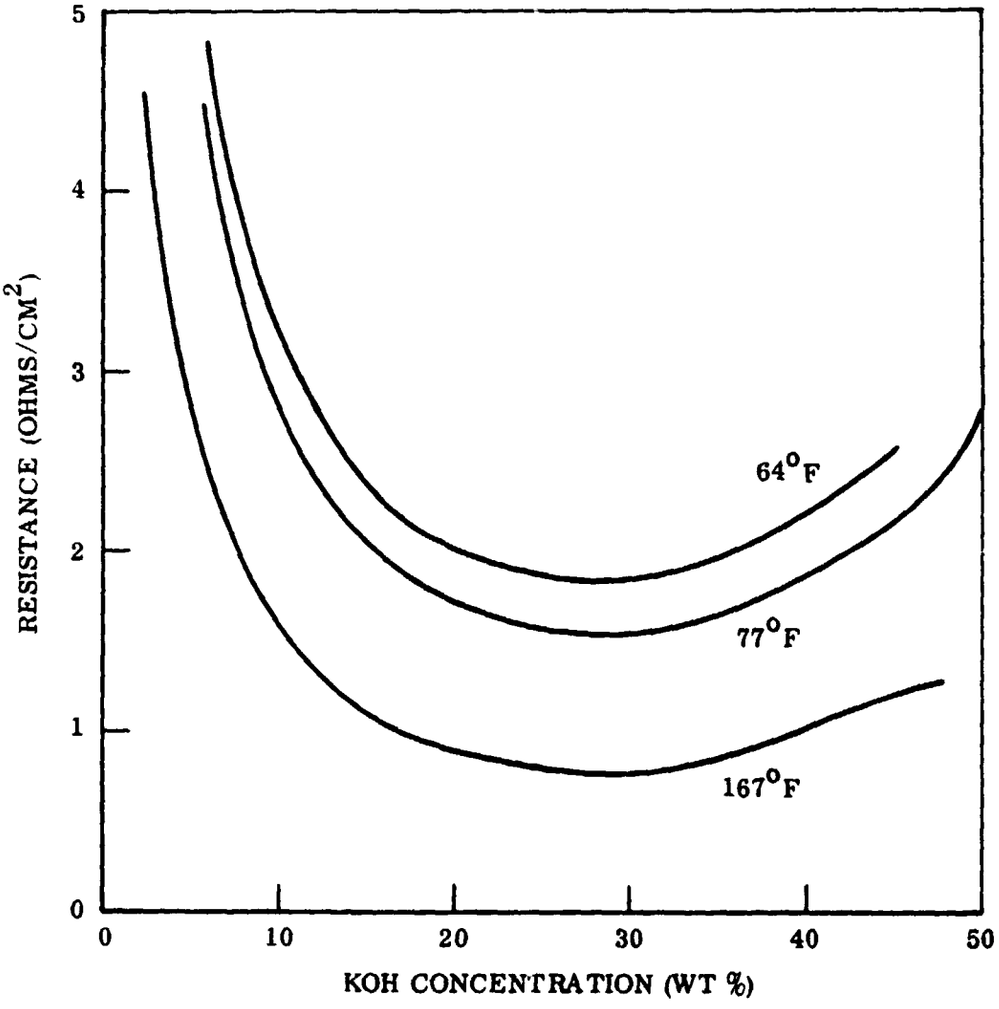

Figure 54 Electrolyte Resistance vs Concentration

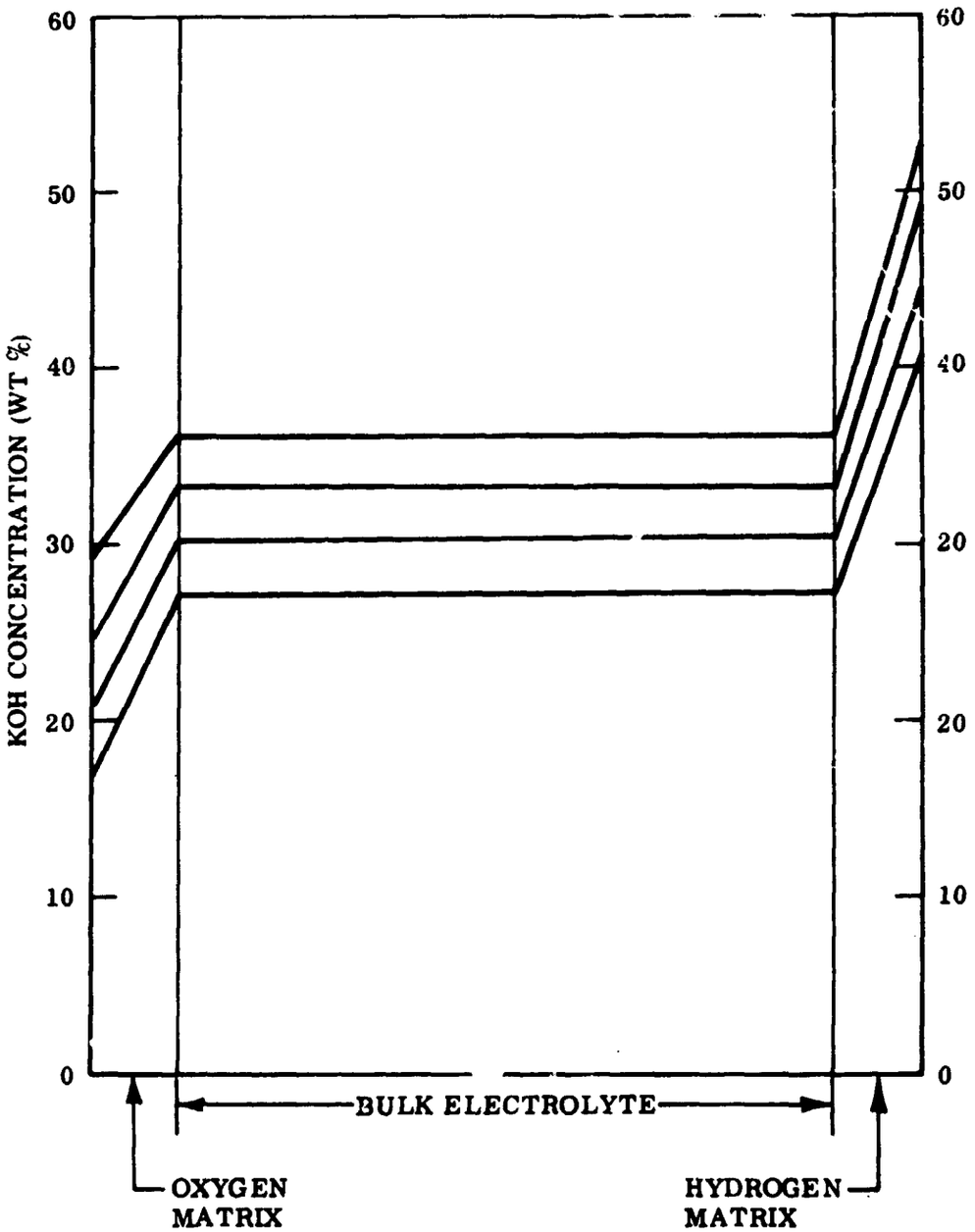

Figure 55 Schematic of Cell Concentration Gradients

2.5 Literature Survey of Hydrazine Detection Amenable to Spacecraft Application

A literature survey was made of hydrazine detection methods with particular attention given to their potential application to spacecraft. The following sources were used.

Pandex and NASA (IAA) files with Lockheed "DIALOG" information retrieval system usage.

Chemical abstracts

Vendor contact

The Lockheed "DIALOG" information retrieval system was used to search the NASA/IAA file.

"DIALOG" System

This system offers the user an interactive command language with which the user can direct a computer to assist in information retrieval. "DIALOG" commands provide means for describing a search interest to the computer, for obtaining results (printouts), and for defining a search interest based on examination of intermediate results. Attached is the cover to the "DIALOG" report for the search carried out on the NASA (IAA) file. A sample page is attached to the cover. A total of 126 references were retrieved from the file, of which 35 references were pertinent to the information desired.

Detection Methods

The literature survey indicates that most analytical procedures for hydrazine consist of oxidation-reduction reactions, acid-base titrations and gasometric methods.

In the area of straight hydrazine detectors, useful in air or liquids, a few of the laboratory techniques have been modified and incorporated into sensors.

Current types utilize the oxidation/reduction reaction, ultraviolet absorption and acid/base (colorimetric) reactions. Specifically, one method makes use of so-called (16,17) detector strips or paper saturated with 2, 4, 5, 7 tetranitrofluorene-9-one (TENF). Upon exposure to hydrazine, there is a color change which is a measure of the hydrazine present. Other hydrazine sensitive reagents include Picryl chlorides, trinitrobenzaldehyde and -dicyanomethylene-2-4-7-trinitro fluorene. This detection method is used on badges for determining approximate hydrazine levels for spacecraft application. In general, the acid-base type of hydrazine detector appears to be the most effective hydrazine sensor.

Director Measurement of Hydrazine in KOH Solutions

Some experimental work with Hydrazine/KOH solutions has been carried out using ultraviolet spectroscopy. Results have not been promising. The literature survey indicates no promising analytical methods for direct detection of hydrazine in a strong potassium hydroxide solution that could be applied to this electrolysis system.

Instrumental Detection Technique

Various detector systems are manufactured specifically for the detection of hydrazine vapor in low concentrations. Three automatic and one manual system are commercially available as follows:

(1) Telydyne, Inc. (Los Angeles, Calif.) manufacturers an instrument which is based on the redox reaction that hydrazine undergoes on the surface of an electrical transducer. The instrument sensitivity is 0.1 ppm and the useful range is up to 100 ppm. The instrument is manufactured both in fixed and portable units and can be hooked up to a warning system. Detector re-calibration is recommended every two to four weeks. The device is subject to interference from certain contaminants.

(2) General Monitors, Inc. (Costa Mesa, California) manufacturers an instrument based on the redox reaction of hydrazine with an aqueous electrolyte. The sensitivity of the instrument is 0 to 5 ppm and the range is 0 to 50 ppm. Both portable and fixed models available with adjustable relays which can be used to sound alarm or control a variety of other functions. Minimum maintenance requires electrolyte change once a month. Interference is caused by sulfur-containing compounds.

(3) Honeywell, Inc., (Minneapolis, Minnesota) manufactures an instrument which utilizes an ultraviolet absorption detector. Sensitivity is 30 ppm. The instrument is portable and can be adapted to a warning system. Interference is caused by a large number of organic compounds.

(4) Mines Safety and Appliance Co. (Pittsburgh, Pennsylvania) manufactures a manual unit which consists of a calibrated 1100 cm^3 hand pump and chemically impregnated filter papers. Sensitivity is 0.5 ppm and the useful range is up to 10 ppm. The advantages of the MSA unit in contrast to the automatic devices are: lower cost, simplicity of operation, reliability, sensitivity, and interference from fewer contaminants. The major disadvantage is that it is operated manually.

Conclusions

Within the limitations proposed for analyzing hydrazine vapor at 1 ppm and in 2-3 molar liquid concentration in KOH, no acceptance system has been reported in the literature search carried out. It is quite evident that an updated literature search is required since for most part this work was carried out in 1972. Based on this literature survey the analysis of hydrazine in KOH would require a separate development effort to expect to be able to demonstrate an analysis technique that could be applied to this program.

3.0 CONCLUSIONS

The basic objective of the contract was to verify the design of key system components, and the concept of an integral system module. The individual components performed quite well except for certain features of the power conditioner and certain new parts of the individual cell assembly. Conclusions relating to each of the sections of this report are presented below.

Pump/Bubble Separator

This was a vendor purchased item which was designed and fabricated to Lockheed requirements. The concept and design of this dual function unit were unquestionably verified and the unit exceeded all its performance requirements. The design should be flight qualifiable with relatively minor adaptation.

Reservoir

The reservoir is also a multi-function component whose performance exceeded its requirements with one exception, size and weight. However, it is felt that the size and weight could be reduced significantly without compromising the performance. The design should be flight qualifiable with relatively minor adaptation.

Baseplate

Performance of the baseplate verified the concept of gas and fluid passages being integral with the module primary structure. However, the particular lamination and annealing sequence is not felt to be a prototype design. Indications are that the baseplate could be, with some design modification, injection molded into a highly reliable structure. It is also felt that a re-evaluation of the materials available for this part would be justified.

Electrodes

The anode performance verified the cell configuration concept. Electrical performance satisfied the design goal. However, problem areas were defined with respect to the availability of a suitable asbestos, and its application on the electrode and the efficient application of the catalyst onto the matrix. Cathode performance was less than the design goal. The problem remains of optimizing the catalyst quantity yet providing uniform dispersal of the catalyst over the electrode matrix. The primary structural membrane, which separates the gas, electrolyte and provides internal support against the elevated gas pressure, has not proven satisfactory and further investigation in this area is necessary.

Molded Cell Spacers

The molded cell spacers performed well and generally exceeded their design requirements. No design changes are anticipated except possibly in the area material used. Further material investigation would be justified on the basis of the gas spacer warpage during annealing.

Cell Stack

The cell stack design proved to be satisfactory; although, assembly is tedious and must be accomplished very carefully. A special fixture should probably be designed to facilitate the assembly procedure, and to insure a more reliable product.

Power Controller

The power controller design was verified in bench testing and exceeded the efficiency goal of 90%. However, when integrated into the module test, efficiency dropped below 90% in the high mode and the unit finally failed. The design is considered satisfactory, but requires debugging.

Feed Tanks

Performance of the tanks met all of the design requirements, and no problem areas were identified.

Heat Exchanger

The prototype heat exchanger which was designed and fabricated on the previous contract was integrated into the prototype module. It was designed to handle a 22 cell stack heat load at ambient temperature. Performance was satisfactory and without problems, including on one occasion, operation in an ambient temperature of 90°F.

Zero Gravity Concept

Each of the major components, as well as the over-all system, was designed to operate in a o-gravity environment. The designs were verified through multi-attitude testing of the major components. Components so tested performed satisfactory and were unsensitive to attitude in the 1 g environment.

References

1. B. M. Greenough, "The Development and Preliminary Design of an Oxygen-Nitrogen Generation System", CR 66940, NAS 1-7706, 18 June 1970.
2. B. M. Greenough, "The Development of a Non-Cryogenic Nitrogen/Oxygen Supply Technique, CR 114912, NAS 9-10405, 17 May 1971.
3. Clark, J. D. and J. R. Smith, "Titrimetric Analysis of Mixtures of Hydrazine and Methyl Hydrazine," Anal. Chemistry: 1188-7, 1961.
4. Malone, H.E., Determination of Mixtures of Hydrazine and 1,1-Dimethyl Hydrazine, Anal. Chemistry 33, 575-7, 1961.
5. Clark, J.D. and J. R. Smith, Titrimetric Analysis of Mixtures of Hydrazine and Methyl Hydrazine, Anal. Chem. 33, 1186-7, 1961.
6. Issue 02 Unclassified Report. AD-841801, NADC-MA-68-39, Analysis of Mixtures Containing Unsymmetrical Dimethyl Hydrazine and Hydrazine-Gas Chromotography.
7. Unclassified Report - 00/06/66 Olin Mathieson Chemical Corporation, New Haven Conn., Calibration of Nitrogen Tetroxide and Hydrazine in Chloroform.
8. Monthly Status Report, NASA-CR-80207, SN-81-8 NAS 7-442, 10 August - 10 September 1966, Research in Chemistry, Quarterly Progress Report.
9. NOTS-TP-4215-AD-377616 00/11/66, Naval Ordnance Test Station, China Lake, Ca. NSOS24331, The Properties and Specification Testing of Unsymetrical Di-methyl Hydrazine (Chemical and Physical) and Methods for Specification Testing of Unsymetrical Di-methyl Hydrazine.
10. Weapons Research Establishment, Salisbury, Australia, Dec. 1965. Mixing and Reaction Studies of Hydrazine and Nitrogen Tetroxide Using Photographic and Spectral Techniques - Bunows, M.C.
11. National Aeronautics and Space Administration. Lewis Research Center, Cleveland, Ohio. ND 315753, Gas Chromatographic Analysis of Hydrazine, Monomethyl Hydrazine and Water in Mixed Hydrazine Cells.
12. NAVWEPS-8788, NOTS-TP-3882 AD-366610, Naval Ordnance Test Station, China Lake, Ca. Aug. 1965 Determination of Hydrazine, 1, 1 Di-methyl Hydrazine Mixtures.
13. AFFTC-TN-59-38, AD-231372, Air Force Flight Test Center, Edwards AFB, Ca., Detection of Liquid Crystal Gases/Reactive Material. (Final Report) 1 Feb. 12 Nov. 1965, Crystal Detectors for Hydrochloric Acid, Hydrogen Fluorides, Hydrazine, Nitrogen Dioxide and Unsymetrical Di-methyl Hydrazine.
14. RADC-TR-64-569 AD 620940 Westinghouse Electric Corp., Pittsburg, Pa., Detailed Procedures for Hydrazine, 1 Di-methyl Hydrazine Assy. Titin II.
15. BSD-TR-338 AD-453038 01/12/64, Space Systems Division, Rocket Research Labs, Eiwards AFB, Ca., Analysis of Hydrazine-Liquid Ammonia Mixtures by Low Temperature Thermogravimetry.
16. Charles A. Plantz, Mine Safety Appliances Company, AMRL-TR-66-162, Colorimetric Personal Dosimeter for Hydrazine Cells, May 1967.
17. Robert F. Rabowski, Captain, USAF, BSC - ARML-TR-68-163, Evaluation of the Use of Commercially Available Detectors for Hydrazine and Nitrogen Dioxide as Colorimetric Dosimeters.

APPENDIX

Computer Printout, Dialog Information Retrieval System

DIALOG INFORMATION RETRIEVAL SYSTEM
LOCKHEED INFORMATION SCIENCES LABORATORY, DEPT/52-50
3251 HANOVER STREET
PALO ALTO, CALIFORNIA 94304
TELEPHONE: (415)493-4411 X46034

TITLE COMPOSIT MATERIALS
DATE/FILE 8-7-72/7
SEARCHER MEINHARDT
REQUESTOR [redacted] Frank Smith
ADDRESS SV 118

TERMINAL 5 8-7-72

COMMAND	USE	TIME	COMMAND	USE	TIME	COMMAND	USE	TIME	COMMAND	USE	TIME
BEGIN	2	.27	IX-ADD	0	.00	IX-DEL	0	.00	IX-DISP	0	.00
EXPAND	5	.22	SELECT	7	1.88	COMBINE	5	.27	LIMIT	0	.00
KEEP	0	.00	DISPLAY	2	.11	SET-HIS	3	.07	TYPE	0	.00
PRINT	3	.05	END	1	.01	PAGE	0	.00	MESSAGE	0	.00
EXPLAIN	0	.00	EXTRACT	0	.00	STAT	0	.00	PUNCH	0	.00
FILE	1	.02	INTERSC	0	.00	LMT-ALL	0	.00	ITEM	1	.04
ERROR	1	.04	EXEC TIME		2.35	SPCH TIME		24.06	PRINT COUNT		126

SET	ITEMS	DESCRIPTION	NO. FILE	SET/A.N.	FMT	ITEM-RANGE
1	1814	E5,I6 COMPOSITE MATERIALS	1 7	19	5	1-126
2	9229	ALUMINUM				
3	202	I*2				
4	2027	[illegible]ION				
5	64	3*4				
6	3639	E15,F16 MECHAN				
7	11	5*4				
8	[illegible]	[illegible]				
9	1376	E6,F14 HYDRAZINE				
10	24334	E6,F11,E12,F13 ANALYSIS				
11	9818	E6,E7,E8 DETECTION				
12	3053	CHEMISTRY				
13	1578	E7,E17,E18 PHYSICAL				
14	0	REACTIONS				
15	48	9*10				
16	8	9*11				
17	63	9*12				
18	16	9*13				
19	126	15+16+17+18				

35/126 = 27.8%

(1)

69X10913# ISSUE 02 CATEGORY 14 AD-841301 NADC-MA-6839 27/05/69
UNCLASSIFIED REPORT, GOVT. & CONTR.
DEVELOPMENT OF AN EXTERNAL DEVICE FOR THE DETECTION OF THE PRESENCE OF CHLORINE TRIFLUORIDE OR MIXED HYDRAZINES (DEVELOPMENT OF EXTERNAL DEVICE FOR DETECTION OF CHLORINE TRIFLUORIDE OR MIXED HYDRAZINES)
KNIGHT, W. F.
NAVAL AIR DEVELOPMENT CENTER, JOHNSVILLE, PA. (NN947215)
AERO MATERIALS DEPT. DATE- 27 MAY 1968 COLL- 15 P REFS

69X10794# ISSUE 02 CATEGORY 27 AD-392194 GR-1-TSF-68
AFRPL-TR-68-113 ESSO-1130 F04611-68-C-0026 00/07/68 CONFIDENTIAL REPORT, GOVT. & CONTR.
DEVELOPMENT OF THERMALLY STABLE LIQUID FUELS, 15 DECEMBER 1967 - 30 JUNE 1968 /U/ (CLASSIFIED NOTATION OF CONTENT DELETED)
BROIS, S. J.; MUNKER, A. H.; OTTEN, E. F.
ESSO RESEARCH AND ENGINEERING CO., LINDEN, N. J. (E4331335)
GOVERNMENT RESEARCH LAB. DATE- JUL. 1968 COLL- 79 P REFS

69X10407C ISSUE 01 CATEGORY 27 AD-391866 R-7437 AFRPL-TR-68-100 AF 04/611/-11407 01/05/68 CONFIDENTIAL REPORT, GOVT. & CONTR.
ENGINEERING PROPERTY DATA ON ROCKET PROPELLANTS /U/ FINAL REPORT, 1 APR. 1966 - 31 MAR. 1968 (CLASSIFIED NOTATION OF CONTENT DELETED)
ROCKETDYNE, CANOGA PARK, CALIF. (RY024740)
CHEMICAL AND MATERIAL SCIENCES DEPT. PLAC- EDWARDS AFB, CALIF. PUBL- AF ROCKET PROPULSION LAB. DATE- 1 MAY 1968 COLL- 42253 P REFS

68X13610# ISSUE 08 CATEGORY 27 R-6639-6 AFRPL-TR-68-12 OR-6
AD-826018 AF 04/611/-11407 00/01/68 UNCLASSIFIED REPORT, GOVT. & CONTR.
ENGINEERING PROPERTY DATA ON ROCKET PROPELLANTS QUARTERLY REPORT, 1 OCT. - 31 DEC. 1967 (ENGINEERING PROPERTIES DATA FOR LIQUID ROCKET PROPELLANTS)
ROCKETDYNE, CANOGA PARK, CALIF. (RY024740)
PLAC- EDWARDS AFB, CALIF. PUBL- AF ROCKET PROPULSION LAB. DATE- JAN. 1968 COLL- 34 P REFS

45893

(2)

67X82292# ISSUE 08 CATEGORY 22 00/06/66 UNCLASSIFIED REPORT, GOVT. & CONTR.
GAS CHROMATOGRAPHIC ANALYSIS OF MIXTURES CONTAINING UNSYMMETRICAL DIMETHYL HYDRAZINE AND HYDRAZINE
GLONA, W.; HAGSTROM, P. A.
OLIN MATHIESON CHEMICAL CORP., NEW HAVEN, CONN. (OU368326)
IN APL ANAL. CHEM. WORKING GROUP 220 MEETING BULL. /CONFIDENTIAL REPORT/ JUN. 1966 P 55-76 REFS SPONSORED BY AF /SEE X67-82287/

LIBRARY CARD ABSTRACT

A hydrazine/water electrolysis process system module design was fabricated and tested to demonstrate component and module performance. This module is capable of providing both the metabolic oxygen for crew needs and the oxygen and nitrogen for spacecraft leak makeup. The component designs evolved through previous R&D efforts, and were fabricated and tested individually and then were assembled into a complete module which was successfully tested for 1000 hours to demonstrate integration of the individual components. A survey was made of hydrazine sensor technology and a cell math model was derived.